

# 1 Ozone trends in homogenized Umkehr, Ozonesonde, and COH 2 overpass records

3 Irina Petropavlovskikh<sup>1,2</sup>, Jeannette D. Wild<sup>3,4</sup>, Kari Abromitis<sup>1,2</sup>, Peter Effertz<sup>1,2</sup>, Koji Miyagawa<sup>5</sup>,  
4 Lawrence E. Flynn<sup>4</sup>, Eliane Maillard Barras<sup>6</sup>, Robert Damadeo<sup>7</sup>, Glen McConville<sup>1,2</sup>, Bryan  
5 Johnson<sup>2</sup>, Patrick Cullis<sup>2</sup>, Sophie Godin-Beckmann<sup>8</sup>, Gerard Ancellet<sup>8</sup>, Richard Querel<sup>9</sup>, Roeland  
6 Van Malderen<sup>10</sup>, Daniel Zawada<sup>11</sup>

7 <sup>1</sup>CIRES, University of Colorado, Boulder, CO, USA

8 <sup>2</sup>NOAA, Global Monitoring Lab, Boulder, CO, USA

9 <sup>3</sup>University of Maryland, Earth System Science Interdisciplinary Center (ESSIC/CISESS), College Park, MD, USA

10 <sup>4</sup>NOAA/NESDIS/Center for Satellite Applications and Research (STAR), College Park, MD, USA

11 <sup>5</sup>National Institute for Environmental Studies (NIES), Tsukuba, Japan

12 <sup>6</sup>Federal Office of Meteorology and Climatology, MeteoSwiss, Payern, Switzerland

13 <sup>7</sup>NASA Langley Research Center, Hampton, VA, USA

14 <sup>8</sup>LATMOS Sorbonne Université, UVSQ-CNRS/INSU, Paris, France.

15 <sup>9</sup>National Institute of Water & Atmospheric Research (NIWA), Lauder, New Zealand

16 <sup>10</sup>Royal Meteorological Institute of Belgium, Uccle (Brussels), Belgium

17 <sup>11</sup>University of Saskatchewan, Saskatoon, SK, Canada

18 *Correspondence to:* Irina Petropavlovskikh (Irina.petro@Noaa.gov)

19 **Abstract.** This study presents an updated evaluation of stratospheric ozone profile trends at  
20 Arosa/Davos/Hohenpeißenberg, Switzerland/Germany, Observatory de Haute Provence (OHP), France, Boulder,  
21 Colorado, Mauna Loa Observatory (MLO) and Hilo, Hawaii, and Lauder, New Zealand with focus on the ozone  
22 recovery period post 2000. Trends are derived using vertical ozone profiles from NOAA’s Dobson Network via the  
23 Umkehr method (with a recent new homogenization), ozonesondes, and the NOAA COHesive SBUV/OMPS satellite-  
24 based record (COH) sampled to match geographical coordinates of the ground-based stations used in this study.  
25 Analyses of long-term changes in stratospheric ozone time series were performed using the updated version (0.8.0) of  
26 the Long-term Ozone Trends and Uncertainties in the Stratosphere (LOTUS) Independent Linear Trend (ILT)  
27 regression model. This study finds a consistency of the trends derived from the different observational records, which  
28 is a key factor to the understanding of the recovery of the ozone layer after the implementation of the Montreal Protocol  
29 and its amendments that control ozone-depleting substances production and release into the atmosphere. The Northern  
30 Hemispheric Umkehr records of Arosa/Davos, OHP, and MLO all show positive trends in the mid to upper  
31 stratosphere with trends peaking at ~+2%/decade. Although the upper stratospheric ozone trends derived from COH  
32 satellite records are more positive than those detected by the Umkehr system, the agreement is within the two times  
33 standard error uncertainty. Umkehr trends in the upper stratosphere at Boulder and Lauder are positive but not  
34 statistically significant, while COH trends are larger and statistically significant (within 2 times standard error  
35 uncertainty). In the lower stratosphere, trends derived from Umkehr and ozonesonde records are mostly negative  
36 (except for positive ozonesonde trends at OHP), however the uncertainties are quite large. Additional dynamical  
37 proxies were investigated in the LOTUS model at five ground-based sites. The use of additional proxies did not  
38 significantly change trends, but equivalent latitude reduced the uncertainty of the Umkehr and COH trends in the

39 upper stratosphere and at higher latitudes. In lower layers, additional predictors (tropopause pressure for all stations,  
40 two extra components of Quasi-Biennial Oscillation at MLO, Arctic Oscillation at Arosa/Davos, OHP and MLO)  
41 improve the model fit and reduce trend uncertainties as seen by Umkehr and sonde.

## 42 **1 Introduction**

43 The WMO Ozone Assessments (WMO, 2018; WMO, 2022), indicate that for some geographical regions, the  
44 stratospheric ozone layer is recovering in accordance with the reduction of ozone depleting substances (ODS) whose  
45 production was restricted by the Montreal Protocol and its amendments. The US Clean Air Act requires NOAA to  
46 monitor prohibited chemicals and the ozone layer to ensure the success of the Montreal Protocol. NOAA's long-term  
47 network of measurements helps to interpret total column and vertically resolved ozone changes and link ozone  
48 recovery to the reduction of ODS levels in the stratosphere, changes in the lower stratosphere that are associated with  
49 climate changes, and to the increases in the troposphere that are influenced by the stratosphere/troposphere exchange  
50 and long-range transported pollution. The ongoing recovery of the stratospheric ozone layer is of great importance to  
51 human health (i.e. cancer from enhanced UV exposures, Madronich et al., 2021), the sustained production of crops,  
52 and the success of fisheries (dangerous algae blooms). For more information see the Environmental Effects  
53 Assessment Panel 2022 Quadrennial Assessment (EEAP, 2023).

54 The Long-term Ozone Trends and Uncertainties in the Stratosphere (LOTUS) study was initiated under Stratosphere-  
55 troposphere Processes And their Role in Climate (SPARC, changed to APARC in 2024) project to reconcile the  
56 differences in defining trend uncertainties between methods outlined in the WMO Assessment (WMO, 2014) and the  
57 SPARC/IO3C/IGACO-O3/NDACC (SI2N) study (Harris et al., 2015). Phase 1 focused on developing best practices  
58 for data merging, trend determination and error analyses. Results focused on analysis of broad latitudinal regions,  
59 near global, Northern and Southern Hemisphere, and Tropics as were used in the SI2N studies. Results are found in  
60 the 2019 report (SPARC/IO3C/GAW, 2019). Phase 2 refined the trend models, and extended the study to gridded,  
61 and GB ozone data sets. The development of methods used in trend detection is built on the community knowledge  
62 gained during the Tiger Team project in early 1990s (Reinsel et al., 2005), collaborations through the SPARC, WMO  
63 and IO3C supported LOTUS activity (Hassler et al., 2014; Harris et al., 2015; Godin-Beekmann et al., 2022) and the  
64 most recent contributions to the WMO Ozone assessment analyses published in Chapter 3, "Update on Global Ozone:  
65 Past, Present and Future" (Hassler et al., 2022).

66 Understanding the causes of the differences between GB and satellite records can create improvements not only in the  
67 internal consistency of data sets, but also in the uncertainties of overall ozone trends. Further, development of  
68 techniques to directly assess uncertainties in the merged records resulting from discrepancies that cannot be completely  
69 reconciled, such as small relative drifts and differences resulting from coordinate transformations and sampling  
70 differences, allows for a more precise estimate of significance of the mean trends. For the GB and satellite data used  
71 in the 2019 LOTUS Report, information on stability and drifts of the measurement was incomplete. The  
72 homogenization of many ozonesonde records was recently addressed and data were reprocessed (Tarasick et al., 2016;  
73 Van Malderen et al., 2016; Witte et al., 2017; Sterling et al., 2018; Witte et al., 2018; Ancellet et al., 2022) while some  
74 instrumental artifacts still need to be addressed (Smit, 2021).

75 The first attempt to evaluate representativeness of the trends derived from GB station records in the middle and upper  
76 stratosphere using SBUV data was done as a part of the LOTUS activity and was discussed in the 2019 LOTUS report.  
77 Comparisons of trends derived from satellite data sub-sampled at the station location (overpass) to those derived from  
78 the relevant zonal average provide a measure of potential sampling errors when comparing satellite and GB trends  
79 (Zerefos et al., 2018; Godin-Beekmann et al., 2022). This paper continues that work by comparing trends derived from  
80 several GB and satellite records that are matched spatially. We further investigate the impact of temporal matching on  
81 trends.

82 The common statistical linear regression trend model used in the 2019 LOTUS Report and the 2022 update (Godin-  
83 Beekmann et al., 2022) was optimized for analyses of the zonally averaged satellite data sets. However, analyses of  
84 the GB and satellite overpass ozone profile data may require reconsideration of additional proxies and optimization  
85 methods to improve interpretation of the processes that impact ozone changes over limited geophysical regions and  
86 reduce trend uncertainties. An assessment of model sensitivities to uncertainties in the volcanic aerosols, solar cycle,  
87 QBO, El Nino Southern Oscillation (ENSO) and other mechanisms also need to be considered in the GB and satellite  
88 overpass record trend analysis. The localized time series for the assessment of dynamical and chemical proxies can  
89 improve attribution of ozone variability, especially in the lower stratosphere, thus reducing uncertainties in the derived  
90 trends. This paper provides an assessment of uncertainties in the derived trends from the NOAA ground-based,  
91 ozonesonde and SBUV/OMPS (zonally averaged and overpass) records and reports improvements in the Multiple  
92 Linear Regression (MLR) trend uncertainties with addition of proxies representing interannual dynamical variability  
93 or long-term changes in atmospheric circulation. Ability of the ground-based and ozonesonde records in capturing  
94 semi-global ozone changes is evaluated by comparing trends derived from the satellite overpass and zonally averaged  
95 records

96 In the LOTUS report, the ozone trends were analyzed at low and middle latitudes, with a focus on the upper and  
97 middle stratosphere. This paper includes middle and low latitude trends assessed in the lower stratosphere and thus  
98 offers an opportunity to test the additional proxy of the tropopause pressure (Thompson et al., 2021).

## 99 **2 Data**

### 100 **2.1 Umkehr and Ozonesonde Records at NOAA**

101 The Dobson Ozone Spectrophotometer has been used to study total ozone since its development in the 1920s  
102 (Staehelin et al., 2018). Dobson records are regularly used in satellite record validation (Bai et al., 2015; Koukouli et  
103 al., 2016; Boynard et al., 2018) and the development of global combined ozone data records (Fioletov et al., 2008;  
104 Hassler et al., 2018). The NOAA Dobson ozone record was homogenized in 2017 to account for inconsistencies in  
105 past calibration records, data processing methods and selection of representative data (Evans et al., 2017). NOAA  
106 Dobson instruments at 4 stations and MeteoSwiss at Arosa/Davos also measure Umkehr profiles, which are derived  
107 as partial column ozone amounts in ~5 km layers. Profiles are derived using an optimum statistical inversion of Dobson  
108 measurements taken continuously at different solar zenith angles (SZAs) (Petropavlovskikh, 2005; Hassler, 2014).  
109 These Umkehr data were recently homogenized to assure the removal of small but significant instrumental artifacts

110 that can impact the accurate detection of stratospheric ozone trends (Petrovskikh et al., 2022, Maillard Barras et  
111 al., 2022). This study focuses on Umkehr records from the MeteoSwiss station of Arosa/Davos, Switzerland, and on  
112 Umkehr records from the NOAA stations of Boulder, Colorado, Mauna Loa Observatory (MLO), Hawaii, Lauder,  
113 New Zealand, and the Umkehr record from Observatory de Haute Provence (OHP), France. NOAA/GML for Umkehr  
114 data means that the NOAA optimization process was applied to the operational records (N-values) prior to the retrieval  
115 of ozone profiles. The source data used in this study are available at <https://doi.org/10.15138/1FF4-HC74> (Miyagawa  
116 et al., 2024). See **Table 1** for details on the GB datasets, locations, source of data and temporal extent of data used.  
117 Umkehr measurements are typically made twice per day when there is no cloud obstruction.

118 The ozonesonde instrument has been flown at 4 NOAA stations since the 1980s. Evolving instrumentation and  
119 standard operating procedures led to the development of data homogenization methods by NOAA and the international  
120 community (i.e., ASOPOS-1, Smit, 2014) to resolve record inconsistencies in the NOAA (Sterling et al., 2018),  
121 Canadian (Tarasick et al., 2016) and SHADOZ (Southern Hemisphere Additional Ozonesondes) networks (Witte et  
122 al., 2017; Witte et al., 2018). The effort was extended in the ASOPOS-2 (Smit et al., 2021) activity and included a  
123 larger group of stations that are part of the NDACC (Network for Detection of Atmospheric Composition Change)  
124 and WMO GAW (World Meteorological Organization Global Atmosphere Watch program) networks. The error  
125 budget for each profile is calculated and included in the archived files (Sterling, 2018). Modern ozonesonde  
126 instruments measure ozone at high vertical resolution, on the order of 100 m (Thompson et al., 2019) depending on  
127 the balloon ascent velocity and the time response of the instrument.

128 The sondes constitute an essential component of satellite calibration and cross-calibration (Hubert et al., 2016),  
129 verification and improvement of climate chemistry and chemistry-transport models (Wargan et al., 2018; Stauffer et  
130 al., 2019). The Dobson total ozone, Umkehr and ozonesonde profile records provide key measurements for upper and  
131 middle stratospheric ozone trend calculations, and are part of the NOAA benchmark network for stratospheric ozone  
132 profile observations (SPARC/IO3C/GAW, 2019; Godin-Beekmann et al., 2022; WMO, 2022).

133 The ozonesonde data are used for trend analyses from OHP, Boulder, and Lauder stations where we have Umkehr  
134 observations. Ozonesondes are launched at Hilo, Hawaii, which is nearly co-located with MLO. Ozonesonde data  
135 for the Arosa/Davos panel are selected from Hohenpeißenberg (HOH), Germany station that is in close vicinity to  
136 Arosa/Davos station. Sonde measurements are typically measured once or twice per week, varying somewhat with  
137 station operational procedures.

138 Data for the NOAA GML ozonesonde records are publicly available from the NOAA Global Monitoring Lab (GML)  
139 at <https://gml.noaa.gov/aftp/data/ozwv/Ozonesonde/>. We use the ‘100 Meter Average Files’ in each station directory.  
140 Other sonde datasets used in this study are also available at several other data centers including the World Ozone and  
141 Ultraviolet Radiation Data Centre (WOUDC, [www.woudc.org](http://www.woudc.org)), Network for the Detection of Atmospheric  
142 Composition Change (NDACC, [www.ndacc.org](http://www.ndacc.org)) data centers, or at the Harmonization and Evaluation of Ground-  
143 based Instruments for Free-Tropospheric Ozone Measurements (HEGIFTOM, <https://hegiftom.meteo.be/>) archive.  
144 Table 1 denotes the source of each dataset used in this study.

145 The ozonesonde data is of significantly higher vertical resolution (even when used as 100 m averages) than the Umkehr  
146 data layers of approximately 5000 m. In order to create a dataset with comparable resolution, we use the Umkehr

147 averaging kernels (AK) to smooth the sonde data. Details appear in Appendix A. We cap the sonde profile at Umkehr  
 148 layer 5 (16–32 hPa) as there is not sufficient sonde information at higher altitudes to meet the requirements of the AKs  
 149 for layers 6 and above. We further match the ozonesonde data to the dates when both Umkehr and sonde data are  
 150 available using  $\pm 24$  hours to find a match, then generate the ozonesonde monthly mean. Appendix D explores the  
 151 impact of temporal sampling on trends. The final matched dataset, with AK averaging, is publicly available at  
 152 <https://doi.org/10.15138/1FF4-HC74> (Miyagawa et al., 2024).

153  
 154 **Table 1: GB datasets, location, instrument type, temporal extent, data record source. For the trend calculations we remove**  
 155 **data during volcanic periods from 1982–1984 and 1991–1994.**

Location	WOUD C Station #	Instrument	Date Range used in trend calculations	Source
Arosa/Davos Arosa, Switzerland (46.8° N, 9.7° E) Davos, Switzerland (46.8° N, 9.8° E)	035	Umkehr	1980 – 2018 2018 – 2020	Optimization by NOAA/GML
Hohenpeißenberg (HOH), Germany (47.8° N, 11.0° E)	099	Ozonesonde	1980 – 2020	NDACC
Observatory de Haute Provence (OHP), France (43.9°N, 5.8° E)	040	Umkehr	1983 – 2020	NOAA/GML
		Ozonesonde	1991 – 2020	NDACC* (same as HEGIFTOM)
Boulder, Colorado (40.0° N, 105.3° W)	067	Umkehr	1980 – 2020	NOAA/GML
		Ozonesonde	1980 – 2020	NOAA/GML - 100m average data
Mauna Loa Observatory (MLO), Hawaii (19.5°N, 155.6°W)	031	Umkehr	1982 – 2020	NOAA/GML
Hilo, Hawaii (19.7° N, 155.1° W)	109	Ozonesonde	1982 – 2020	NOAA/GML - 100m average data

Lauder, New Zealand (45.0°S, 169.7°E)	256	Umkehr	1987 – 2020	NOAA/GML
		Ozonesonde	1987 – 2020	NDACC

156 \*Note, data from the “Corrected Ozone partial pressure” column is used for trend analyses

157 **2.2 The NOAA Cohesive (COH) Station Overpass Ozone Profile Datasets**

158 NASA and NOAA have produced satellite measurements of ozone profiles through the Solar Backscatter Ultraviolet  
159 (SBUV) on the sequence of Polar Orbiting Environmental Satellites (POES) since 1978. This measurement series is  
160 extended with the related Ozone Mapping and Profiler Suite (OMPS) nadir profiler (NP) instruments using similar  
161 measurement techniques and retrieval algorithms. These combine to provide nearly 45 years of continuous data (1978  
162 – present). This single instrument type dataset eliminates many homogeneity issues including varying vertical  
163 resolution, or instrumentation differences. Version 8.6 SBUV data incorporates additional calibration adjustments  
164 beyond the Version 8 release (McPeters et al., 2013). Small but evident biases remain (Kramarova et al., 2013a).  
165 Several methods have been historically used to combine these datasets into a continuous series. The NASA MOD  
166 version 1 dataset based on SBUV and OMPS v8.6 (Frith, 2014) combines data from all available satellites with no  
167 modification or bias adjustments. NASA has developed an alternate processing for the SBUV and OMPS data (v8.7)  
168 which incorporates new calibrations at the radiance level, and updated a priori with improved troposphere.  
169 Additionally, the a priori is chosen to be representative of the local solar time of the measurement. MOD v2 is based  
170 on the v8.7 processing (Frith et al., 2020), and further applies an adjustment to the v8.7 data to shift all measurements  
171 to a nominal measurement time of 1:30 PM local time.

172 The NOAA SBUV/2 and OMPS Cohesive dataset (further referred to as COH) combines data from the SBUV/2 and  
173 OMPS instruments using NASA’s version 8.6 for the SBUV/2 data and NOAA/NESDIS version 4r1 for the OMPS  
174 Suomi National Polar-orbiting Partnership (SNPP) data. This dataset uses correlation-based adjustments providing  
175 an overall bias adjustment plus an ozone-dependent factor (Wild et al., 2016) to moderate the remaining biases  
176 between instruments in the series. The resulting profile product is a set of daily or monthly zonal means and is publicly  
177 available at [https://ftp.cpc.ncep.noaa.gov/SBUV\\_CDR](https://ftp.cpc.ncep.noaa.gov/SBUV_CDR). Zones are 5° wide in latitude, identified by the central latitude  
178 (2.5°, 7.5°, etc.). Contributing satellites and their period of use is shown in Table 2.

179 **Table 2: Satellite mapping for COH data series.**

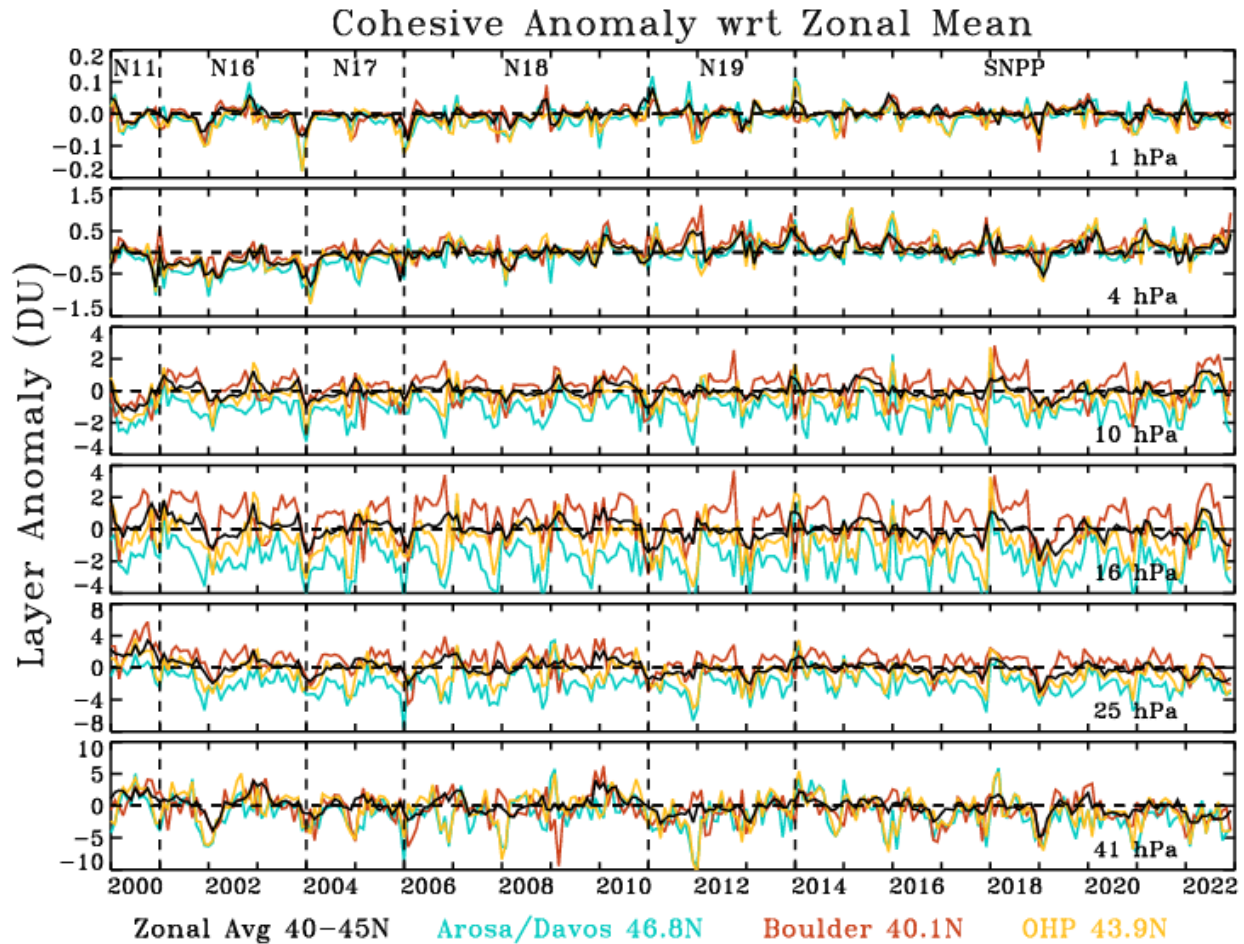
Satellite	Dates
Nimbus 07	10/1978 – 5/1989
NOAA 11 (ascending)	6/1989 – 12/1993
NOAA 09	1/1994 – 6/1997
NOAA 11 (descending)	7/1997 – 12/2000
NOAA 16	1/2001 – 12/2003
NOAA 17	1/2004 – 12/2005

NOAA 18	1/2006 – 12/2010
NOAA 19	1/2011 – 12/2013
SNPP	1/2014 – present

180 A previous version of this dataset using OMPS v3r2 has been used in climate reviews and trend studies (Godin-  
181 Beekmann et al., 2022; Weber et al., 2022a, 2022b) including Chapter 3 of the WMO Ozone Assessment (Hassler et  
182 al., 2022). Appendix B examines the differences between the data versions. The impact on trends is limited to less  
183 than 1% per decade, well within the precision of the trend results.

184 We create the overpass data at a ground station by collecting all profiles from a satellite within a  $\pm 2/20^\circ$   
185 latitude/longitude box centred on the station. The box size is chosen to ensure that one to four points are found per  
186 day. Fewer points are found if the orbit passes directly over the station; more points are found if the orbits straddle  
187 the station. The collected profiles are inverse-distance weighted to the station location and averaged. COH style  
188 adjustments are applied (Wild et al., 2016) creating a COH overpass time series from 1978 to present. This dataset is  
189 available on the NOAA website at [https://ftp.cpc.ncep.noaa.gov/SBUV\\_CDR/overpass](https://ftp.cpc.ncep.noaa.gov/SBUV_CDR/overpass).

190 Figure 1 shows the ozone anomaly time series for the 40–45° N zonal average data, and for the data at 3 stations in or  
191 near the zone. Anomalies are calculated with respect to the zonal average climatology. The series shown are for the  
192 layer data with the bottom pressure of the layer displayed on the right side of the graph. This depiction retains the  
193 information about the relative differences between the stations and the zonal average. In the mid-stratosphere (25–10  
194 hPa) the biases between the stations are most pronounced with Arosa/Davos usually showing less ozone and Boulder  
195 usually showing more ozone. At the uppermost layers (1 and 4 hPa), and the lowest layer (41 hPa) the bias between  
196 stations is reduced. The anomalies for Arosa/Davos and OHP, which are geographically closer than Boulder, are often  
197 nearly anticorrelated with the Boulder anomalies especially in the second half of the year. Indeed at 16 hPa in  
198 particular, one can see that often the Boulder anomalies are positive when the Arosa/Davos and OHP anomalies are  
199 negative.

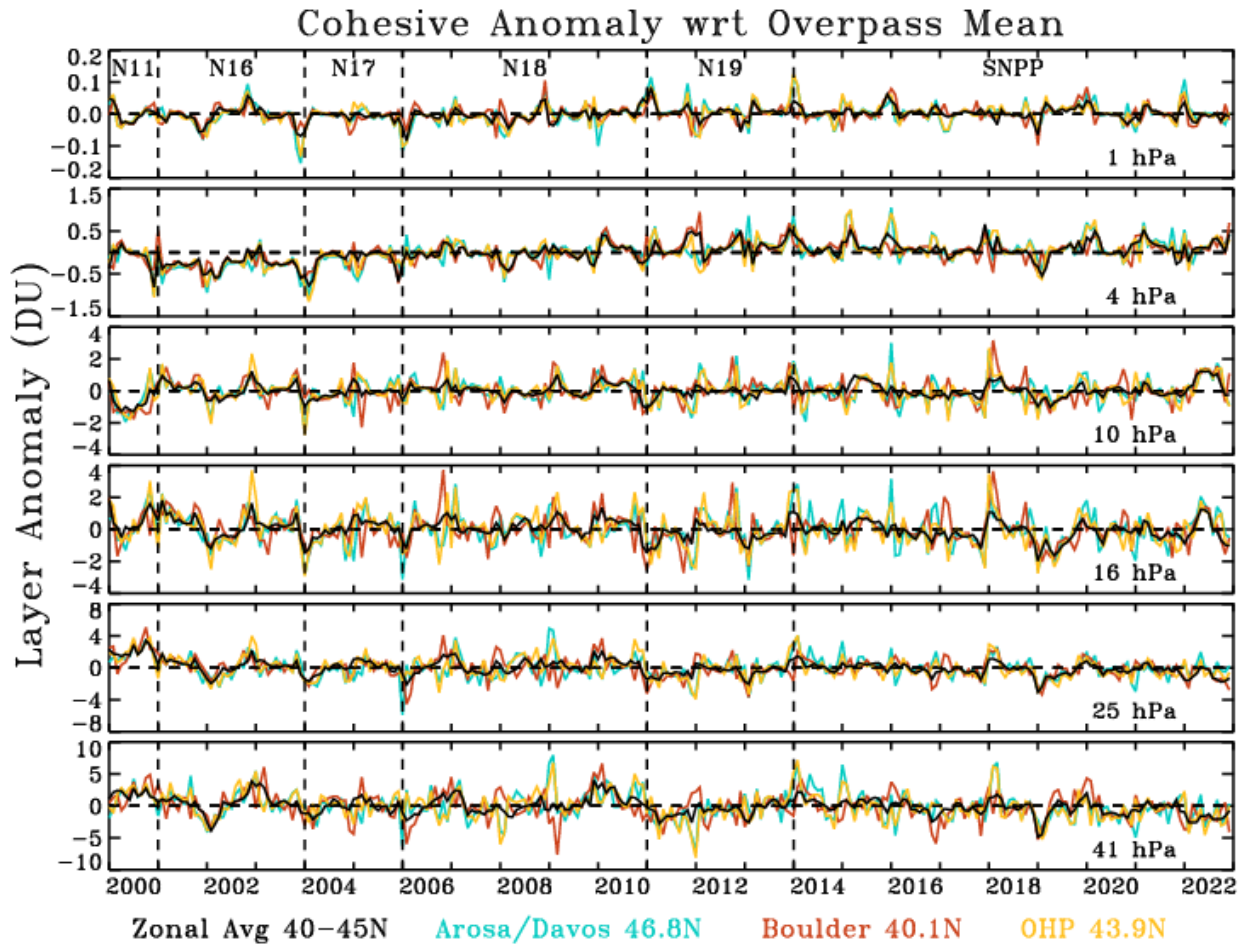


200

201 **Figure 1. Monthly ozone anomaly relative to the zonal mean monthly averages. This process leaves intact the trend for**  
 202 **each site and the zone, and accentuates the differences between the station values since all anomalies are referenced to the**  
 203 **zonal product. Evident at 4 hPa is a positive trend from 2002 to 2013, then a levelling out after.**

204 Figure 2 also shows the anomalies for the 40-45° N zonal average with the station anomalies, but each anomaly is  
 205 now created using the climatology derived from each separate dataset. This removes the bias between the stations and  
 206 the zones. At 1 hPa, Arosa/Davos appears to display the most variation (largest peaks and dips) in the anomalies.  
 207 Since the anomaly for each site is now based on the seasonality of each site's data the structure in the anomalies is  
 208 more uniform. For example, now at 16 hPa, the difference between Boulder and the two sites Arosa/Davos and OHP  
 209 in the latter half of the year is removed. In 2012, where the Boulder anomaly was positive with respect to the zonal  
 210 average seasonal value, and the Arosa/Davos and OHP sets were negative with respect to the zonal seasonal average,  
 211 all are now of the same sign with respect to their own seasonal averages. Nonetheless, there are events where one  
 212 station shows opposite anomalies to the other two, for example early 2009 at 41 hPa, when the Boulder anomaly is  
 213 negative, and Arosa/Davos and OHP are positive. Thus, it is noted that when comparing daily or monthly data values  
 214 from GB and satellite data, the overpass data will reveal a different structure than the zonal data. The trend calculations  
 215 in this paper are based on the datasets of Fig. 2, where the seasonal behavior is removed using the station seasonality.  
 216





217  
 218 **Figure 2. Monthly ozone anomaly relative to the monthly climatology for each station overpass dataset. This process leaves**  
 219 **intact the trend for each site and the zone, and shows the consistency among the stations when each station climatology is**  
 220 **removed. This dataset is used for the trends calculations. Evident at 4 hPa is a positive trend from 2002 to 2013, then a**  
 221 **levelling out after. Trends are run on this dataset.**

222 The COH overpass and zonal datasets have a similar vertical granularity as the Umkehr dataset, but use somewhat  
 223 different pressures for the demarcation of the top and bottom of each layer. Since no additional smoothing is required,  
 224 we simply use interpolation and integration to convert the COH layer profiles to the Umkehr layers. We exclude layers  
 225 1 to 4 since there is little sensitivity in SBUV and OMPS NP in these layers (Kramarova et al., 2013b). The overpass  
 226 monthly-mean dataset in this study uses all COH data matched to dates when Umkehr data also exists. This dataset is  
 227 publicly available at [https://gml.noaa.gov/aftp/ozwv/Publications/2023\\_Umkehr\\_Ozone\\_Trends\\_Paper/](https://gml.noaa.gov/aftp/ozwv/Publications/2023_Umkehr_Ozone_Trends_Paper/). Appendix  
 228 D explores the impact of temporal sampling on trends.

229 This study also uses a specialized zonal monthly-mean COH product which is the average of all daily profiles with an  
 230 Umkehr match at the associated GB station. Zones used for most stations are the 5° wide zone which includes the  
 231 geographic station latitude (Arosa/Davies: 47.5° N, OHP: 42.5° N, MLO: 17.5° N). Boulder and Lauder, however,  
 232 are located directly on the border of two zones, so the zonal product in this study is the mathematical average of the  
 233 two adjacent zones (Boulder: 37.5° N and 42.5° N, Lauder 42.5° S and 47.5° S).

## 234 3 Methods

### 235 3.1 LOTUS Model overview - the Reference Model

236 The Long-term Ozone Trends and Uncertainties in the Stratosphere (LOTUS) activity is a project of SPARC  
237 (Stratosphere-Troposphere Processes and their Role in Climate) and has produced a statistical Multiple Linear  
238 Regression (MLR) model called the LOTUS model (<https://usask-arg.github.io/lotus-regression/index.html>).

239 The 2019 LOTUS report (SPARC/IO3C/GAW, 2019) and update (Godin-Beekmann et al., 2022) have quantified  
240 stratospheric ozone trends and evaluated their uncertainties. The LOTUS model is a general-least-squares approach  
241 MLR model. This study uses version 1 (v 0.8.0) with the independent linear trends (ILT) configuration. The  
242 independent linear terms represent the ozone depletion period (pre-1997), the ozone recovery period (post-2000) and  
243 an optional gap period (1997–2000). We will call the terms “pre”, “post” and “gap” for short. The version 0.8.0 adds  
244 an option to enforce continuity across the gap period which is used in this study. The regression uses an interactive  
245 procedure (Cochrane and Orcutt, 1949) and the autocorrelation coefficient is adjusted with each iteration. The  
246 covariance matrix is modified accordingly to account for measurement gaps (Savin and White, 1978).

247 The LOTUS model (further referred as reference model in this study) is written here:

$$248 \hat{y}(t, z) = \beta_0(t, z)C_{pre}(t) + \beta_1(t, z)C_{post}(t) + \beta_2(t, z)Linear_{pre}(t) + \beta_3(t, z)Linear_{post}(t) + \sum_{i=4}^n \beta_i X_i(t, z) + \varepsilon(t, z) \quad (1)$$

249 where  $\hat{y}(t, z)$  is the estimated ozone at time  $t$  and altitude  $z$ ;  $\beta$  are the fitted coefficients of the model; the residual  
250 term,  $\varepsilon(t, z)$  is the difference between the LOTUS model and the input data.  $C_{pre}$  and  $C_{post}$  are the constant terms as  
251 defined by:

$$252 Constant_{pre} = \begin{cases} 1 & \text{for } t < 1997 - Jan \\ 1 - mt & \text{for } 1997 - Jan \leq t < 2000 - Jan \\ 0 & \text{for } t \geq 2000 - Jan \end{cases}$$

$$253 Constant_{post} = \begin{cases} 0 & \text{for } t < 1997 - Jan \\ mt & \text{for } 1997 - Jan \leq t < 2000 - Jan \\ 1 & \text{for } t \geq 2000 - Jan \end{cases}$$

254 where  $m=0.029135$  and  $t$  = month starting in January 1980 and ending in December 2020. Indeed, the constant terms  
255 are only constant in the “pre” and “post” periods. The 3-year “gap” period is represented by a line of slope  $m$   
256 connecting the two constant (pre and post period bias) terms.

257 The linear terms of the model are defined as:

$$258 linear_{pre} = \begin{cases} mt - b & \text{for } t < 1997 - Jan \\ 0 & \text{for } t \geq 1997 - Jan \end{cases}$$

$$259 linear_{post} = \begin{cases} 0 & \text{for } t < 2000 - Jan \\ mt & \text{for } t \geq 2000 - Jan \end{cases}$$

260 where  $m=0.008487$ ,  $b = -1.700240$ , and  $t$  = month starting in January 1980 and ending in December 2020.

261 Natural variability is a complicating factor in deriving trends associated with the changes in the ozone depleting  
262 chemistry. LOTUS fits predictor variables as proxies for natural variability to the ozone data so that one can interpret  
263 the resulting linear trend as a trend due to the changes in chemistry. The summation term is the summation of the  
264 predictors used as a proxy for the dynamical induced ozone variability.

265 The natural variability proxies in the LOTUS model v 0.8.0 are Aerosol Optical Depth (AOD), El Niño/ Southern  
266 Oscillation (ENSO), and the Quasi-Biennial Oscillation (QBO) in the form of the first two principal components (also  
267 known as an empirical orthogonal function analysis). The data sources for each are described in Table 3.

268 Large sulfur dioxide (SO<sub>2</sub>) levels reaching the lower stratosphere following major volcanic eruptions (i.e. El Chichon,  
269 Pinatubo or Hunga) can impact the validity of ozonesonde measured values (Yoon et al., 2022). However, SO<sub>2</sub> is not  
270 long-lived gas and is soon converted to sulphate aerosols that can alter observations by ozone remote sensing systems.  
271 Both Umkehr and satellite ozone profiles from SBUV and OMPS are highly uncertain and/or biased because of high  
272 aerosol load during volcanic eruptions (DeLuisi et al, 1989; Petropavlovskikh et al., 2005, 2022; Bhartia et al, 1993,  
273 Torres et al., 1995, Bhartia et al, 2013). It is recommended that the data for 2 to 3 years after the El-Chichon and  
274 Pinatubo large volcanic eruptions should not be used in trend analyses. Therefore, we exclude data during the volcanic  
275 periods (1982–1983 and 1991–1993) from the analyzed time series. Moreover, this study is focused on the linear trend  
276 analyses after 2000 when there are no large stratospheric aerosol perturbations that significantly influence  
277 stratospheric ozone variability over the middle latitudes and therefore impact trend and uncertainty estimates. Since  
278 we have eliminated the data during the volcanic period, this study does not include the AOD proxy in the calculations.  
279 We define the ‘reference’ model (RM) as the proxies most commonly used for the dynamical proxies which is  
280 equivalent to the LOTUS model v 0.8.0 minus the AOD term. The representative equation is:

$$281 \sum_{i=4}^n \beta_i(t, z) X_i(t) = \beta_4(t, z) QBO_A(t) + \beta_5(t, z) QBO_B(t) + \beta_6(t, z) ENSO(t) + \beta_7(t, z) Solar(t) \quad (2)$$

282 The Quasi-biennial Oscillation (QBO) is derived from the Singapore radiosonde profiles (1979–2020) that detect  
283 variability in the direction of the tropical winds in the lower stratosphere. It also shows that zonal wind variation  
284 propagates downward with an average period of ~28 months [Wallace, 1973]. The principal component analysis of  
285 the 100–10 hPa zonal winds can describe the majority of the wind variability. The reference model (and LOTUS v  
286 0.8.0) use the two leading modes of the calculated empirical orthogonal functions (EOF) for trend analyses [Wallace  
287 et al., 1993].

288 The El Niño/ Southern Oscillation (ENSO) is a periodic mode of climate variability of the atmosphere and sea surface  
289 temperatures associated with the equatorial Pacific Ocean with periods ranging from 2–8 years. The Multivariate  
290 ENSO index (MEI) is produced by the NOAA Physical Sciences Laboratory and is derived from the EOF analysis of  
291 sea surface temperature, sea level pressure, outgoing terrestrial radiation, and surface winds in the area of the Pacific  
292 basin from 30° S to 30° N and from 100° E to 70° W (Wolter and Timlin, 2011). Temperature anomalies in the  
293 troposphere with corresponding stratospheric temperature anomalies during El Niño/ La Niña events modulate the  
294 tropical upwelling of the Brewer-Dobson circulation (BDC) and thus the meridional transport of ozone in the  
295 stratosphere. (Diallo et al., 2018).

296 The solar cycle is the 11-year periodic cycle of solar activity and solar irradiance that reaches the Earth’s atmosphere.  
297 The change in UV radiation that is absorbed by the atmosphere, most notably in the upper stratosphere, leads to  
298 changes in atmospheric temperature and the photochemistry which produces ozone. (Lee and Smith, 2003). The 10.7  
299 cm solar radio flux data is used as the proxy for the solar cycle in the LOTUS model.

300 Seasonal components in the form of Fourier harmonics were added into the LOTUS model with version 0.8.0. Godin-  
301 Beekman et al. (2022) showed in their Fig. 7 that the model fit for the ozone profile satellite and model records is

302 improved by adding seasonal components to the proxies, increasing the adjusted R-squared ( $R^2$ ) from 0.3 or less to  
 303 0.3 to 0.5. The seasonality and relevant contributions of some predictor's variables are compensated in this study by  
 304 adding the seasonal components to the fitted predictors. Seasonal components are represented in the model by sine  
 305 and cosine functions with periods of 12 and 6 months that describe the variability of the proxies on these timescales.  
 306 So, for each fitted predictor in the model

307  $\beta_i(t, z)X(t)$  where  $i > 1$

308 a seasonal variation in the form of Fourier components is added as follows:

309 
$$\beta_m(t, z) = \beta_{m,0}(z) + \sum_{i=1}^2 \beta_{m,1,i}(z) \sin\left(\frac{2\pi it}{12}\right) + \sum_{i=1}^2 \beta_{m,2,i}(z) \cos\left(\frac{2\pi it}{12}\right)$$

### 310 **3.2 The Extended Model - Adding Predictors**

311 Recent publications (i.e. Petropavlovskikh et al., 2019; Szlag et al., 2020; Godin-Beekmann et al, 2022; Millan et al.  
 312 2024) highlight the need to reduce the trend uncertainties in the lower stratosphere (LS). There is still a discrepancy  
 313 between modeled and observed ozone trends in the LS but large uncertainties make comparisons difficult. In this  
 314 study, we test additional predictors in the model to account for dynamical variability of ozone in the stratosphere, thus  
 315 improving the model performance and reducing the uncertainty of the trends. The argument for additional predictors  
 316 is that the LOTUS model was developed for the regression of zonally averaged ozone data, which reduces some  
 317 variability that might be impacting the ground-based records on regional bases. Impact of additional proxies in trend  
 318 analyses were reported in other publications (Weber et al, 2022a, Bernet, 2023 and references therein), and were  
 319 mostly found to improve the statistical model fit at high latitudes where the impact of the descending branch of the  
 320 Brewer-Dobson circulation and Arctic/Antarctic oscillations has contributed to additional variability in stratospheric  
 321 ozone records.

322 In what we define as the 'extended' model, we add single additional predictors (one at a time) in the model as such:

323 
$$\sum_{i=4}^n \beta_i(t, z)X_i(t) = \beta_4(t, z)QBO_A(t) + \beta_5(t, z)QBO_B(t) + \beta_6(t, z)ENSO(t) + \beta_7(t, z)Solar(t) + \beta_8(t, z)X_{predictor}(t)$$

324 The fitted predictors contain Fourier components, like in the reference model, to allow for seasonal variation.

325 We test the following additional predictors as described below to assess the impact on trends and uncertainties:

- 326 • Quasi-Biennial Oscillation (QBO): Two notable disruptions to the otherwise relatively periodic QBO have  
 327 occurred during the study period: 2015–2016 and in 2020 (Diallo, et. al 2022). Two additional leading modes  
 328 of the calculated empirical orthogonal functions (EOF) are tested to improve the trend model fit during the  
 329 anomalous QBO years.
- 330 • Arctic/Antarctic Oscillation (AO/AAO): the pattern of surface air pressure anomalies in the polar region and  
 331 certain mid-latitude regions. The AO/AAO has strong correlations (Lawrence et al 2020) with stratospheric  
 332 ozone through the strength of the polar vortex. The positive phase of the AO or AAO in the winter months  
 333 is associated with low activity in the vertically propagating planetary Rossby waves, a strong polar vortex, a  
 334 low vortex wavenumber, and low stratospheric temperatures. Thus, the positive (negative) phase of the  
 335 AO/AAO is correlated to low (high) ozone anomalies especially in the winter months (Lawrence et al, 2020).

- 336 • North Atlantic Oscillation (NAO): Similar to the Arctic Oscillation, this is a pattern of surface air pressure  
337 anomalies between certain regions in the high altitudes of the North Atlantic Ocean. This index is calculated  
338 by the pressure difference between the Azores high and the subpolar low.
- 339 • Eddy Heat Flux (EHF): The flux of heat through a zonal plane by transport due to the Brewer-Dobson  
340 circulation, here averaged from 45–75° N/S (use EHF S for Lauder only). This represents the planetary wave  
341 activity that drives transport of ozone.
- 342 • Tropopause Pressure (TP): Pressure level of boundary between the troposphere and the stratosphere. In this  
343 study, we use the monthly mean pressure level of the tropopause from the NOAA National Centers for  
344 Environmental Prediction (NCEP) reanalysis product. As the troposphere warms due to release of GHGs  
345 and the stratosphere cools due to ODSs destroying stratospheric ozone, the tropopause is rising (Meng et al.,  
346 2021). Thompson et al, (2021) and Stauffer et al., (2023) found that the lower stratospheric ozone trends in  
347 tropics become slightly positive when recomputed with respect to the tropopause height (which has its own  
348 trend). This finding indicates that ozone depletion in the lower stratosphere (i.e. Ball et al., 2020) is driven  
349 by climate-change-related changes in transport and mixing in the lower stratosphere. Therefore, we are  
350 testing the TP proxy in the model to account for non-chemical ozone losses in order to assess chemical  
351 attribution of ozone trends.
- 352 • Equivalent Latitude (EqLat): Geographical latitude of the isoline encircling the area of equal Potential  
353 Vorticity (PV) (Lary et al, 1995). The EqLat normalizes the range of PV values that change with season and  
354 interannually and makes it convenient for interpretation of ozone variability and trends (i.e. Wohltmann et al  
355 2005). The dataset was generated from GMI CTM analyses (private communications with Susan Strahan,  
356 June 2021) for each ground-based station overpass criteria (latitude and longitude envelope, see above) and  
357 at several altitude levels coincident with Umkehr ozone profile layers. Appendix C discusses a COH dataset  
358 based on EqLat instead of geometric latitude. No advantage was found by using the EqLat coordinate system  
359 for the COH zonal dataset.

360 Source datasets for all predictors in the reference and extended models are shown in Table 3.

361 **Table 3: List of predictors either previously used (bolded) in the LOTUS 0.8.0 (reference) model and additional predictors**  
362 **evaluated in this study for a future use in the extended LOTUS trend regression model. Note, two components of the QBO**  
363 **predictors were used in the reference model (i.e. Godin-Beekmann et al., 2022). We added two more components in the**  
364 **extended model for tests described in this paper.**

Predictor	Description	Source
<b>ENSO</b>	<b>El Nino/Southern Oscillation</b>	<b>Monthly Mean Multivariate ENSO Index</b> <a href="https://psl.noaa.gov/enso/mei.old/">https://psl.noaa.gov/enso/mei.old/</a> <sup>1</sup>

Solar	Solar 10.7cm flux	<a href="https://spaceweather.gc.ca/forecast-prevision/solar-solaire/solarflux/sx-5-en.php">https://spaceweather.gc.ca/forecast-prevision/solar-solaire/solarflux/sx-5-en.php</a>
QBO	Quasi-Biennial Oscillation	Principal Component Analysis of the Monthly Mean Zonal Wind <a href="https://www.geo.fu-berlin.de/met/ag/strat/produkte/qbo/qbo.dat">https://www.geo.fu-berlin.de/met/ag/strat/produkte/qbo/qbo.dat</a>
AOD	AOD is included in the LOTUS model, but not used in this study	
AO	Arctic Oscillation, Monthly Mean index	<a href="http://www.cpc.ncep.noaa.gov/products/precip/CWlink/daily_ao_index/monthly_ao_index.b50.current.ascii">http://www.cpc.ncep.noaa.gov/products/precip/CWlink/daily_ao_index/monthly_ao_index.b50.current.ascii</a>
AAO	Antarctic Oscillation, Monthly Mean index	<a href="https://www.cpc.ncep.noaa.gov/products/precip/CWlink/daily_ao_index/ao/aao.shtml">https://www.cpc.ncep.noaa.gov/products/precip/CWlink/daily_ao_index/ao/aao.shtml</a>
NAO	The North Atlantic Oscillation, monthly mean index	<a href="https://www.cpc.ncep.noaa.gov/products/precip/CWlink/pna/norm.nao.monthly.b5001.current.ascii.table">https://www.cpc.ncep.noaa.gov/products/precip/CWlink/pna/norm.nao.monthly.b5001.current.ascii.table</a>
EHF	Eddy Heat Flux	Cumulative Mean (from September to April) of Heat Flux at 100 hPa from MERRA2 reanalysis averaged over 45–75° N (45–75° S for Lauder), deseasonalized. It is kept constant from April to Sep. <a href="https://acd-ext.gsfc.nasa.gov/Data_services/met/ann_data.html">https://acd-ext.gsfc.nasa.gov/Data_services/met/ann_data.html</a>
TP	Tropopause Pressure	Monthly Mean NCEP-NCAR reanalysis (Kalnay et al., 1996); Tropopause pressure at the lat/lon of each station, deseasonalized.  <a href="ftp://ftp.cdc.noaa.gov/Datasets/ncep.reanalysis.derived/tropopause/pres.trop.mon.mean.nc">ftp://ftp.cdc.noaa.gov/Datasets/ncep.reanalysis.derived/tropopause/pres.trop.mon.mean.nc</a>
EqLat	Equivalent Latitude	Monthly Mean equivalent latitude derived from MERRA2 -GMI CTM potential vorticity (PV) contours on 31 potential temperature surfaces

		[Susan Strahan, private communication, 8/24/2022]. The PV at each station is determined by a 1/distance weighted average of the values in a $\pm 2^\circ$ latitude, $\pm 2^\circ$ longitude grid, then converted to EqLat on the Umkehr layers.
--	--	---

365 <sup>1</sup> Since the incorporation of the ENSO index into the LOTUS model, NOAA GSL has updated the index to v1.2.  
 366 <https://psl.noaa.gov/enso/mei/>. However, for consistency with results from the Godin-Beekmann (2022) paper we use the  
 367 old MEI index that is part of the LOTUS v 0.8.0 package.

368 All proxies are used as is. No de-trending (removal of the long-term trend in proxy) is applied to the proxies. Therefore,  
 369 we interpret any changes to the trends derived with additional proxies as approximations of trends driven by chemistry  
 370 and transport related to climate change. These are rough approximations as some feedbacks are known to impact  
 371 chemistry (e.g. changes in stratospheric temperature).

### 372 3.3 The Full Model - Combining Additional Predictors

373 After we have determined the impact of the additional predictors singly, we discern which predictors should be  
 374 combined to constitute the 'Full Model'. Prior to selecting additional predictors for the 'Full Model', we perform  
 375 correlation tests to identify any cross correlations between predictors. We select predictors that are not highly  
 376 correlated (less than +/- 0.2) to ensure that all predictors are largely independent. We use the square of the Pearson  
 377 correlation coefficient  $R^2$  for each pair of the predictors to test our assumptions. We find that ENSO, Solar, QBO  
 378 (1,2,3,4), AAO, AO, EHF (N and S), and TP (at each station) have correlations less than +/- 0.2 (with the exception  
 379 of  $R^2 = 0.3$  for EHF (N) and AO). Therefore, any of these predictors can be combined in the 'Full Model'. We find  
 380 that NAO has a correlation of .38 with AO so we do not use these two predictors in the same model.

381 We also test the independence of EqLat proxies calculated at several geographic locations (defined by the latitude and  
 382 longitude of each Umkehr station) and by selecting a proxy at several altitude levels centered in the middle of Umkehr  
 383 layers 3–9. We find that the  $R^2$  between the TP and EqLat in the lower stratosphere (Umkehr layer 3) can be large but  
 384 anticorrelated -0.7 (Boulder), moderate 0.4 (MLO and Lauder), while close to zero at Arosa/Davos and low at OHP  
 385 (-0.2). In the middle and upper stratosphere, the  $R^2$  varies from -0.5 to -0.4 (MLO), 0.2 to 0.3 (Arosa/Davos and OHP),  
 386 0.5 to 0.6 (Boulder), and 0.4 to 0.7 (Lauder). EqLat has mostly low correlations ( $< \pm 0.3$ ) with all other proxies except  
 387 for higher correlations with QBO B in layers 5 (-0.3) and 6 (-0.4), and QBO A in layer 7 (0.3) at MLO; and with AO  
 388 in layer 8 (0.3) at OHP and Arosa/Davos. Also, EqLat has no correlation with the TP proxy in layer 4 in Boulder, in  
 389 layer 9 at Lauder, and in layers 8 and 9 at OHP. Since there are occasional high correlations between EqLat and TP  
 390 proxies, we do not use them together in the 'Full trend Model'.

## 391 4 Results

### 392 4.1 Reference Model Trend Results

393 First, we discuss the reference model trends derived from the COH overpass, Umkehr and ozonesonde records at 5  
 394 geographic locations. All datasets are deseasonalized with a climatology computed from a subset of data taken from  
 395 1998–2008 prior to the trend analysis. Trend results are presented in Fig. 3 and organized in 5 panels. Each panel

396 shows trends at selected pressure/altitude levels detected from Umkehr (green), COH (orange) and ozonesonde (blue)  
397 records at Arosa/Davos, OHP, Boulder, MLO/Hilo and Lauder ground-based stations. Ozonesonde data for the  
398 Arosa/Davos panel are selected from Hohenpeißenberg, Germany station that is in close vicinity to Arosa/Davos  
399 station. We show trends for layers where the measurement is of highest quality: Umkehr (layer 3 through 8), COH  
400 (layers 5 through 9) and ozonesonde (layers 3 through 5) records.

401 The Umkehr data used in this analysis is the monthly mean of all available Umkehr data (one or two measurements  
402 per day). The sonde and COH monthly means use only those profiles that have corresponding Umkehr measurements  
403 on that date. We explore the impact of temporal sampling on trends in Appendix D. For COH with the Umkehr  
404 matched data (see Figure A12), trends are slightly larger at OHP but well within the error bars. At all other stations  
405 the COH trends are not impacted by sampling. At OHP the ozonesonde trends matched to Umkehr (see Figure A13)  
406 are slightly larger at layer 4 only and well within the error bars; while at Lauder in layers 4 and 5 trends are smaller,  
407 but barely within the error bars.

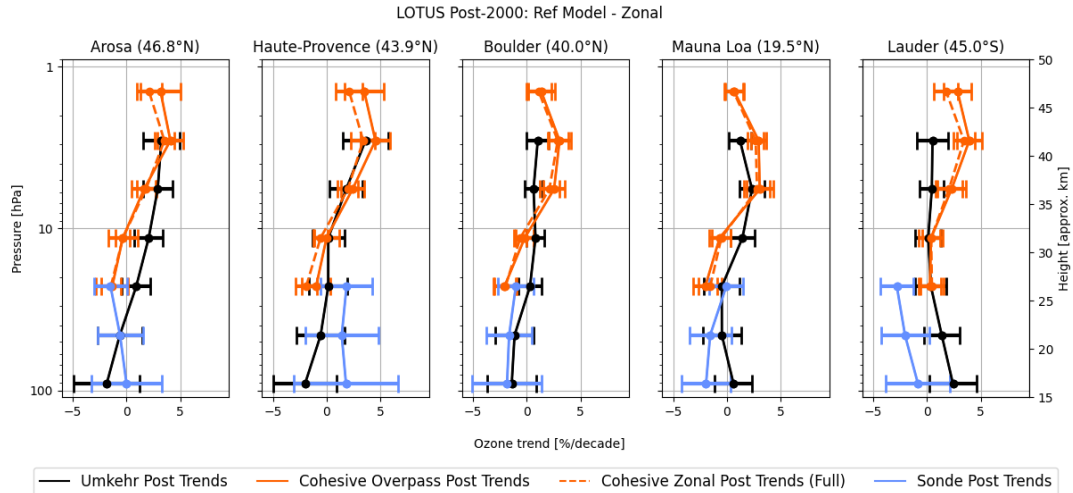
408 Figure 3 shows that in the upper (above 10 hPa) stratosphere, Umkehr (black) and COH (orange) trends are positive  
409 and agree within the error bars ( $\pm 2$  standard errors). The exception is found at 8–2 hPa pressure level over the Lauder  
410 station, where Umkehr trends are near zero and COH trends are  $\sim +3$ – $4$  %/decade. The error bars show  $\pm 2$  standard  
411 errors, and the fact that they do not overlap suggests that the differences in trends are statistically significant. This  
412 could be related to the relatively large uncertainties in the instrumental corrections applied to homogenize the Umkehr  
413 record (Petropavlovskikh et al, 2022). Björklund (2023) discusses relative drifts in Umkehr, ozonesonde, FTIR and  
414 MW ozone records over Lauder. The authors are not able to identify instrumental artifacts that may have caused the  
415 discrepancies in the co-located records, but point out that it is not related to the sampling biases.

416 In the middle stratosphere (60–10 hPa) agreement between Umkehr and COH is within uncertainty of the trend except  
417 at Arosa/Davos where COH trends are statistically different from Umkehr trends at 16–8 hPa. COH trends at 32–16  
418 hPa are mostly negative ( $-2$ – $3$  %/decade) with the exception of Lauder where trends are near zero and similar to  
419 Umkehr trends. Umkehr trends between 32–16 hPa are close to zero. The ozonesonde trends (blue) agree with COH  
420 (orange) and Umkehr (black) trends in layer 32–16 hPa at Arosa/Davos, Boulder and MLO. However, at OHP  
421 (Lauder) the ozonesonde trends are found to be positive at  $+2 \pm 2.2$  %/decade (negative at  $-3 \pm 1.5$  %/decade) and  
422 significantly different from the near-zero trends seen in the COH and Umkehr results.

423 In the lower stratosphere (125–63 hPa), Umkehr trends vary between small positive ( $+1$ – $2$  %/decade at Hilo and  
424 Lauder) and negative ( $-2$ – $3$  %/decade at Arosa/Davos, OHP and Boulder); however, trend uncertainties are the largest  
425 (2 standard errors are 2–3 %/decade, see Table 4 below) in comparison to the middle and upper stratospheric trends.  
426 Ozonesonde trends at OHP station are positive ( $+2$  %/decade), and negative over Lauder ( $-2$  %/decade). They also  
427 feature large uncertainties ( $\pm 4.2$  %/decade at OHP) that are larger than the uncertainties found in Umkehr trends which  
428 could be caused by the limited sampling (see Appendix D, Figure A11). Sonde trends at Hilo show negative trend  
429 values with large uncertainties. But the data in this study at Hilo is not corrected for the ozonesonde drop off after  
430 2014 known to occur at this station (Stauffer, 2022), so the deviation from the Umkehr results at these levels may be  
431 misleading.



432 Figure 3 also shows trends derived from the zonal-mean COH data associated with each station (orange dashed line).  
 433 These are shown for comparison with the overpass COH data (solid line) to study the impact of the spatial sampling  
 434 biases on the trends. Though Figs. 1 and 2 show clear interannual differences between the records from the individual  
 435 stations, and the associated zonal average, we find very small differences in trends (mostly in the upper stratosphere  
 436 at middle latitude stations). Therefore, the station overpass sampling provides trends that are representative of the  
 437 zonal averaged trends (Zerefos, 2018) and the discrepancies in trends between GB and satellite records do not strongly  
 438 depend on the spatial sampling differences.



439  
 440 **Figure 3:** The 2000–2020 ozone trends are shown at 7 altitude/pressure levels. The LOTUS model v 0.8.0 is used for trend  
 441 analyses. Umkehr trends (black), COH (orange) and ozonesonde (blue) are shown for 5 ground-based stations:  
 442 Arosa/Davos, OHP, Boulder, MLO and Lauder (panels left to right). Ozonesonde data for the Arosa/Davos panel are  
 443 selected from Hohenpeißenberg, Germany that is in close vicinity to Arosa/Davos. Trends from the zonal-mean COH data  
 444 (orange dashed line) are shown for comparison with the overpass COH data (solid line). The error bars indicate  $\pm 2$  standard  
 445 errors.

446 **4.2 Standard Error of Reference Model**

447 **Table 4:** Standard Error (SE) for the Reference model 2000–2020 trend for five ground-based station locations  
 448 (Arosa/Davos, OHP, Boulder, MLO and Lauder). Results are provided for trend analyses of the Cohesive satellite (COH),  
 449 Dobson Umkehr (UMK) and ozonesonde (SND) records and for Umkehr. The layers are selected to represent the best  
 450 quality of data. Values of SE shown are the actual errors in DU/decade.

LOTUS Model Proxy Tests: Standard Error for Reference Model																
Height	Umkehr	Arosa/Davos			OHP			Boulder			MLO			Lauder		
(hPa)	Layer	UMK	COH	SND	UMK	COH	SND	UMK	COH	SND	UMK	COH	SND	UMK	COH	SND
1-2	9		0.92			0.91			0.62			0.43			0.63	
2-4	8	0.85	0.59		1.06	0.68		0.51	0.52		0.52	0.37		0.72	0.57	
4-8	7	0.69	0.59		0.77	0.54		0.41	0.52		0.58	0.62		0.57	0.66	
8-16	6	0.66	0.68		0.75	0.59		0.42	0.43		0.55	0.49		0.61	0.56	
16-32	5	0.66	0.75	0.76	0.89	0.68	1.10	0.54	0.51	0.77	0.82	0.55	0.75	0.73	0.54	0.73
32-63	4	1.05		1.04	1.13		1.55	0.90		1.04	0.90		0.94	0.83		1.16

63-127	3	1.55		1.60	0.15		2.10	1.15		1.63	0.87		1.07	1.11		1.50
--------	---	------	--	------	------	--	------	------	--	------	------	--	------	------	--	------

451  
452 We will use the standard error of the linear (trend) term in Equation 1 to evaluate the success of the additional proxies  
453 to improve understanding of trend values. The standard error is an output of the regression code, and indicates the  
454 uncertainty in the trend value. Smaller Standard Errors indicate increased confidence in the trend result. We use the  
455 standard error as a metric instead of standard deviation to reduce dependence on the number of points in the trends  
456 model. The **Table 4** provides the Standard Errors for the Reference Model fit and represents uncertainty of the trend  
457 in DU of the mean ozone in each layer at the station. The standard errors of the trend detected in three co-located  
458 ozone records at each station (or in the nearby location as in case of Arosa/Davos or MLO comparisons) do not  
459 significantly differ, although in general ozonesonde errors are slightly larger than Umkehr errors most likely due to  
460 the larger sampling errors in ozonesonde monthly mean record. Also, the errors in trends detected in COH layers 5–8  
461 are on average smaller than for Umkehr trends (with the exception of layer 7 at Boulder, MLO and Lauder) which  
462 could be explained by an overpass method that averages several satellite profiles from adjacent orbits and therefore  
463 reduces meteorological scale variability in averaged ozone data.

#### 464 **4.3 Adjusted R<sup>2</sup>**

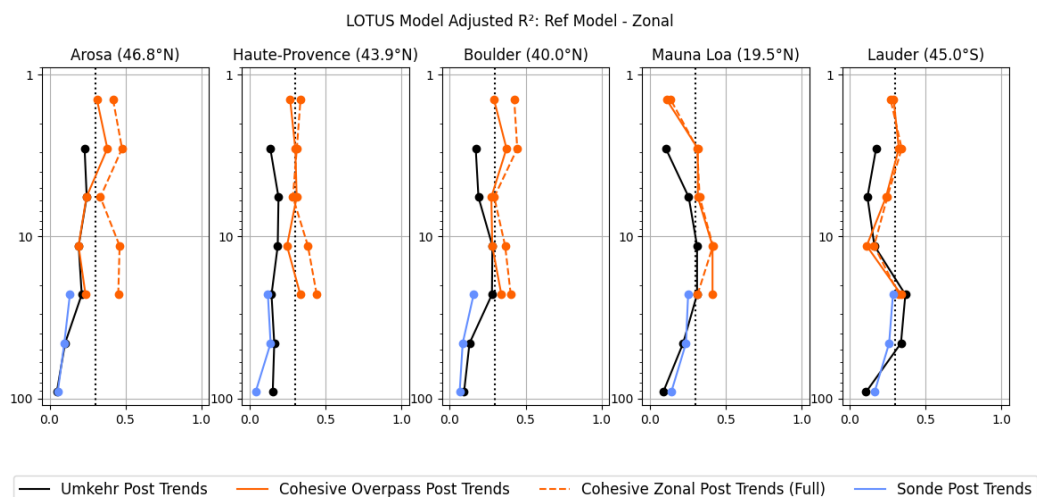
465 The adjusted R<sup>2</sup> values of the 2000–2020 trends are shown in Fig. 4 and Table 5 for the data fit using the Reference  
466 model. The adjusted R<sup>2</sup> is a modified version of R<sup>2</sup> that adjusts for the number of predictors in a regression model and  
467 represents the ‘goodness’ of the model fit to the data. For COH adjusted R<sup>2</sup> is shown for both the overpass and the  
468 zonal datasets.

469 Though values are significantly less than the high values usually seen when comparing data that includes the prevalent  
470 seasonal variation, the adjusted R<sup>2</sup> values for the COH zonal mean record are similar in magnitude and vertical shape  
471 to the results of the (60°S–60°N) broadband trend analyses published in Godin-Beekmann (2022), Fig. 7 varying  
472 between 0.1 and 0.5. We designate the average values (0.3) as a threshold for satisfactory fit indicating conformance  
473 with prior LOTUS results. We indicate in bold in Table 5 adjusted R<sup>2</sup> values of 0.3 or greater to note achievement of  
474 that threshold and include vertical dashed line in Fig. 4 for reference.

475 The adjusted R<sup>2</sup> for the Reference model fit is slightly better for the zonal mean COH data than for the COH overpass  
476 over the Northern middle latitude stations. This is expected as much of the variability of the time series is reduced in  
477 the zonal average as compared to the station overpass data as shown in Fig. 2, and more easily explained by the  
478 typically used predictors. Indeed, the goal of this study is to determine if the additional predictors help to explain the  
479 additional variation as measured at point locations.

480 The model fit to the GB data is similar to the COH overpass results in the middle stratosphere (layers 5 and 6), but the  
481 model explains less ozone variability in the Umkehr records in the upper stratosphere (layers 7 and 8). In the lower  
482 stratosphere (layers 3, 4 and 5), the model fit to the ozonesonde and Umkehr records is similar with the exception of  
483 Lauder (Umkehr has larger adjusted R<sup>2</sup> in layers 4 and 5). The adjusted R<sup>2</sup> for COH overpass in layer 5 is similar to  
484 Umkehr and sonde with a larger difference at OHP. The adjusted R<sup>2</sup> in the lower stratosphere is less than in the middle  
485 stratosphere, which points to other processes (e.g., transport) that drive ozone variability. In this paper we investigate

486 improvement to the trend model fit by introducing additional proxies that can improve representation of the  
 487 dynamically-driven ozone variability in the stratosphere.



488  
 489 **Figure 4: The adjusted  $R^2$  is plotted as a function of altitude/pressure for the LOTUS model fit to the Umkehr (black),**  
 490 **ozonesonde (blue), COH overpass (orange, solid), and COH zonal-mean (orange, dashed). Results are shown in 5 panels**  
 491 **that represent trend analyses of ozone records over Arosa/Davos (Hohenpeißenberg for sondes), OHP, Boulder, MLO (Hilo**  
 492 **for sondes) and Lauder ground-based stations.**

493 **Table 5: Similar to Table 4, but for the adjusted  $R^2$ . Values of 0.30 and above are indicated in Bold as a threshold to**  
 494 **indicate a satisfactory fit**

LOTUS Model Proxy Tests: Adjusted R2 for Reference Model																
Height	Umkehr	Arosa/Davos			OHP			Boulder			MLO			Lauder		
(hPa)	Layer	UMK	COH	SND	UMK	COH	SND	UMK	COH	SND	UMK	COH	SND	UMK	COH	SND
1-2	9		<b>0.31</b>			0.27			0.29			0.11			0.29	
2-4	8	0.23	<b>0.38</b>		0.14	<b>0.30</b>		0.17	<b>0.37</b>		0.11	<b>0.32</b>		0.17	<b>0.32</b>	
4-8	7	0.25	0.25		0.19	<b>0.31</b>		0.19	0.27		0.26	<b>0.32</b>		0.12	0.24	
8-16	6	0.19	0.19		0.19	0.25		0.28	0.28		<b>0.31</b>	<b>0.41</b>		0.16	0.11	
16-32	5	0.21	0.24	0.13	0.14	<b>0.33</b>	0.14	0.28	<b>0.34</b>	0.16	<b>0.31</b>	<b>0.41</b>	0.25	<b>0.37</b>	<b>0.34</b>	0.26
32-63	4	0.10		0.10	0.16		0.24	0.13		0.09	0.22		0.24	<b>0.34</b>		0.20
63-127	3	0.05		0.05	0.15		0.25	0.09		0.02	0.09		0.14	0.11		0.10

495 .

496 **4.4 Reference Model P-Values:**

497 The p-values are often used to evaluate statistical significance of predicted results and results labelled “significant” if  
 498 they remain below a threshold of 0.05. However, Chang et al. (2021) argued as Wasserstein et al. (2019) does that all  
 499 trends should be reported with their associated p-values and a thorough discussion of the certainty of trend detection  
 500 as described by the p-values. Therefore, the p-values can be used for understanding the certainty of the trend. Under  
 501 the IGAC TOAR activity, p-values are scored to define a consistent scale for comparison of the trends between  
 502 different analyses (see Table 3, Chang et al., 2023).

503 **Table 6: Similar to Table 4 but for p-values. Values of less than 0.05 (high certainty of trend detection) are shown in blue**  
 504 **and with bolded numbers. Values between .05 and 0.1 (blue, not bolded) indicate medium certainty, between 0.1 and 0.33**  
 505 **(orange) - low certainty of trend detection, and above 0.33 (red) - very low certainty or no evidence of trend detection.**

LOTUS Model Reference Model P Values																
Pressure	Umkehr	Arosa/Davos			Haute-Provence			Boulder			Mauna Loa			Lauder		
(hPa)	Layer	UMK	COH	SND	UMK	COH	SND	UMK	COH	SND	UMK	COH	SND	UMK	COH	SND
1-2	9		<b>0.00</b>			<b>0.00</b>			<b>0.03</b>			0.10			<b>0.00</b>	
2-4	8	<b>0.00</b>	<b>0.00</b>		<b>0.00</b>	<b>0.00</b>		<b>0.05</b>	<b>0.00</b>		<b>0.02</b>	<b>0.00</b>		0.47	<b>0.00</b>	
4-8	7	<b>0.00</b>	<b>0.01</b>		<b>0.02</b>	<b>0.00</b>		0.12	<b>0.00</b>		<b>0.00</b>	<b>0.00</b>		0.43	<b>0.00</b>	
8-16	6	<b>0.00</b>	0.62		0.84	0.98		0.05	0.66		<b>0.01</b>	0.17		0.85	0.50	
16-32	5	0.17	0.08	<b>0.05</b>	0.87	0.15	0.12	0.58	<b>0.00</b>	0.21	0.56	<b>0.00</b>	0.93	0.61	0.62	<b>0.00</b>
32-63	4	0.55		0.57	0.62		0.41	0.21		0.12	0.61		0.11	0.10		0.07
63-127	3	0.23		1.00	0.17		0.46	0.22		0.26	0.47		0.08	<b>0.03</b>		0.58

506 Table 6 provides p-values for the Reference Model. These are further used as a baseline for comparison to model fits  
 507 with additional predictors. P-values of the reference model fit suggest a high certainty ( $p < 0.05$ ) in detected trends in  
 508 the COH data in layers 7, 8 and 9 at almost all stations with the exception of the higher p-value (0.1, medium certainty)  
 509 found at MLO in layer 9. Also, high certainty in derived trends is reached for COH records in layer 5 at Boulder and  
 510 MLO.  
 511

512 Umkehr trend analyses also show high confidence in trend detection at Arosa/Davos and MLO stations in layers 6, 7  
 513 and 8, at OHP in layers 76 and 8, and in Boulder in layers 6 and 8. For the ozonesonde data the high confidence (i.e.  
 514 low uncertainty) is found for Hohenpeißenberg, and Boulder trends detected in layer 5, and at Lauder in layers 4 and  
 515 5.

516 The medium level of the certainty ( $0.05 < p \leq 0.10$ ) is found in trends detected in layer 5 of COH ozone time series at  
 517 Arosa/Davos, layer 3 of ozonesonde at MLO, and in layer 4 of ozonesonde and layer 3 of Umkehr at Lauder.

518 Low certainty in detected trends at p-value of 0.10 (not inclusive) to 0.33 is found in Umkehr layer 3 and 5 at  
 519 Arosa/Davos; in COH layer 5 and Umkehr layer 3 at OHP; in Umkehr layers 3 4, and ozonesonde layers at Boulder;  
 520 in ozonesonde layer 4 and COH layer 6 record at MLO.

521 Highest (lowest certainty) p-values ( $> 0.33$ ) were found in layer 6 of COH overpass records at most stations (except  
 522 for MLO where p-values are medium high). We note that the COH trends are close to zero and the uncertainty envelope  
 523 crosses the zero line. Therefore, the statistical trend model cannot separate trends from zero due to unexplained high  
 524 ozone variability in this layer. . Similarly, near-zero Umkehr trends with relatively large SE in layer 6 at OHP and  
 525 Lauder, layer 5 at all (except Arosa/Davos) stations, and in layers 3 and 4 at MLO show the same level of high p-  
 526 values thus suggesting that additional proxies should be added in the trend model to assess the impacts of the natural  
 527 variability and instrumental noise on trend uncertainty.

528 It is also important to note that the reference trend model fit to ozone in Umkehr layers 7 and 8 at Lauder has high p-  
 529 values, which is related to the near-zero trends that shows large disagreement with COH trend. This difference could  
 530 be caused by remaining instrumental step changes that were not fully removed during the record homogenization  
 531 (Petropavlovskikh et al., 2022).

532 While near-zero trends and high p-values are found in the fit of the Hilo ozonesonde record in layer 5, the p-values in  
 533 layer 4 show only medium p-values for near zero trends. It is possible that infrequent launches of ozonesonde  
 534 observations at Hilo could create the temporal sampling bias and appear noisy. The ozonesonde record at

535 Hohenpeißenberg has sufficiently frequent sampling (3 times per week) for successful trend analyses (Chang et al.,  
536 2020; Chang, 2023 preprint), but the p-values remain high in layers 3–4. The p-values for Umkehr fit at Arosa/Davos  
537 are in the medium to high range for layers 3, 4, 5, but somewhat smaller which could be due to non-zero trends in  
538 layers 3 and 5. The p-value difference could be also related to the different location of the ozonesonde (HOH) and  
539 Umkehr (Arosa/Davos) observations, thus the records could contain different atmospheric variability that might  
540 impact the model fit.  
541 We will discuss changes to the p-values in the next section after we add more proxies to the trend model in an attempt  
542 to improve confidence in trend detection.

### 543 5 Trends with the Extended Model - testing the addition of single predictors

544 The LOTUS styled Reference Model is developed and optimized for zonal average datasets. Modeling and trend  
545 analysis for GB and satellite overpass data may improve by the addition of other proxies not used in the reference  
546 model to improve capturing processes that impact ozone changes over limited geographical regions. The Extended  
547 Model tests the addition of single predictors to see if fit statistics can be improved for GB and overpass datasets. We  
548 judge success of the Extended Model by examination of the reduction in the Standard Error of the trend term, and by  
549 evaluation of the impact on the adjusted  $R^2$  of the model fit. Table 7 displays the change in the Standard Error of the  
550 post 2000 trend for each proxy tested determined as  $SE_{ref} - SE_{ext}$  as a percent of  $SE_{ref}$ . As such positive values  
551 correspond to the desired reduction of SE, and are highlighted in the table in blue. Low impact changes in the SE are  
552 highlighted in white, and increases in SE (negative values) are highlighted in red. It may seem unusual for the addition  
553 of proxies to increase the SE (negative values in the table) which indicates less confidence in the fit. But these SE are  
554 the uncertainty in the trend term, not in the overall model fit. The new proxies considered each have a possible trend  
555 and associated error budget for that trend. Whether the additional proxy increases trend uncertainty can depend on  
556 how well the trend of the new proxy can be characterized. The adjusted  $R^2$  is a better indicator of the overall model  
557 improvement. Figure 5 displays the adjusted  $R^2$  for the Extended Model for each proxy tested. Values of 0.30 and  
558 above are indicated in bold as a threshold to indicate a satisfactory fit.

559 **Table 7: Change in Standard Error (SE) of the post-2000 trend estimate, in percent of SE of Reference Model for adding**  
560 **single predictors. Panel a: Tropopause Pressure; b: Equivalent Latitude; c: QBO terms C and D; d: AO/AAO; e: NAO; f:**  
561 **Eddy Heat Flux. Cells with reduced (increased) SE have blue (red) background, while cells with low impact changes (<0.5**  
562 **%) have no colours.**

563 a)

a) LOTUS Model Test: Difference [%] in Standard Error: Tropopause Pressure vs Reference Model																
Pressure (hPa)	Umkehr Arosa/Davos			Haute-Provence			Boulder			Mauna Loa				Lauder		
	Layer	UMK	COH	SND	UMK	COH	SND	UMK	COH	SND	UMK	COH	SND	UMK	COH	SND
1-2	9		0.3			0.1			0.5			1.4			3.0	
2-4	8	-0.7	-0.5		-0.1	-0.4		-0.2	0.4		-0.6	-0.3		1.3	2.6	
4-8	7	-0.3	0.0		0.3	1.3		0.3	-0.2		2.6	0.3		3.7	1.4	
8-16	6	-1.1	-0.7		0.0	0.3		0.7	-0.2		0.6	0.8		3.1	5.4	
16-32	5	-0.2	2.1	-0.9	1.1	5.3	2.4	-0.4	0.6	0.6	4.5	9.3	2.7	0.0	0.7	2.4
32-63	4	6.6		6.1	5.9		9.9	3.4		7.5	7.0		6.1	8.0		9.4
63-127	3	12.8		10.2	12.8		10.7	6.8		6.0	5.8		4.6	9.8		7.9

564

565 b)

LOTUS Model Test: Difference [%] in Standard Error: Equivalent Latitude vs Reference Model																
Pressure	Umkehr	Arosa/Davos			Haute-Provence			Boulder			Mauna Loa			Lauder		
(hPa)	Layer	UMK	COH	SND	UMK	COH	SND	UMK	COH	SND	UMK	COH	SND	UMK	COH	SND
1-2	9		8.4			2.9			1.9			-7.2			2.9	
2-4	8	-0.5	0.7		0.1	1.2		-0.4	1.5		-3.5	-5.4		1.0	3.1	
4-8	7	3.8	3.2		2.1	0.6		5.4	4.1		-2.6	-3.9		0.5	1.2	
8-16	6	6.1	8.3		2.5	10.9		2.4	7.8		5.3	7.8		3.4	7.7	
16-32	5	7.9	10.6	5.9	1.9	13.4	8.7	-1.9		1.4	0.3	0.7	0.7	0.8	3.9	-1.1
32-63	4	-1.4		-1.8	3.2		0.6	-0.2		-0.5	0.3		1.0	-0.2		-0.6
63-127	3	1.3		2.0	-1.4		-3.3	-0.8		-0.4	9.6		2.3	1.4		0.6

566

567 c)

c) LOTUS Model Test: Difference [%] in Standard Error: QBO C/D vs Reference Model																
Pressure	Umkehr	Arosa/Davos			Haute-Provence			Boulder			Mauna Loa			Lauder		
(hPa)	Layer	UMK	COH	SND	UMK	COH	SND	UMK	COH	SND	UMK	COH	SND	UMK	COH	SND
1-2	9		-1.6			-0.2			0.5			-0.5			-3.3	
2-4	8	-0.8	3.1		-0.3	9.1		2.9	4.6		-3.5	-0.3		-1.7	-0.4	
4-8	7	-0.1	1.5		0.3	3.3		-2.7	-1.2		-6.1	-4.2		1.8	1.4	
8-16	6	0.5	-1.3		1.1	-0.3		-2.4	0.7		-0.4	0.8		-2.5	-2.9	
16-32	5	-0.8	1.3	0.0	-0.9	3.0	2.8	0.6	0.6	0.1	7.1	8.4	10.1	-3.1	-0.6	1.1
32-63	4	0.9		0.2	2.0		-0.9	2.7		-1.8	2.9		6.5	-1.6		-1.9
63-127	3	-0.3		-0.8	5.7		-0.2	0.3		-4.2	0.4		3.0	-2.8		-3.2

568

569 d)

d) LOTUS Model Test: Difference [%] in Standard Error: AO/AAO vs Reference Model																
Pressure	Umkehr	Arosa/Davos			Haute-Provence			Boulder			Mauna Loa			Lauder		
(hPa)	Layer	UMK	COH	SND	UMK	COH	SND	UMK	COH	SND	UMK	COH	SND	UMK	COH	SND
1-2	9		1.2			-1.6			0.3			-1.9			-0.5	
2-4	8	-0.8	0.0		-3.8	-1.2		-0.8	-0.4		-2.1	-2.4		0.8	-1.9	
4-8	7	-0.7	1.7		-4.2	-2.6		3.2	4.7		1.2	-3.4		1.2	-1.2	
8-16	6	-0.2	-0.6		-2.4	-3.9		1.2	0.5		1.6	-1.6		-0.3	2.5	
16-32	5	-1.2	-0.4	-1.2	0.5	-2.1	-2.4	0.2	-0.6	-2.1	3.9	1.8	0.7	-1.6	-1.5	1.4
32-63	4	5.8		7.8	0.4		4.6	-1.2		-1.7	7.6		1.7	-0.7		2.5
63-127	3	13.1		12.9	5.5		6.8	-1.4		-3.2	4.4		1.3	-1.1		2.4

570

571 e)

e) LOTUS Model Test: Difference [%] in Standard Error: NAO vs Reference Model																
Pressure	Umkehr	Arosa/Davos			Haute-Provence			Boulder			Mauna Loa			Lauder		
(hPa)	Layer	UMK	COH	SND	UMK	COH	SND	UMK	COH	SND	UMK	COH	SND	UMK	COH	SND
1-2	9		0.5			-2.5			-0.2			-3.7			-1.3	
2-4	8	-0.2	0.0		-3.1	-1.9		-0.4	-1.9		-1.7	-3.8		-2.0	-1.8	
4-8	7	-0.6	0.7		-2.0	-2.0		0.0	3.9		2.6	-1.1		-2.8	-2.4	
8-16	6	0.2	-0.9		-1.7	-3.4		-2.2	-2.8		2.4	-0.4		-2.0	-0.5	
16-32	5	-0.5	-1.2	-1.1	0.7	-2.2	-4.0	-0.4	-1.4	-1.2	-1.4	-0.7	-3.0	-2.5	-4.3	-1.5
32-63	4	2.6		3.1	-0.6		-0.9	-0.2		0.4	1.5		-0.8	-2.6		-4.8
63-127	3	10.6		6.7	2.7		1.0	0.4		-2.7	1.7		-0.5	-2.3		-4.9

572

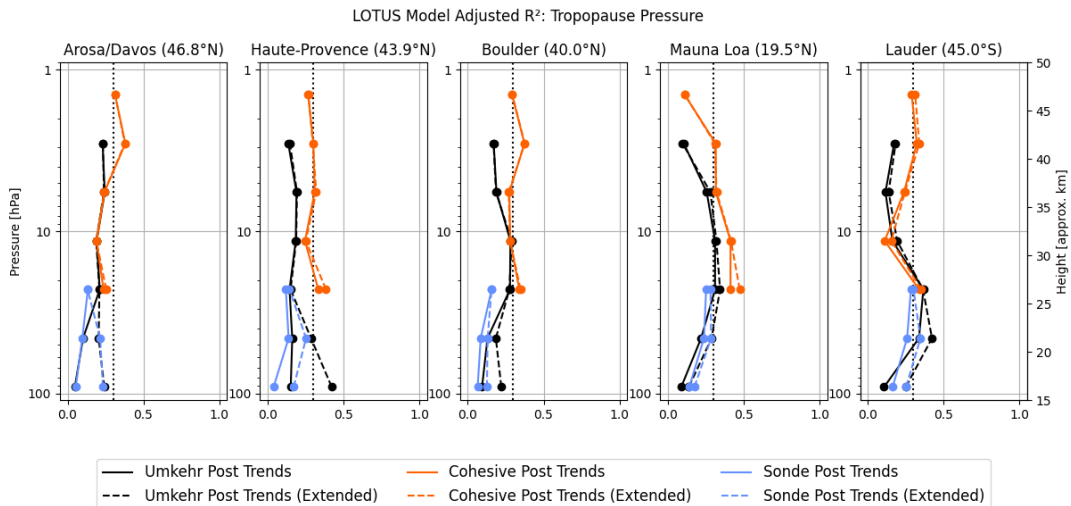
573 f)

LOTUS Model Test: Difference [%] in Standard Error: Eddy Heat Flux vs Reference Model																
Pressure	Umkehr	Arosa/Davos			Haute-Provence			Boulder			Mauna Loa			Lauder		
(hPa)	Layer	UMK	COH	SND	UMK	COH	SND	UMK	COH	SND	UMK	COH	SND	UMK	COH	SND
1-2	9		5.0			4.5			4.4			-3.2			0.2	
2-4	8	-1.4	4.6		2.6	6.0		3.1	8.8		-1.6	-3.3		0.7	1.9	
4-8	7	-2.7	-3.4		-0.4	-3.9		-3.0	-2.3		5.0	-4.4		1.8	4.5	
8-16	6	-3.1	-3.2		-2.5	-4.8		-2.4	-3.5		-1.1	0.4		-0.2	1.1	
16-32	5	-3.4	-2.8	-3.2	-2.2	-3.7	-2.5	-2.6	-2.4	-2.5	9.3	-0.4	4.3	0.7	2.4	0.7
32-63	4	-1.9		-1.6	-2.0		-1.8	-2.7		-3.5	8.8		3.1	1.9		1.6
63-127	3	1.5		1.4	-0.9		-1.6	-2.5		-3.8	0.9		0.9	2.1		1.1

574

575 **5.1 Tropopause pressure (TP)**

576 Adding the TP proxy to the standard LOTUS model produces the most consistent results between different techniques  
 577 (COH, Umkehr and ozonesonde) and also have similar magnitude of standard error changes among different latitudes  
 578 (i.e. Arosa/Davos, OHP, Boulder, MLO, Lauder). The most significant impact in improving the SE is found in the  
 579 lower stratosphere (layers 3, 4) and in the middle stratosphere (layer 5) at the MLO tropical station. The impact of the  
 580 TP proxy on the COH trend uncertainty in the model stratosphere (layer 5) is somewhat larger, likely due to the  
 581 satellite AK extending into the lower stratosphere. Similarly, larger reduction of the standard error in the Umkehr  
 582 trends in the lowermost stratosphere (layer 3) in comparison to the AK-smoothed ozonesonde record could be due to  
 583 sampling biases in the ozonesonde record. Adding the TP proxy to the Reference Model improves the adjusted  $R^2$  in  
 584 layers 3–5, whereas the SE improvements are also consistent across geo-locations and measurement techniques. The  
 585 TP proxy only explains ozone variability near the tropopause because changes in both parameters are linked to the  
 586 same dynamical processes (i.e. irreversible mixing). In the middle and upper stratosphere ozone variability is not  
 587 linked to the processes that change TP, thus using this proxy add error to the model fit. Several improvements resulted  
 588 in adjusted  $R^2$  to exceed the 0.3 threshold (Umkehr at OHP in layer 3, sonde and Umkehr at Lauder and MLO in layer  
 589 4) and in many cases the adjusted  $R^2$  increased by more than 0.02 (see Fig. 5a).



590

591

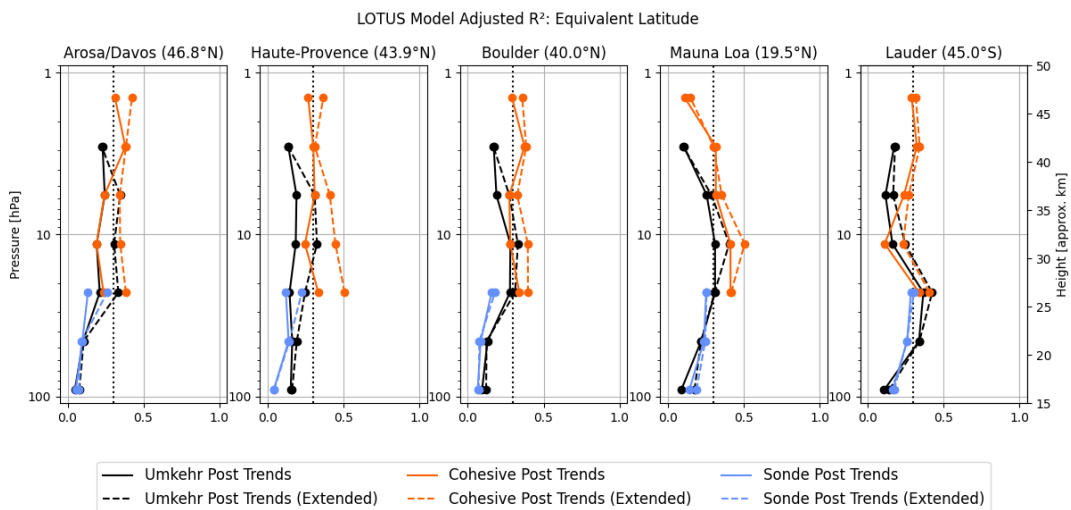
592 **Figure 5 a) Similar to Figure 4, but adjusted  $R^2$  results are shown for both Reference model (solid line) and the Extended**  
 593 **model (Dashed line, Full) for COH overpass (orange), Umkehr (black) and ozonesonde (blue) trend. Extended model**  
 594 **includes additional TP proxy.**

595 **5.2 Equivalent Latitude (EqLat)**

596 In the mid-latitudes, the addition of EqLat as a predictor shows consistent results across measurement techniques and  
 597 stations with few exceptions. The reduction in the SE of the model fit is evident in the COH data in the upper  
 598 stratosphere (above 4 hPa or ~ 40 km), but is less pronounced in Umkehr profiles. The impact on MLO SE of the trend  
 599 fit in the upper stratosphere is negative (in both COH and Umkehr records) which can be explained by the fact that  
 600 the EqLat is much closer to geometric latitude near the equator than at the middle/high latitudes and therefore its use  
 601 as a proxy would not provide any additional information in interpretation of the tropical upper stratospheric ozone  
 602 variability. It could also suggest that the addition of EqLat will overfit the record.

603 The ozone record trend fits in the middle stratosphere (32–4 hPa or 25–40 km) benefit from adding the EqLat proxy  
 604 at most locations. Improvement in the SE of the trends in the lower stratosphere (127–63 hPa or ~15–20 km) is  
 605 minimal, limited to some locations and instrumental records (Arosa/Davos Umkehr and HOH sonde, MLO Umkehr  
 606 and sonde, and Lauder Umkehr and ozonesonde), which could be related to the location of subtropical jet that  
 607 modulates mixing of tropical and subtropical (and occasionally polar) air masses and influences the strat/trop  
 608 exchange. Unexpectedly, the addition of the EqLat proxy to the MLR statistical model for trend detection in Boulder  
 609 Umkehr and ozonesonde lower stratospheric ozone records increases the uncertainties of the fit, while the influence  
 610 of subtropical jet on Boulder lower stratosphere is well known (Manney et al, 2018). Perhaps, the data analyses also  
 611 need to consider the tropopause variability.

612 In terms of the impact on the adjusted  $R^2$ , the EqLat proxy significantly improves model fit for multiple instruments,  
 613 mostly in layers 5–7, and in COH fit in layer 9 (see Fig. 5b). The adjusted  $R^2$  improvements also often exceeded 0.3  
 614 threshold. No significant improvement is found in the ozonesonde model fit in layer 5 with the exception of the OHP  
 615 and Hohenpeißenberg records (0.1 increase).



616

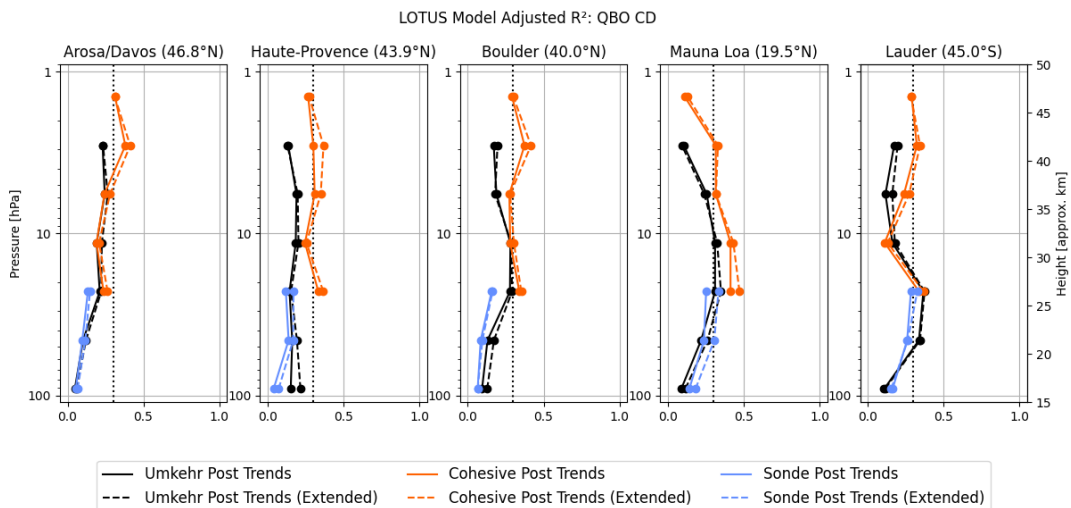
617

618 **Figure 5 b) the same as a), but Extended model includes Equivalent Latitude proxy.**



619 **5.3 Extra QBO terms C and D**

620 QBO is an important driver of ozone variability at tropical stations. Based on the results of adding 2 extra terms of the  
 621 QBO to the standard model, the recommendation could be to exercise this option only for the tropical station trends.  
 622 At the Northern middle latitudes (i.e. in Arosa/Davos, OHP and, to a lesser degree, in Boulder) an improvement to the  
 623 trend SE uncertainties in layer 8 is noted. There seems to be a similar pattern for the upper stratosphere in trends  
 624 derived with Heat Flux. Tweedy et al. (2017) show that the first two EOFs of the QBO did not describe the anomalous  
 625 QBO behavior, while Anstey et al. (2021) show that the addition of two more EOFs of the QBO could capture the  
 626 effect of the disruptions on the zonal winds. Therefore, including additional QBO EOFs could benefit attribution of  
 627 ozone variability in the middle stratosphere (layers 4 and 5) in the tropical latitudes (reduced errors in MLO/Hilo  
 628 trends) and in the upper stratosphere (layer 8 in COH and in some Umkehr trends) in the NH middle latitude stations  
 629 (Arosa/Davos, OHP, Boulder) related to the global circulation pattern that are also represented by the Heat Flux proxy.  
 630 A slight reduction in the errors at SH middle latitude (sonde at Lauder, New Zealand) could be invoked by the EqLat  
 631 variability that has a small correlation with the QBO-D proxy and sampling bias. Reduction of SE in the trend fit of  
 632 the layer 5 ozonesonde (up to 2.8 %) and COH (up to 3.0%) records at OHP is not found in the Umkehr results, which  
 633 suggests overfitting and sampling bias (see results in Appendix D).  
 634 The addition of extra QBO terms slightly improves the adjusted  $R^2$  model fit (see Fig 5, c) for all COH station overpass  
 635 records in layer 8 (except at MLO) and occasionally improves Umkehr adjusted  $R^2$  (Boulder and Lauder). The most  
 636 significant improvement is found at MLO in layers 3–5 in all three instrument records.

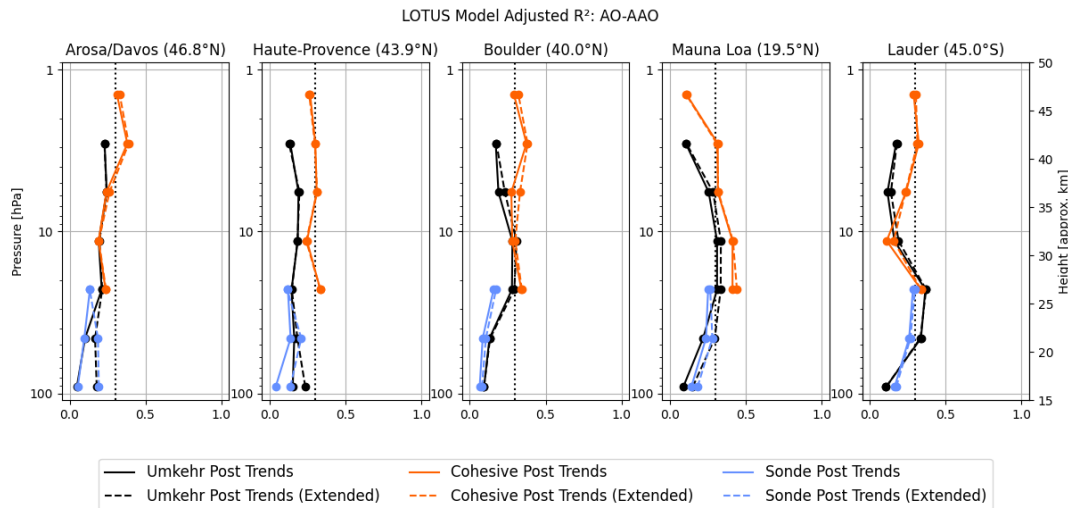


637  
 638  
 639 **Figure 5 c) the same as a), but Extended model includes 2 extra QBO terms as an additional proxy.**

640 **5.4 Arctic and Antarctic Oscillations (AO/AAO)**

641 AO/AAO proxies reduce SE (blue colored cells) in the lower stratosphere (layers 3 and 4) at Arosa/Davos, OHP, and  
 642 MLO, although the reduction somewhat differs between the Umkehr and ozonesonde records. At the same time, at  
 643 Boulder and Lauder the SE does not show an improvement after the addition of the AO/AAO proxy (AAO is used

644 instead of AO at Lauder). In the middle stratosphere (layer 7), a reduction in SE is found over Boulder in both COH  
 645 and Umkehr records. The addition of AO/AAO proxies improves the SE of the trend at MLO and Lauder but only in  
 646 Umkehr records, while it worsens the COH SE. At Lauder, the COH SE in layer 6 shows an improvement, but not in  
 647 Umkehr record. Since results in the middle stratosphere (layers 5–7) are not always consistent among different  
 648 techniques (reductions are not in the same layers) it could indicate statistical model overfit into the record’s noise, or  
 649 vertical smoothing of the Umkehr or COH technique that combines ozone variability in the layer with a portion of  
 650 ozone variability in the adjacent layers, thus partially or completely reducing the correlation with the proxy.  
 651 The addition of the AO predictor increases the adjusted  $R^2$  in the lower stratosphere at Arosa/Davos, OHP and MLO  
 652 (see Fig. 5d). Also, a small enhancement of the adjusted  $R^2$  is seen in the middle and upper stratosphere, including in  
 653 Umkehr layers 6 and 7 and COH layers 6, 7 and 9 over Boulder, as well as in Umkehr fit in layers 5–7 at MLO, and  
 654 at Lauder (AAO) for Umkehr and COH records in layer 6. These results are not very consistent across different  
 655 geolocations, but seem to be consistent across instrumental records at some stations (Umkehr and ozonesonde in the  
 656 lower layers, and COH and Umkehr in the upper layers).

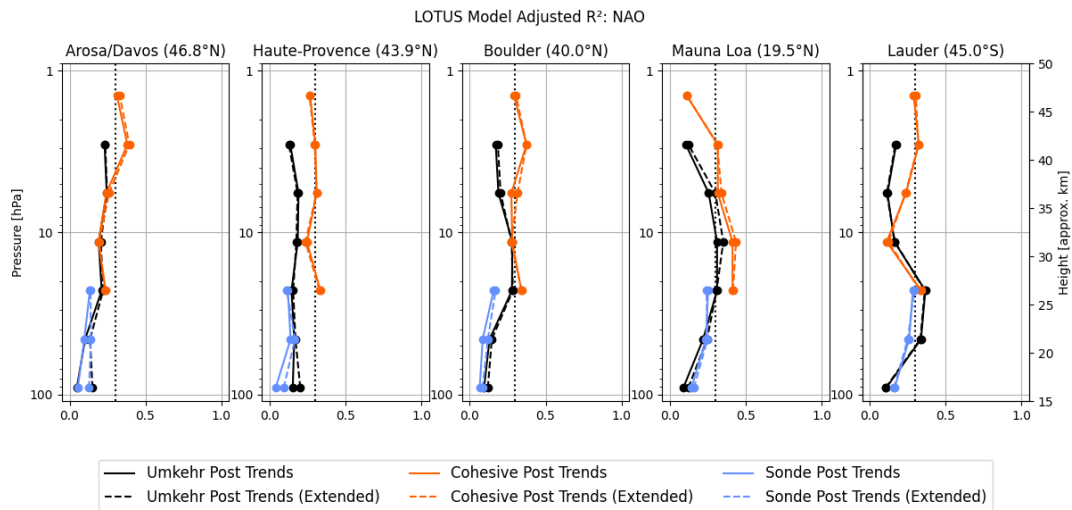


657  
 658 **Figure 5 d) the same as a), but extended model includes AO/AAO proxy.**

659 **5.5 North Atlantic Oscillation (NAO)**

660 Including the NAO proxy in the trend model appears to have a similar pattern (i.e., in latitude and altitude) of changes  
 661 in the standard error as compared to the result of inclusion of the AO/AAO proxy. It is not a surprise, since indices of  
 662 the NAO and AO are highly correlated in time due to their common link to the downward propagation of stratospheric  
 663 anomalies. Standard errors are somewhat reduced in the lower stratospheric layers at the middle NH latitude and  
 664 tropical Umkehr records, but the change is less significant than in AO/AAO cases. The impacts on ozonesonde trend  
 665 uncertainties are very minimal and inconclusive at Boulder (layers 5 and 4), Hohenpeißenberg (layer 3 and 4), and  
 666 OHP (layer 3). The impacts on Lauder are similar or stronger (SE is increased for both Umkehr and sonde records) to  
 667 the impacts of the AO/AAO. In the middle and upper stratosphere, the standard errors are typically increased. The  
 668 exception is found in layer 7 of the COH record at Boulder and Arosa/Davos, and in layers 6 and 7 of the Umkehr  
 669 record at MLO. Similar negative results are found when AO/AAO proxies are added, which suggests that the observed

670 time series are overfitted and potentially some instrumental or sampling anomalies are misinterpreted with addition  
 671 of these proxies (see Fig. 5e).



672

673

674 **Figure 5 e) the same as a) but extended model includes NAO as an additional proxy.**

675 **5.6 Eddy Heat Flux (EHF)**

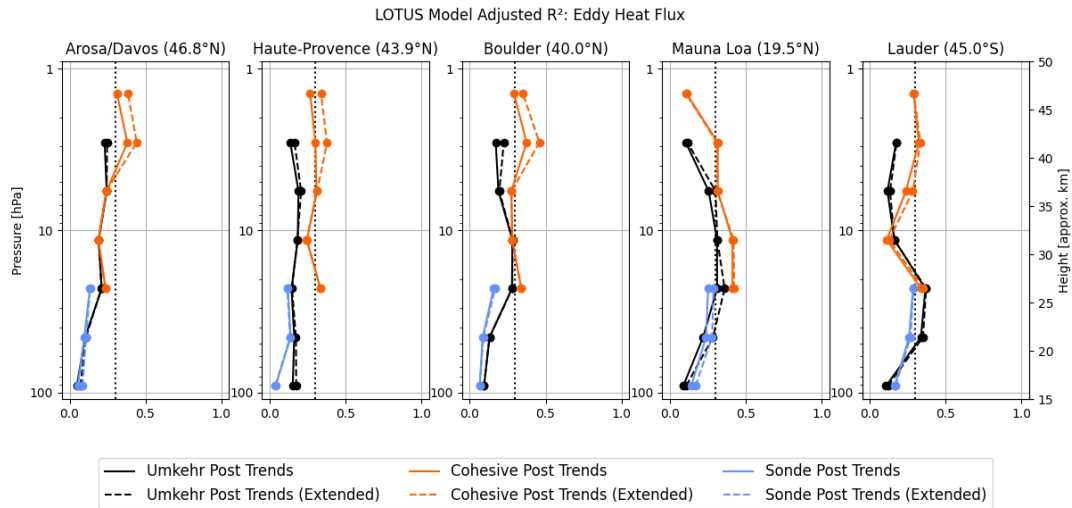
676 The EHF represents a dynamical proxy for assessment of the impact of the Brewer Dobson Circulation (BDC). It is  
 677 expected to have an impact on the upper stratospheric ozone by accelerating the transport in the upper branch that  
 678 brings more ozone at higher latitudes (i.e. Arosa/Davos) and middle latitudes (i.e. OHP, Boulder, and Lauder). It could  
 679 possibly represent changes in the lower branch of the BDC circulation and the expansion of the tropical band, thus  
 680 modulating ozone in the lower stratosphere at tropics (i.e. MLO). In the Southern middle latitudes (i.e. Lauder), the  
 681 correlations could be related to the shift in the subtropical wave activities to the higher latitudes in response to the  
 682 ozone hole healing.

683 The addition of the EHF predictor leads to the reduced SE uncertainties in the upper stratosphere in COH and Umkehr  
 684 trends at OHP and Boulder, and in COH only trends at Arosa/Davos. It has a much smaller reduction of SE for the  
 685 Lauder trend and even an increase in uncertainties if used to fit upper stratospheric ozone time series at MLO. At the  
 686 same time, the SE in the Umkehr and ozonesonde middle stratosphere (layers 4–5) at MLO is substantially reduced,  
 687 including smaller improvements at Lauder. In the lower stratospheric (layer 3) ozone trend SE in Umkehr and sonde  
 688 records at MLO, Lauder and Arosa/Davos are somewhat reduced when using the EHF proxy.

689 Addition of the EHF predictor seems to have an impact in the upper stratosphere increasing the adjusted R<sup>2</sup> for COH  
 690 records in layers 8 and 9 in all but MLO or Lauder records, which indicates impact of the BDC upper branch on the  
 691 middle NH latitudes (see Fig. 5f). In contrast to the COH, the Umkehr adjusted R<sup>2</sup> has not changed significantly,  
 692 which possibly suggests a high measurement noise in the station records. There is, however, a small increase in  
 693 adjusted R<sup>2</sup> in the Umkehr record in layer 7 at MLO (whereas COH does not show a change).

694 The increase in adjusted R<sup>2</sup> is found at MLO in Umkehr and sonde layers 4 and 5, including a small increase in layer  
 695 3, which probably is related to the EHF-driven changes in the middle stratosphere. Ozone variability in Umkehr and

696 sonde records at MLO appears to contain information about the circulation changes in the shallow BDC branch.



697

698 **Figure 5 f) the same as a) but extended model includes EHF as an additional proxy.**

## 699 **6 The Full Model - adding multiple predictors**

700 In this paper we seek to develop an improved model and thus trend estimates for point located measurements of ozone  
701 through modifications of a model optimized for zonal data. Our criteria for model improvement are based on reduction  
702 of the SE of the trend with either improvement (at best) or moderate impact (at worst) on the model adjusted  $R^2$ . From  
703 the results of the previous section, we see several opportunities to improve the model and improve confidence in the  
704 trend estimates. This section examines if the gains of the above are improved while adding several predictors together.  
705 As stated above the TP as a predictor exhibits the most consistent results for all stations and measurement techniques.  
706 The other predictors have successes in SE reduction, but only at some layers, and some stations. Some results are  
707 instrument dependent.

708 Based on the tests above we expect combining predictors can improve the model fit and trend SE reduction, but it is  
709 clear that the predictor selection should vary by station and level. Appendix E details the choices made for the Full  
710 Model which combines 1 to 3 additional proxies beyond the Reference Model.

### 711 **6.1 Predictors added for the Full Model**

712 Reduction of the SE of the trend while improving (or at least not impacting) model adjusted  $R^2$  is the basis of predictor  
713 choice for the Full Model. To qualify a predictor should exhibit consistent results for all measurement techniques.  
714 Improvement at multiple stations is preferred to single station improvements. In general, we avoid combining highly  
715 correlated predictors. Table 8 shows final choices for the Full Model.

716 **Table 8: Added predictors for the Full model are tuned for each layer and each station. For layers 7 to 9 the SE and**  
717 **adjusted  $R^2$  parameters at MLO are not improved by additional predictors, and the original LOTUS based Reference**  
718 **Model is used. Appendix E explains the logic of the predictor selection.**

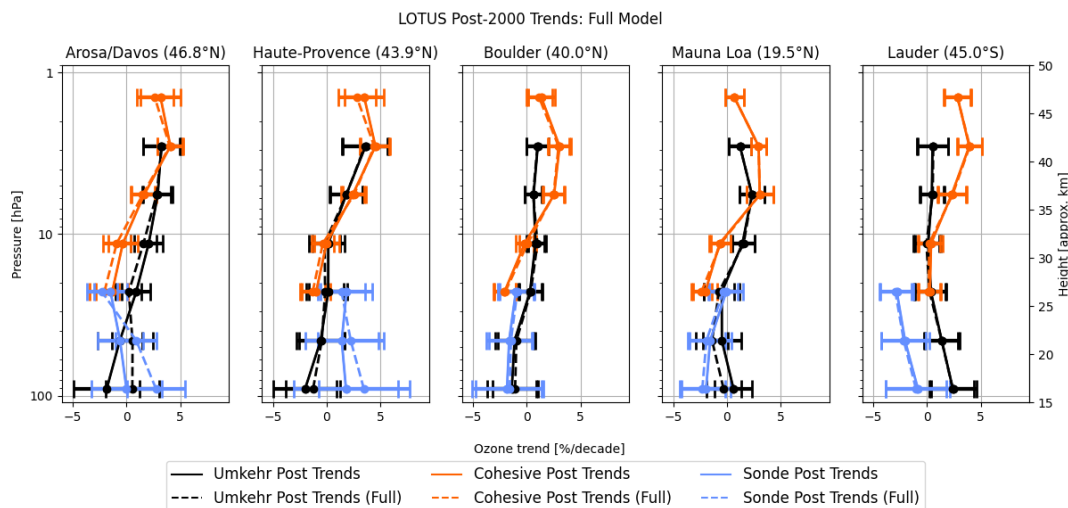
719

LOTUS Full Model predictor selection					
	Arosa/Davos	OHP	Boulder	MLO	Lauder
Layer					
9	EqLat	EqLat	EqLat	Reference only	EqLat
8	EqLat	EqLat	EqLat	Reference only	EqLat
7	EqLat	EqLat	EqLat	Reference only	EqLat
6	EqLat	EqLat	EqLat	EqLat	EqLat
5	EqLat	EqLat	EqLat	EqLat, QBO CD, AO	EqLat
4	TP, AO	TP, AO	TP	TP, QBO CD, AO	TP
3	TP, AO	TP, AO	TP	TP, QBO CD, AO	TP

720

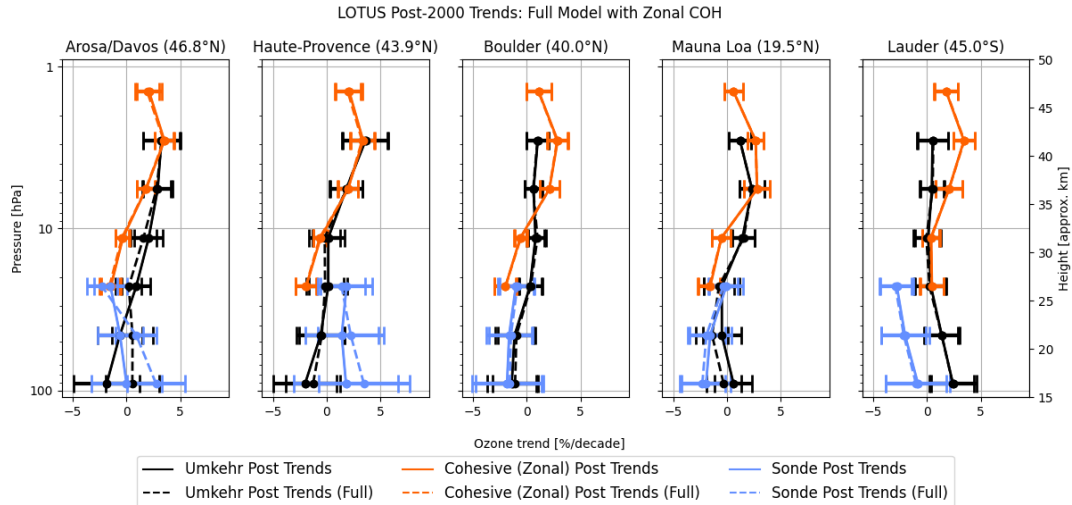
721 **6.2 Impact of the Full Model on trends.**

722 Figure 6a shows the trends for the stations (with COH overpass) for the Reference and Full Models. An impact of the  
 723 Full Model on ozone trends derived in the upper stratosphere (above 16 hPa) is neutral. Addition of proxies to the  
 724 LOTUS model does not change trends which remain the same magnitude as those derived using the Reference Model,  
 725 i.e., positive and statistically significant at the SH and MH middle latitudes and over tropics. The largest difference  
 726 (outside of the SE uncertainty) between upper stratospheric Umkehr and COH trends is found over Boulder, MLO  
 727 and Lauder.



728

729 **Figure 6a: Post 2000 trends for the Full and Reference Model. In this figure the COH data shown in orange is the overpass**  
 730 **data. Solid lines depict Reference Model values (unchanged from Fig. 3). Dashed lines depict Full Model values for all 3**  
 731 **instrument types.**



732

733 **Figure 6b: Post 2000 trends for the Full and Reference Model. In this case the orange lines are with the zonal data instead**  
 734 **of the COH overpass data. Dashed lines depict Full Model values for all 3 instrument types. The Umkehr and sonde trends**  
 735 **are unchanged from Fig. 6a.**

736 In the middle stratosphere, additional proxies do not change trend values across locations and instrumental records  
 737 (outside of the SE). At OHP, Boulder and Lauder Umkehr trends in layer 6 (8–16 hPa) are barely positive while COH  
 738 trends are negative. At Arosa/Davos and MLO, COH trends in layer 6 are barely negative and Umkehr trends are  
 739 significantly positive. Most COH trends in layer 5 (16–32 hPa) are statistically negative (except at Lauder), while  
 740 Umkehr trends are near zero.

741 In the lower stratosphere, Umkehr and sonde trends Arosa/Davos and MLO change after the Full model is used.  
 742 However, Umkehr and sonde trend changes at MLO are within the SE and therefore can be deemed not significant.  
 743 Ozonesonde trends at Arosa/Davos in layer 3 (125–63 hPa) change from zero to positive. Umkehr trends at  
 744 Arosa/Davos in layer 3 change from negative to near zero. Large differences between ozonesonde and Umkehr trends  
 745 at Lauder and OHP remain unchanged after the Full model is applied although respective SE envelopes overlap.

746 Figure 6b also shows the trends for the Reference and Full Models, but the COH data shown is the associated zonal  
 747 data relevant to each station. Incorporation of the additional proxies does not change the trend values for the zonal  
 748 COH data. Impact on error estimates for the trends are discussed next.

## 749 6.2 Impact of the Full Model on the Trend SE

750 Table 9 summarizes the reduction in the SE for the Full model. Selection of the EqLat predictor for the Full model in  
 751 the layers 5–9 and for all stations (except MLO/Hilo, to be discussed later) shows the improvement in the SE (as  
 752 discussed in the previous section). Also, the TP predictor is selected for inclusion to the Full model for trend analyses  
 753 at Boulder and Lauder stations in layers 3 and 4. The combination of several predictors are used for individual stations  
 754 based on the additional reduction in the SE. For the Arosa/Davos and OHP stations we select a combination of the TP  
 755 and AO to reduce the SE almost twice as much in some layers. Inclusion of AO proxy is in support of the interpretation  
 756 of seasonal and interannual ozone variability recorded over stations in Europe that are north of 40 degrees latitudes  
 757 and are exposed to the seasonal events of ozone depleted air masses transported from the Polar region during the

758 spring season (Steinbrecht et al., 2011; Manney et al., 2011; Knudsen and Grooss, 2000; Fioletov and Shepherd, 2003;  
 759 Zhang et al., 2017; Weber et al., 2022a). The strong impact of AO/AAO on the lower stratosphere ozone variability  
 760 are not detected in Boulder or Lauder and we choose not to include it in the Full model for trend analyses at these  
 761 stations.

762 **Table 9: Change in post 2000 trend SE in the Full Model as a % difference of the Reference Model. Color coding is the**  
 763 **same as introduced in Table 7.**

764

LOTUS Model Test: Difference [%] in Standard Error: Full Model vs Reference Model																
Pressure	Umkehr	Arosa/Davos			Haute-Provance			Boulder			Mauna Loa			Lauder		
(hPa)	Layer	UMK	COH	SND	UMK	COH	SND	UMK	COH	SND	UMK	COH	SND	UMK	COH	SND
1-2	9		8.4			2.9			1.9			0.0			2.9	
2-4	8	-0.5	0.7		0.1	1.2		-0.4	1.5		0.0	0.0		1.0	3.1	
4-8	7	3.8	3.2		2.1	0.6		5.4	4.1		0.0	0.0		0.5	1.2	
8-16	6	6.1	8.3		2.5	10.9		2.4	7.8		5.3	7.8		3.4	7.7	
16-32	5	7.9	10.6	5.9	1.9	13.4	8.7	-1.9		1.4	13.6	13.0	13.3	0.8	3.9	-1.1
32-63	4	8.7		10.0	6.1		9.4	3.4		2.7	17.3		10.3	8.0		7.4
63-127	3	20.3		18.5	13.5		12.8	6.8		2.2	8.0		5.6	9.8		6.8

765

766 The MLO/Hilo location is close to the Tropical belt and therefore has different processes impacting stratospheric  
 767 ozone variability as discussed in the previous section. We find that EqLat proxy can be added to the Full model in  
 768 layer 6 and 5 (similar to other stations); however, above layer 6, EqLat or TP is not useful for interpretation of tropical  
 769 ozone variability and therefore we believe the trend model in these layers should remain as it currently is used in  
 770 Godin-Beekmann et al. (2022) analyses. The EqLat and TP are mildly correlated (-0.4) in the stratosphere, and  
 771 therefore we decided against combining both of these proxies in the Full model. However, we also found that adding  
 772 AO and QBO C/D proxies in layers 3, 4 and 5 improved the model fit and reduced the SE. These combined additional  
 773 proxies are not correlated and reduce SE more than when using them separately.

774 The Full Model showed impacts on the SE in the upper stratosphere (above 8 hPa). The trend errors were reduced  
 775 with the exception of Umkehr trends at 4–2 hPa over Boulder and Arosa/Davos where errors did not change. No  
 776 changes in SE are found at MLO with additional proxies, thus the Full Model is kept the same as the Reference Model  
 777 for this station in the upper stratosphere.

778 Similarly, in the middle stratosphere SE were mostly reduced after the Full Model was applied (except for slightly  
 779 larger SE in trends derived from ozonesonde at OHP and from Umkehr at Boulder).

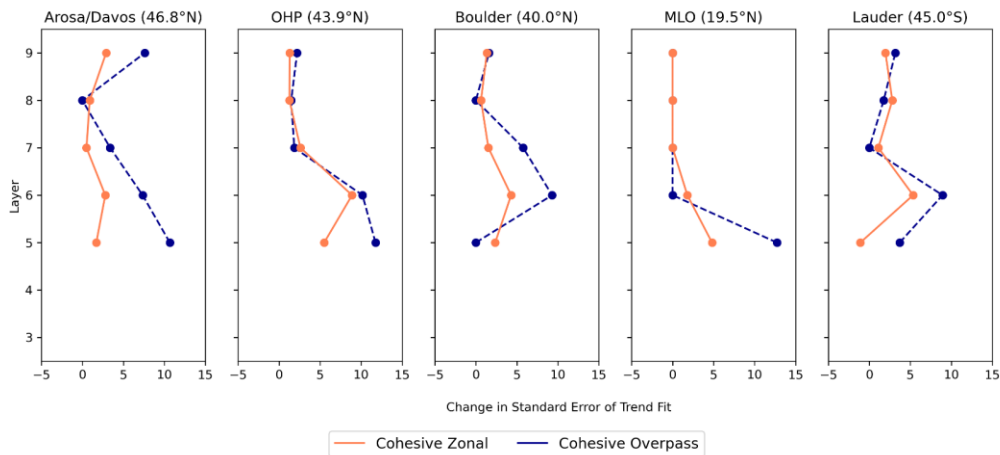
780 After applying the Full Model in the lower stratosphere, we still found high uncertainty due to higher ozone variability  
 781 (natural variability), but SE were reduced. Arosa/Davos and MLO Umkehr and sonde trends changed after Full Model  
 782 was used. Change in ozonesonde trends at HOH in layer 3 (125–63 hPa) goes from zero to positive and trend detection  
 783 becomes highly confident (p-value <0.05). Umkehr trends at Arosa/Davos in layer 3 changed from negative to near  
 784 zero but results have low certainty (p-value >0.1). Larger trend differences remain between ozonesonde and Umkehr  
 785 at Lauder and OHP after the Full Model is applied.

786 **Table 10: Change in Standard Error of Trend, as percent of Reference Model SE, for the COH overpass data and zonal**  
 787 **data at the 5 ground stations. MLO Full Model in layers 9-7 is the same as the Reference Model (change is marked as NA).**

788

LOTUS Model Proxy Tests: (% difference of SE of Trend): overpass and zonal COH											
Height	Umkehr	Arosa/Davos		OHP		Boulder		MLO		Lauder	
(hPa)	Layer	Overpass	Zonal	Overpass	Zonal	Overpass	Zonal	Overpass	Zonal	Overpass	Zonal
1-2	9	7.61	2.89	2.20	1.30	1.61	1.34	NA	NA	3.17	1.97
2-4	8	0.00	0.90	1.47	1.26	0.00	0.63	NA	NA	1.75	2.76
4-8	7	3.39	0.47	1.85	2.55	5.77	1.53	NA	NA	0.00	1.11
8-16	6	7.35	2.75	10.17	8.98	9.30	4.30	0.00	1.79	8.93	5.34
16-32	5	10.67	1.74	11.76	5.54	0.00	2.36	12.73	4.81	3.70	-1.11

789



790

791 **Figure 7: Change in Standard Error of Trend, as percent of Reference Model SE, for the COH overpass data (blue) and**  
 792 **COH zonal data (red) at the 5 ground stations.**

793 It is instructive to ponder if the addition of proxies that yield improvements via reduction of the standard error in the  
 794 localized GB or overpass measurements also have the potential to improve uncertainties in the zonal data. To explore  
 795 this Table 10 and Fig. 7 show the percent change in SE of the trend when adding the proxies for the Full model.  
 796 Values are shown for both the COH overpass and the COH zonal data. In general, except when the improvement in  
 797 the SE for the overpass COH is small (3% or less), addition of proxies has much less impact on the zonal results than  
 798 on overpass results. This suggests that indeed the Reference LOTUS model is well tuned for zonal datasets, but can  
 799 be improved with select addition of proxies for overpass or localized GB data.

### 800 6.3 Impact of the Full Model on adjusted R<sup>2</sup>

801 Table 11 shows the adjusted R<sup>2</sup> for the Full Model. In the upper stratosphere, the Full Model increases the adjusted  
 802 R<sup>2</sup> above 8 hPa (except in Umkehr at 4–2 hPa). Over MLO there is no change because the Full Model is kept the same  
 803 as the Reference Model for layers 7, 8 and 9.

804 **Table 11: Adjusted R<sup>2</sup> of the Full Model. Values of 0.30 and above are indicated in Bold as a threshold to indicate a**  
 805 **satisfactory fit. Compare to Table 4 containing values for the Reference Model.**

806



LOTUS Model Proxy Tests: (Adjusted R <sup>2</sup> of the Full Model)																
Height	Umkehr	Arosa/Davos			OHP			Boulder			MLO			Lauder		
(hPa)	Layer	UMK	COH	SND	UMK	COH	SND	UMK	COH	SND	UMK	COH	SND	UMK	COH	SND
1-2	9		0.42			0.37			0.36			0.11			0.32	
2-4	8	0.23	0.39		0.14	0.31		0.17	0.39		0.11	0.32		0.18	0.34	
4-8	7	0.35	0.35		0.31	0.41		0.27	0.33		0.26	0.32		0.17	0.27	
8-16	6	0.31	0.35		0.33	0.45		0.33	0.40		0.40	0.51		0.25	0.23	
16-32	5	0.34	0.38	0.26	0.25	0.51	0.23	0.31	0.40	0.18	0.44	0.53	0.39	0.42	0.41	0.29
32-63	4	0.23		0.25	0.29		0.27	0.19		0.18	0.42		0.38	0.42		0.31
63-127	3	0.31		0.31	0.44		0.21	0.22		0.11	0.19		0.24	0.25		0.21

807 In the middle stratosphere (32–8 hPa) adjusted R<sup>2</sup> increases are found in all records (although smaller increases are  
808 found in ozonesonde and Umkehr records at OHP, Boulder and Lauder at 32–64 hPa). At Arosa/Davos, Boulder and  
809 Lauder the adjusted R<sup>2</sup> in the COH and Umkehr trend models increase and continue to be very close in value. The  
810 COH adjusted R<sup>2</sup> is larger at OHP and MLO than in Umkehr and sonde records thus suggesting that overpass  
811 conditions might have smoothed some natural variability observed in the GB records. In general, the adjusted R<sup>2</sup> is  
812 the largest at the 32–64 hPa level. This suggests that the Full Model shows an improvement for regional trend analyses  
813 in the middle stratosphere.

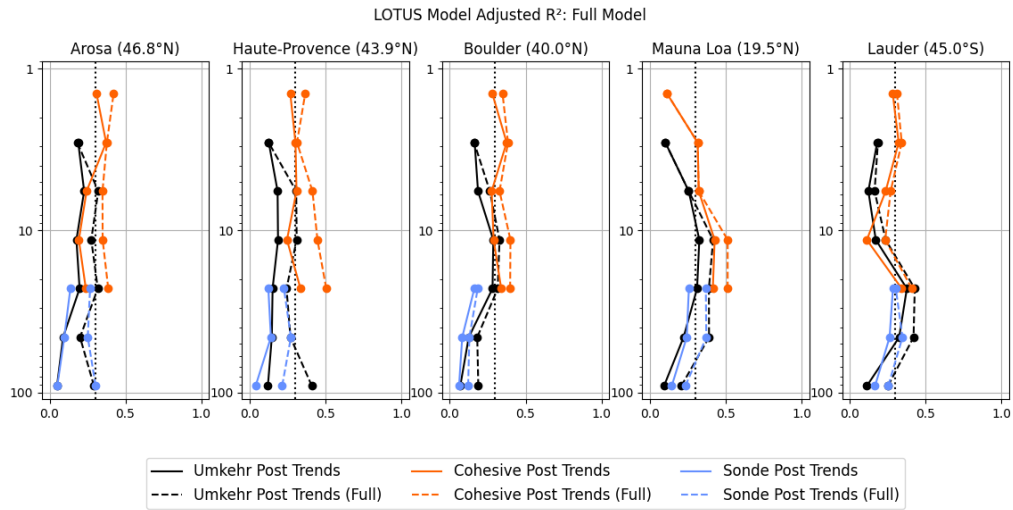
814 Although Umkehr and sonde trend changes at MLO in the lower stratosphere are within the SE and therefore can be  
815 deemed not significant, the adjusted R<sup>2</sup> is increased which suggests a better model fit in the Full Model. The adjusted  
816 R<sup>2</sup> increases in both Umkehr and ozonesonde data, while the largest increases are found in the Arosa/Davos, OHP and  
817 MLO records.

818 In the lower stratosphere, the adjusted R<sup>2</sup> remains low in both Umkehr and sonde records at Boulder (only TP is added  
819 for the Full model). While the p-values at 63–32 hPa are significantly reduced (see discussion in the next section),  
820 they still remain relatively high. These results suggest that additional research is needed to identify the best set of  
821 proxies for Boulder records in the lower stratosphere. At Lauder, the ozonesonde record shows smaller adjusted R<sup>2</sup> as  
822 compared to Umkehr partially due to low sampling biases.

823 It is valuable to further explore the impact of the Full Model on the adjusted R<sup>2</sup> for the zonal and overpass COH data.  
824 Fig. 8a shows the adjusted R<sup>2</sup> for the Reference and Full Models at each of the 5 stations using the COH overpass  
825 data. In all cases the Full Model improves the adjusted R<sup>2</sup> except for MLO layers 7, 8 and 9 where the Full and  
826 Reference Model are identical. The most significant improvements are seen by Umkehr at layers 3 to 7, COH overpass  
827 at Layers 5, 6 and 7, and sonde layers 3–5. Figure 8b shows similar results using COH zonal data instead of overpass.  
828 There is practically no further improvement in the adjusted R<sup>2</sup> for the zonally averaged COH results (except for a  
829 small increase for MLO layer 5). Comparison of results reveals that for OHP the implementation of the Full model  
830 for the COH overpass data (Fig. 8a, dashed line) improves the adjusted R<sup>2</sup> to values nearing that of the Reference  
831 Model zonal data in layer 7 and below (Fig. 8b, solid line). For MLO and Lauder the use of the Full Model on the  
832 COH overpass data improves the adjusted R<sup>2</sup> over the Reference Model beyond the improvement seen in the COH  
833 zonal results for layers 5 and 6. At Arosa/Davos and Boulder the implementation of the Full Model does not fully  
834 reach the magnitude of the COH zonal adjusted R<sup>2</sup>.

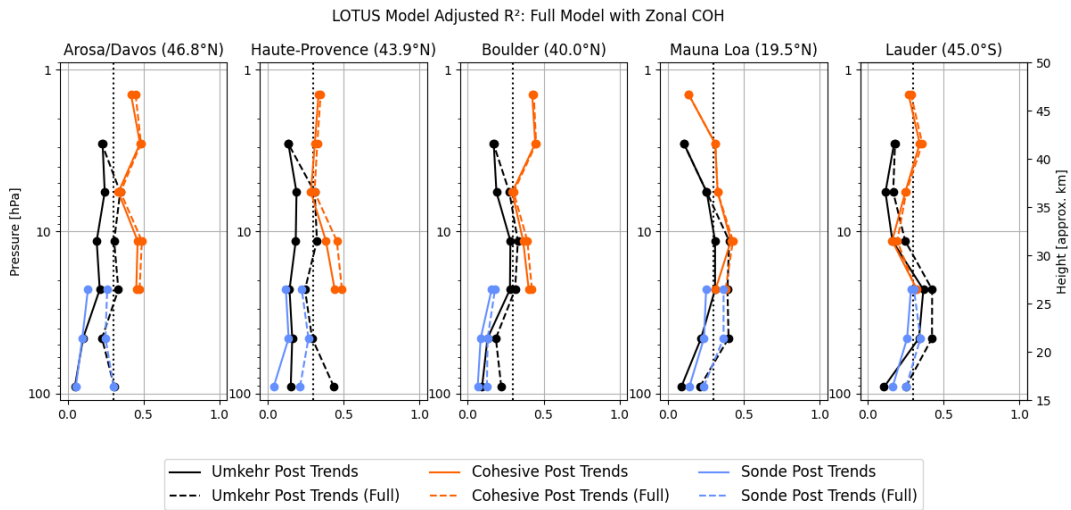
835

836



837  
838  
839

**Figure 8a: Adjusted R<sup>2</sup> for the Full Model (dashed lines) and Reference Model (solid lines) at 5 stations. The COH data in this figure is the overpass data at each station.**



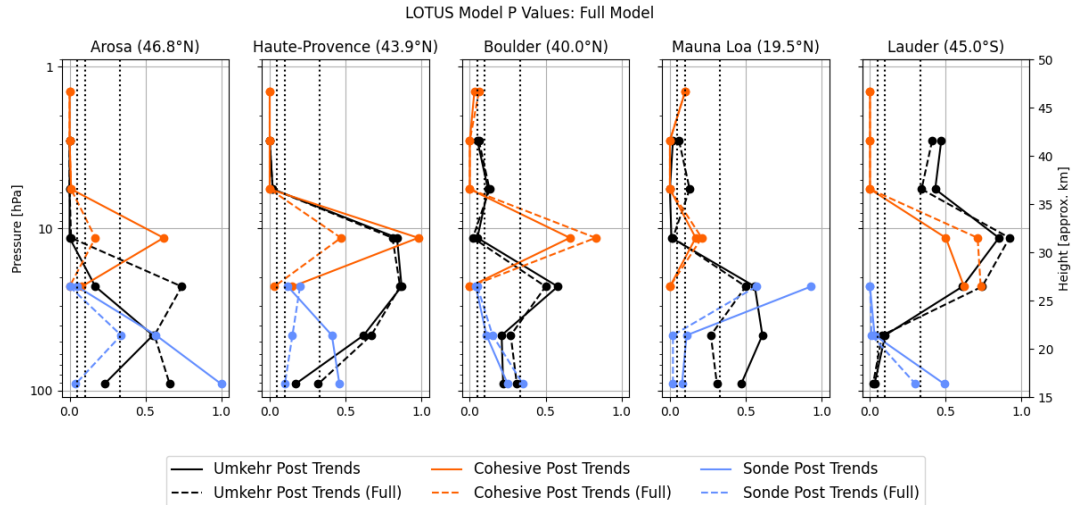
840

841

842

843

**Figure 8b: Adjusted R<sup>2</sup> for the Full Model (dashed lines) and Reference Model (solid lines) at 5 stations. The COH data in this figure is the zonal data for each station. The Umkehr and sonde lines are identical to those in Fig. 8a.**



844  
 845 **Figure 8c: the same as b, but for the p-values. Vertical dotted lines indicate limits for the high (<0.05), medium-high**  
 846 **(between 0.05 and 0.1), medium (between 0.1 and 0.3) and low confidence (>0.3).**

### 847 6.3 Examination of the p-values of the Full Model

848 In the upper stratosphere (above 8 hPa), the confidence in Umkehr trends remained high (see Figure 8c) for most  
 849 stations except at Boulder (medium to low) and Lauder (very low, although some improvement was found). COH  
 850 trends confidence was very slightly degraded over Boulder at 1–2 hPa, but mostly has not changed.

851 In the middle stratosphere (between 32 and 8 hPa), p-values were significantly reduced in COH records. At 8–16 hPa  
 852 remained high, but at 16–32 hPa the confidence improved (continued) to high over Arosa/Davos and OHP (Boulder  
 853 and MLO). In case of Umkehr analyses in layer 8–16 hPa at Arosa/Davos, Boulder and MLO the confidence remained  
 854 high. However, at 16–32 hPa the Umkehr trend detection confidence was degraded over Arosa/Davos and Lauder.  
 855 For the ozonesonde record, the p-values remained low (<0.05) except at MLO where some improvement was found  
 856 after the Full Model was used, but the p-value remained high. It suggests that some instrumental records have either  
 857 high atmospheric or instrumental noise and therefore perhaps high certainty in trend detection cannot be achieved with  
 858 linear trend models. For near zero trends with high variability, the p-values are not a good criterion for trend  
 859 detectability.

860 In the lower stratosphere (between 125 and 32 hPa), analyses of p-values for the Full Model fit show significant  
 861 improvement for Umkehr trends at MLO between 63–32 hPa (while the p-value was increased at other stations at this  
 862 level). In addition, improvement in p-values was found for ozonesonde trends at all stations. Specifically, very low p-  
 863 values for the Full model were reached at Arosa/Davos (125–63 hPa), OHP (125–63 and 63–32 hPa), MLO (125–63  
 864 and 63–32 hPa), and Lauder (63–31 hPa).

### 865 7 Summary of the Full Model findings.

866 We find that upper stratospheric trends in COH overpass and Umkehr records detect ozone recovery with high  
 867 confidence ( $p < 0.05$ ) above 8 hPa (with the exception of near-zero positive Umkehr trends over Lauder and Boulder).

868 We note the largest difference between Umkehr and COH trends (outside of the SE uncertainty) at Boulder, Mauna  
869 Loa and Lauder.  
870 Confidence for the middle stratosphere (between 32 and 8 hPa) trends vary between high, medium and low. Although  
871 most of the trends are narrowly different from zero (especially when error bars are considered), there are some  
872 differences in results across instrumental groups: trends in COH and sonde (except at OHP) between 32 and 16 hPa  
873 tend to be small negative, while Umkehr trends are slightly positive. Some trends are statistically different from zero.  
874 However, instrument-specific error bars often overlap and thus making differences in trends not significant.  
875 Confidence in lower stratosphere trends is highly variable and even lower than in the middle stratosphere due to higher  
876 ozone variability unaccounted for by Solar, QBO and ENSO proxies used in the Reference Model. However, high  
877 confidence ( $p < 0.05$ ) is still found in ozonesonde trends at Arosa/Davos, OHP, MLO and Lauder (although not at all  
878 layers). Umkehr trends in the lower stratosphere show lower confidence than ozonesonde trends (except at Lauder  
879 and Arosa/Davos in the lowermost altitudes). The low confidence levels could be related to the near-zero trends  
880 derived from Umkehr data, whereas ozonesonde trends are often different from zero lines. Also, we apply AK-  
881 smoothing to the sondes to account for the wide AKs in the Umkehr retrieval. We tested the impacts of the AK on  
882 ozonesonde trends (see Appendix A) and did not find any significant impacts. Most notably, ozonesonde and Umkehr  
883 trends significantly disagree in the lower stratosphere at OHP and Lauder and therefore require further investigation.  
884 The instrumental drifts and differences in Lauder trends are also discussed in Bjorkland et al. (2023 preprint) and are  
885 consistent with our findings.

## 886 **8 Conclusions.**

887 This paper is a follow up to Godin-Beekmann et al. (2022) with a focus on the GB record trend assessment. Therefore,  
888 our trend analyses focus on the questions:

- 889 1) Do proxies for evaluating trends of GB stations need to be different from those of the optimized set for zonal  
890 data?
- 891 2) Are station records representative of the small geophysical region or semi-global changes?
- 892 3) Do uncertainties of the zonal averaged trends improve with additional proxies?

893  
894 The Full Model developed in this paper for station and overpass data adds proxies to the LOTUS models of Godin-  
895 Beckmann (2022). Our trend analysis of stratospheric ozone records from the Umkehr, ozonesonde and COH station  
896 overpass data at 5 geographical regions using the Full Model (LOTUS v 0.8.0) show similar trends to those published  
897 in Godin-Beekmann et al. (2022) paper. We analyze trends for instrumental records converted to 7 Umkehr layers that  
898 represent ozone changes in the upper, middle and lower stratosphere over NH and SH middle latitudes and over high  
899 tropics of the NH. We also analyze GB station records at Arosa/Davos, Hohenpeißenberg and OHP separately in  
900 contrast to the “European regional” trend analyses presented in Godin-Beekmann et al. (2022) and included COH  
901 overpass records for comparisons with the GB records. Our analyses include evaluation of the adjusted  $R^2$  (aka  
902 goodness of the model fit), standard error and p-values.

903 We also investigate differences between satellite trends as detected in the records sampled for individual geographical  
904 locations (spatial and temporal overpass criteria) versus zonal average datasets. We find that COH overpass ozone  
905 records capture ozone variability of the ground-based station records (Umkehr and sonde) better than COH zonal data.  
906 We do not find that the COH zonal record is improved by using EqLat instead of geometric latitude to construct the  
907 dataset (see Appendix C), but EqLat can be an important additional proxy at some levels for GB data. To determine  
908 the improvement to the model fit we use the Standard Error and adjusted  $R^2$  for the Full and Reference model fit.  
909 Using the Reference model for the zonal mean COH data we find slightly better adjusted  $R^2$   
910 than for the COH overpass data fit over the Northern middle latitude stations. This is expected as much of the  
911 variability of the overpass time series is reduced in the zonal average data. Therefore, we also explore the impact of  
912 additional predictors in the trend model fit applied to the more variable GB and satellite COH overpass data to  
913 determine if that will reduce the SE and improve the adjusted  $R^2$ . We also apply the Full model to the zonally averaged  
914 data to assess the benefits of additional proxies to further reduce trend uncertainties.  
915 We find that adding predictors (with few exceptions) does not change the trends but often reduces SEs and increases  
916 the adjusted  $R^2$  (with the exception of the upper stratospheric ozone trends at MLO). We also find that the p-values  
917 are useful for interpretation of improvements of the model fit in the data, although improvements in the SE do not  
918 always result in improved confidence in derived trends, especially when the trends are close to zero. In these cases we  
919 conclude that either longer records are needed to discern trend information outside of the atmospheric noise or further  
920 research into the inconsistencies between instrumental records and homogenization procedures is required. We also  
921 find the small changes in trends in the lower stratosphere and improvements in the model fit after additional proxies  
922 are used. However, the sampling tests indicate that trends can depend on the temporal selection of the records when  
923 AK are used to smooth ozonesonde high resolution profiles (see discussion in Appendix D).  
924 This paper concludes that additional proxies bring improvements to trend detectability for GB and gridded satellite  
925 data analyses and better agreement is achieved between satellite overpass and GB trends. We also find that zonally  
926 averaged and gridded satellite records produce comparable trends over the studied middle latitudes and subtropical  
927 regions. Therefore, the GB trends are representative of the stratospheric ozone changes over the semi-global area.  
928 Finally, zonally averaged data do not benefit from addition of proxies beyond what LOTUS model uses for global  
929 trend detection whereas the uncertainties in GB and gridded trends are significantly reduced and sometimes (Boulder,  
930 MLO, Lauder) become comparable to the uncertainties of the zonally averaged trends in the upper and middle  
931 stratosphere. Based on analyses presented in this paper we strongly recommend using additional proxies for trend  
932 analyses of GB and gridded satellite stratospheric ozone records. Additional proxies should be selected based on the  
933 latitude and altitude of the observational ozone record to adequately represent stratospheric transport and mixing  
934 processes impacting interannual and seasonal ozone variability.

935 **Appendices**

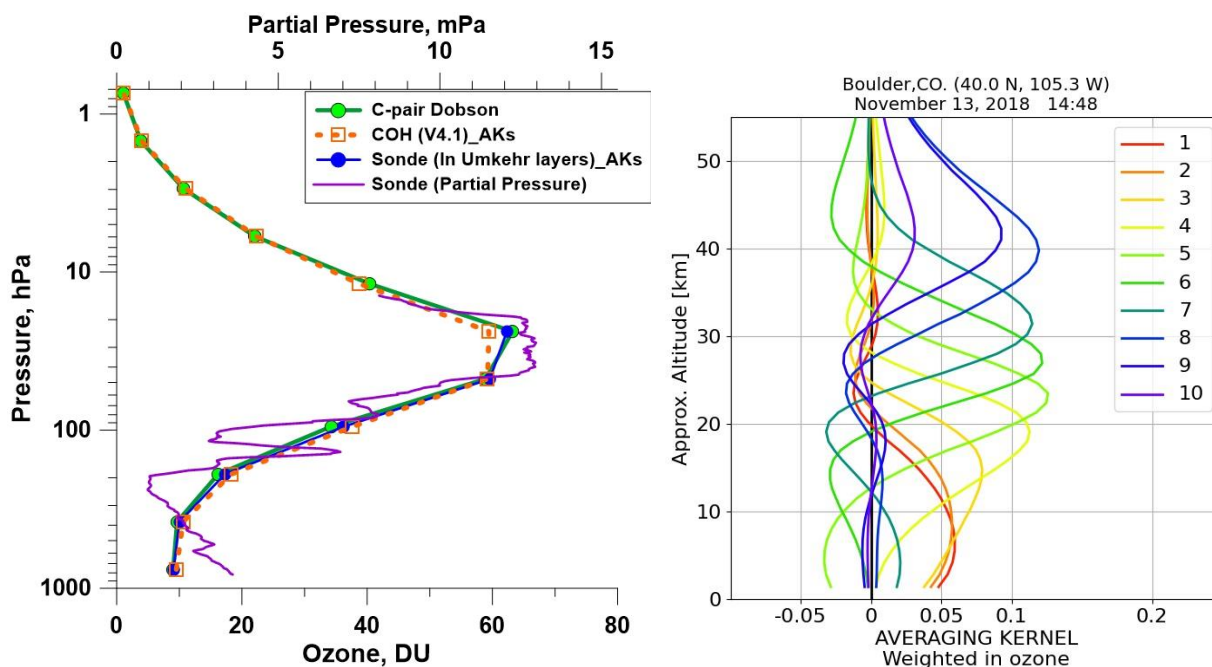
936 **Appendix A: AK Smoothing for ozonesondes**

937 Ozonesonde profiles have high vertical resolution (purple line in Fig. A1) in comparison to the Umkehr (green solid  
 938 line) or COH (orange dashed line) ozone profiles. Each Umkehr layer is referenced to the atmospheric pressure at the  
 939 bottom of the layer, which is constructed using half of the pressure in the layer below. Averaging Kernels (AK) as  
 940 shown in Fig. A1, panel b, define the granularity of the Umkehr vertical grid. In order to compare trends from three  
 941 instrumental records in the same vertical system, we convert the ozonesonde and COH profiles to the Umkehr layers  
 942 and DU. The COH overpass data is in units of DU, but on different layers than the defined Umkehr layers, so only  
 943 vertical grid modification is required. The sonde profiles (purple thin line) are in units of partial pressure and are first  
 944 converted to DU, then converted to the Umkehr grid (blue solid line in panel a). Conversion to the Umkehr grid can  
 945 be done either by interpolation, or by AK smoothing. The equation describing the process of applying AK smoothing  
 946 is

947 
$$Ozone_{smoothed}(i) = Ozone_{apriori}(i) + \sum_j AK_{ij} \{Ozone_{true}(j) - Ozone_{apriori}(j)\}$$

948

949 where AK is the Averaging Kernel for layer i,  $Ozone_{smoothed}$  is the smoothed ozone result,  $Ozone_{true}$  is the  
 950 ozonesonde profile, and  $Ozone_{apriori}$  is the Umkehr a priori (climatological) profile. The AK for each Umkehr layer  
 951 is used as a weighting function applied to the ozonesonde profile ( $Ozone_{true}$ ) prior to the integration which simulates  
 952 the Umkehr optimal estimation method used for estimating the ozone content in the targeted layer (Rodgers, 2000).  
 953



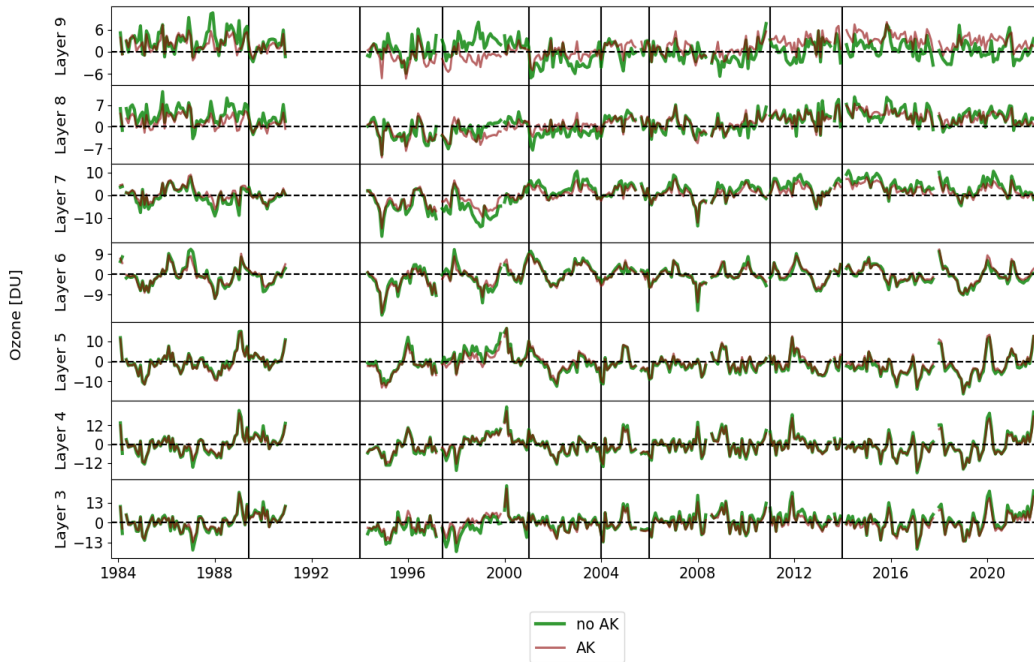
954

955 **Figure A1: a) An example of ozone observations over the Boulder, CO station. The purple line is 100-m averaged ozone**  
956 **partial pressure (hPa) vertical profile measured by sonde on 13 November, 2018 . The green line with solid circles is the**  
957 **ozone profile derived from Dobson Umkehr observations on the same day. The blue line with blue dots is the ozonesonde**  
958 **profile converted to the Umkehr layers and smoothed with the Umkehr AK. The orange dashed line with open squares is**  
959 **the COH ozone profile observed over Boulder on the same day and interpolated to the Umkehr layer vertical grid. b) The**  
960 **Umkehr AK for the ozone profile derived from observations in Boulder on 13 November, 2018. Each line represents the**  
961 **smoothing function for one of 10 Umkehr layers (see color legend).**

962 Although the ozonesonde measurement typically reaches altitudes between 32 and 10 hPa, the balloon often bursts  
963 before reaching the top of layer 6 (16 hPa), therefore only partially covering the ozone content in that layer. We also  
964 note that Umkehr AKs are relatively wide and therefore will incorporate (weight in) ozone variability from the layer  
965 above and layer below of the targeted Umkehr layer. (See layer 6, green line in Fig. A1, panel b.) Therefore, there  
966 are two sources of error in ozonesonde comparisons with Umkehr ozone in layer 6: a) burst level for ozonesonde does  
967 not reach the top of the layer 6, thus the integrated ozone is smaller than expected. b) the Umkehr AK for layer 6 is  
968 relatively wide and therefore the Umkehr layer partially contains information from above the burst altitude of the  
969 ozonesonde, thus making smoothed ozonesonde concentration lower than expected. In order to avoid these errors, we  
970 only show ozonesonde results up to layer 5.

971 Similarly, we explored smoothing COH profiles with Umkehr AKs. Figure A2 demonstrates the time series of the  
972 COH ozone over the Mauna Loa station. The trend model was fitted to the COH record with and without AK applied.  
973 The reference trend model included proxies and trends. To focus on ozone variability that contributes to the trends we  
974 subtracted the modeled ozone variability from the COH data and then added the trend component back. The COH  
975 record residuals in Fig. A2 are shown in Umkehr layers where COH is either smoothed with AK (red lines) or not  
976 (green lines). We notice that the AK-smoothing of the COH profile in layer 9 does not have a lot of independent  
977 information from layer 8. In this example it clearly shows that the trends in layer 8 are embedded in the COH layer 9  
978 ozone time series, which was confirmed when we compared trends derived from the AK-smoothed COH in layers 8  
979 and 9. In case of the integrated COH ozone record, the trends in layers 8 and 9 differed. In order to avoid biasing the  
980 COH trends at layer 9 we decided to not apply Umkehr AKs for COH smoothing and only use COH profiles  
981 interpolated into the Umkehr layers. This result makes sense since COH overpass data are derived from UV  
982 backscatter radiances also using an Optimal Estimation technique. COH overpass data has a comparable vertical  
983 resolution to Umkehr, simply with different layer definitions. Interpolation makes the most sense for rendering COH  
984 data in the Umkehr vertical coordinate system.

COH Time Series at Mauna Loa, Proxy Tested: AKs



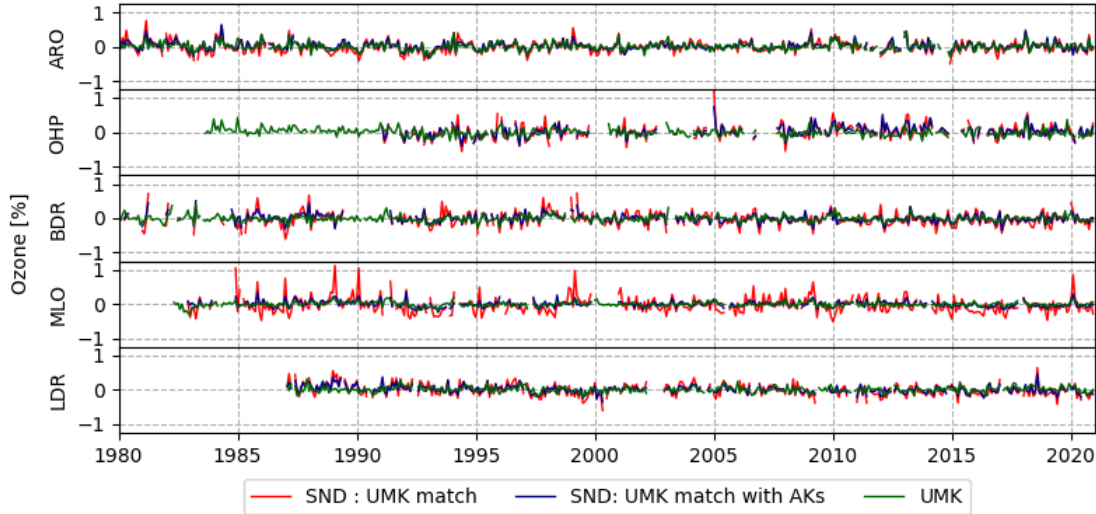
985

986 **Figure A2: Modified residuals (seasonal cycle, Solar, QBO, and ENSO are removed, but trend is retained) of COH overpass**  
 987 **data at Mauna Loa (20N, 156W). Red: AK smoothed to Umkehr layers; Green: Interpolated to Umkehr layers. Vertical**  
 988 **lines show the dates of satellite records in COH. The largest impact of the AK is seen between 1997 and 2001 where two**  
 989 **curves separate in layers 7, 8 and 9, and also after 2001 in layer 9.**

990 Figure A3 demonstrates time series of monthly mean ground-based records the lower stratosphere at 5 stations. The  
 991 Umkehr data (blue) are compared with the ozonesonde anomalies either interpolated to the Umkehr layer 3 (green),  
 992 or ozonesonde profiles matched with Umkehr profiles in time and smoothed using the Umkehr averaging kernels  
 993 (crimson). All three datasets have been deseasonalized using their respective climatological (using 1998-2008  
 994 climatology) average monthly mean ozone. The application of the Averaging Kernels has the effect of smoothing the  
 995 temporal variability.



### Deseasonalized Time Series: Comparisons between UMK and SND : Layer 3



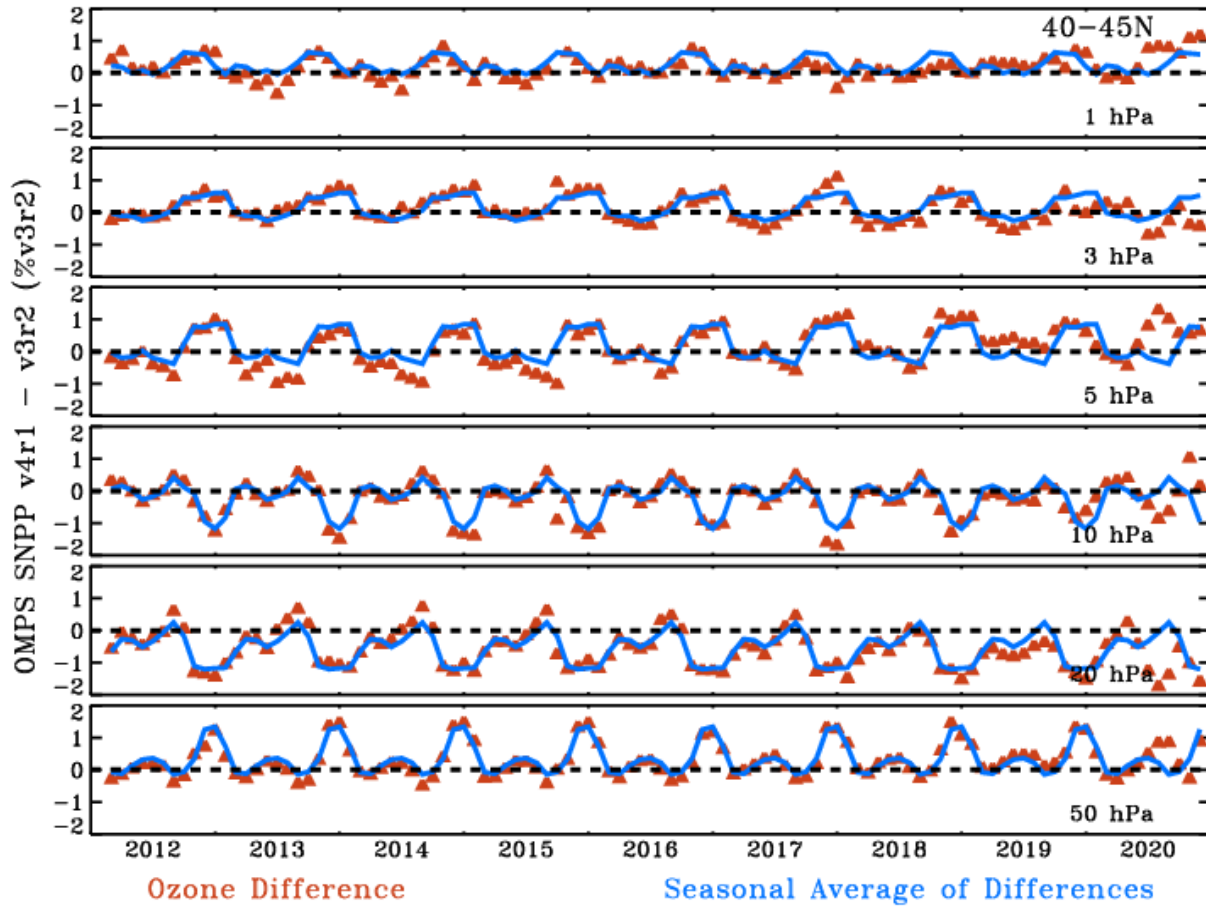
996

997 **Figure A3: Time series of monthly averaged and de-seasonalized (in %) ozone anomalies of Umkehr (green) and**  
998 **ozonesondes records are compared at 5 ground-based stations. Ozonesonde data are either calculated using only profiles**  
999 **that are interpolated in Umkehr layer 3 (blue) or matched with Umkehr profile in time and smoothed with the Umkehr**  
1000 **averaging kernels (crimson).**

### 1001 **Appendix B: COH using OMPS v3r2 vs OMPS v4r1**

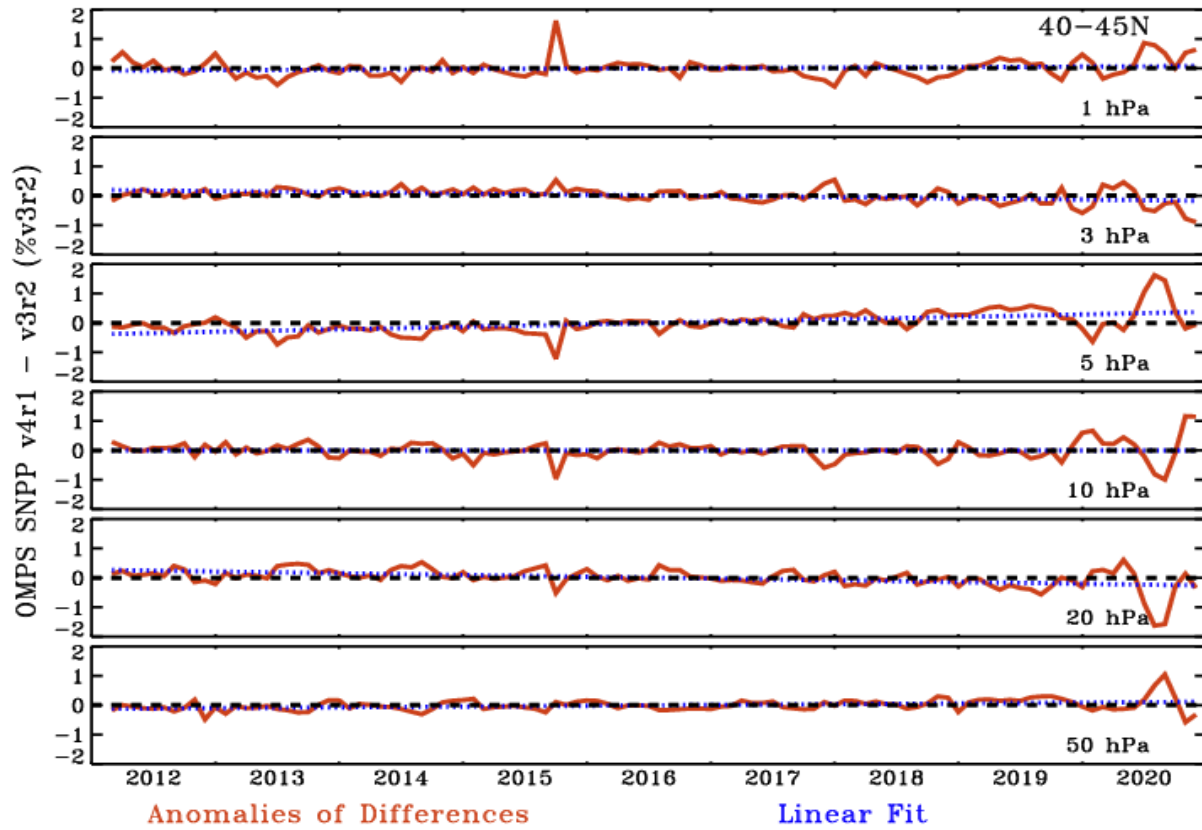
1002 OMPS SNPP v4r1 uses updated SDRs as input which incorporate unified and consistent calibration algorithms  
1003 removing artificial jumps caused by operational changes, instrument anomalies, or contamination for anomaly views  
1004 of the environment or spacecraft. Also included are new interpolated band-passes, and updated soft calibration based  
1005 on the new input SDR's.

1006 Differences between the v3r2 and v4r1 versions of the resulting COH dataset are typically less than 1 percent (Fig.  
1007 A4 and A5). Small seasonal variation is apparent at all levels. Larger differences are visible in 2020 when the soft  
1008 calibration for v3r2 is extended beyond its period of relevance. Figure A6 shows the drift between the two versions.  
1009 Drift between the datasets is less than +/- 1% at all levels. This is a reasonable estimate of the resulting expected trend  
1010 difference in using the newest COH version as compared to the v3r2 results used in Godin-Beekmann (2022).



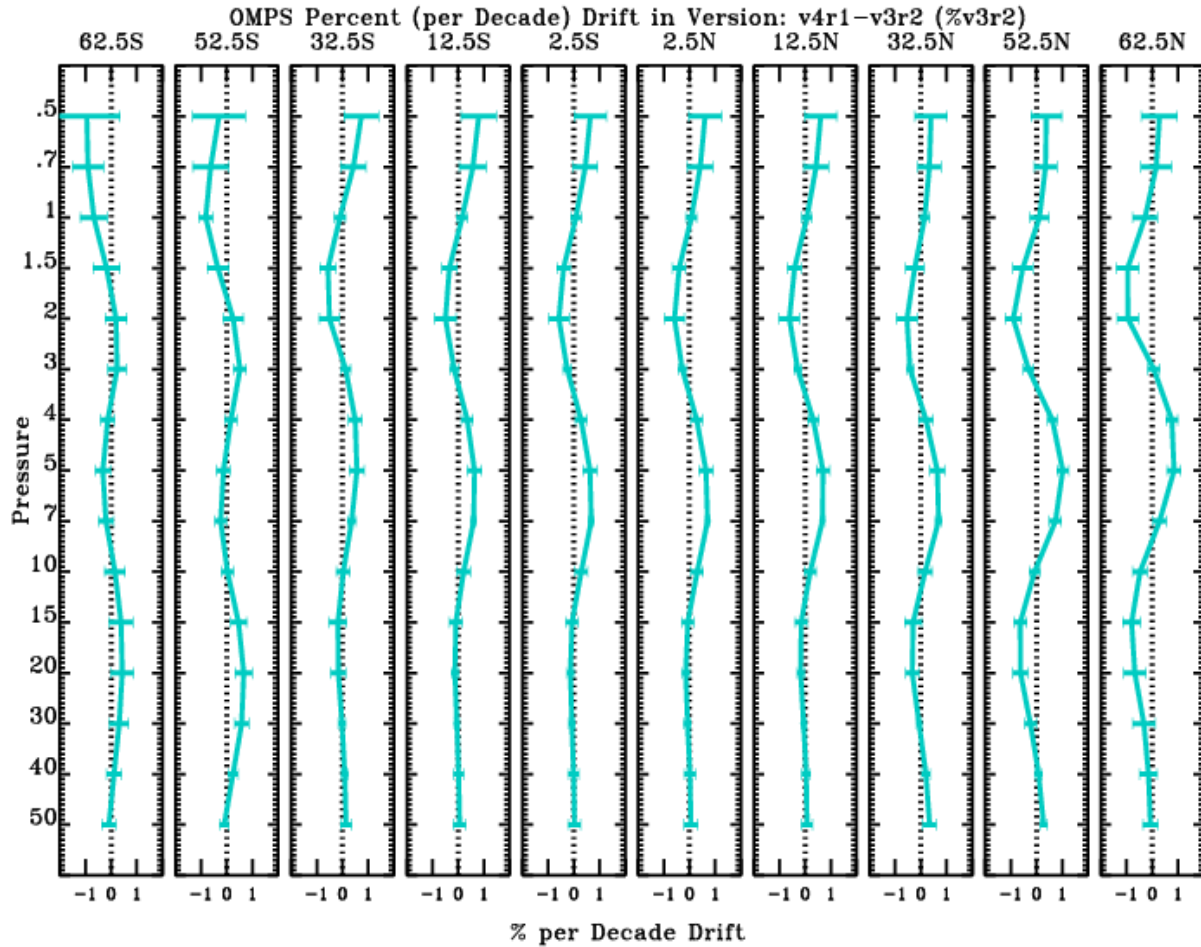
1011  
 1012  
 1013  
 1014  
 1015  
 1016  
 1017

Figure A4: Differences in the COH monthly average zonal product as generated from SNPP v4r1 and v3r2 processing. Also shown is the annual cycle in this difference as depicted by the average over all years for each month. Exhibited at 40-45N is a less than 2% difference with an annual cycle. A somewhat different pattern is seen in 2020 where the soft calibration for v3r2 is extended beyond its period of relevance.



1018  
 1019  
 1020  
 1021

Figure A5: Anomalies of the differences in version (v4r1 vs v3r2) in the COH monthly average zonal product at 40-45N. Anomalies are enhanced in 2020. Also shown as a blue dotted line is a linear least square fit to the anomalies representing the drift between the two versions.



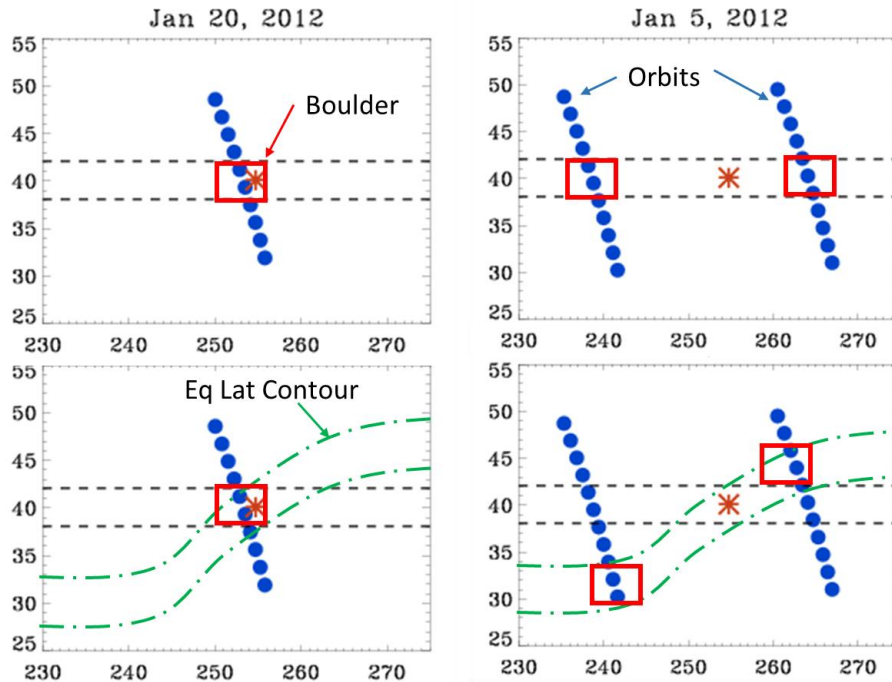
1022

1023 **Figure A6 shows the drift between the two versions (v4r1 vs v3r2) as function of pressure level at 10 latitudes.**

1024 **Appendix C: Impact of using equivalent latitude in generation of the COH product**

1025 The COH overpass data used in this paper collects all profiles during the day within a latitude and longitude box of  
 1026 +/- 2 degrees by +/- 20 degrees, then generates a 1/distance averaged value for the station. The box is based on  
 1027 geometric latitude and longitude. With 15 orbits per day, the chosen box size guarantees 2 to 4 possible profiles within  
 1028 the box depending on whether the orbit overpasses or straddles the site as shown in Fig. A7. Also shown is a scenario  
 1029 when the equivalent latitude (EqLat) near the site is particularly non-zonal. In such cases the profiles selected using  
 1030 a geometric coordinate box will select SBUV profiles from an Eq Lat that is different from that of the measurement  
 1031 station.

1032



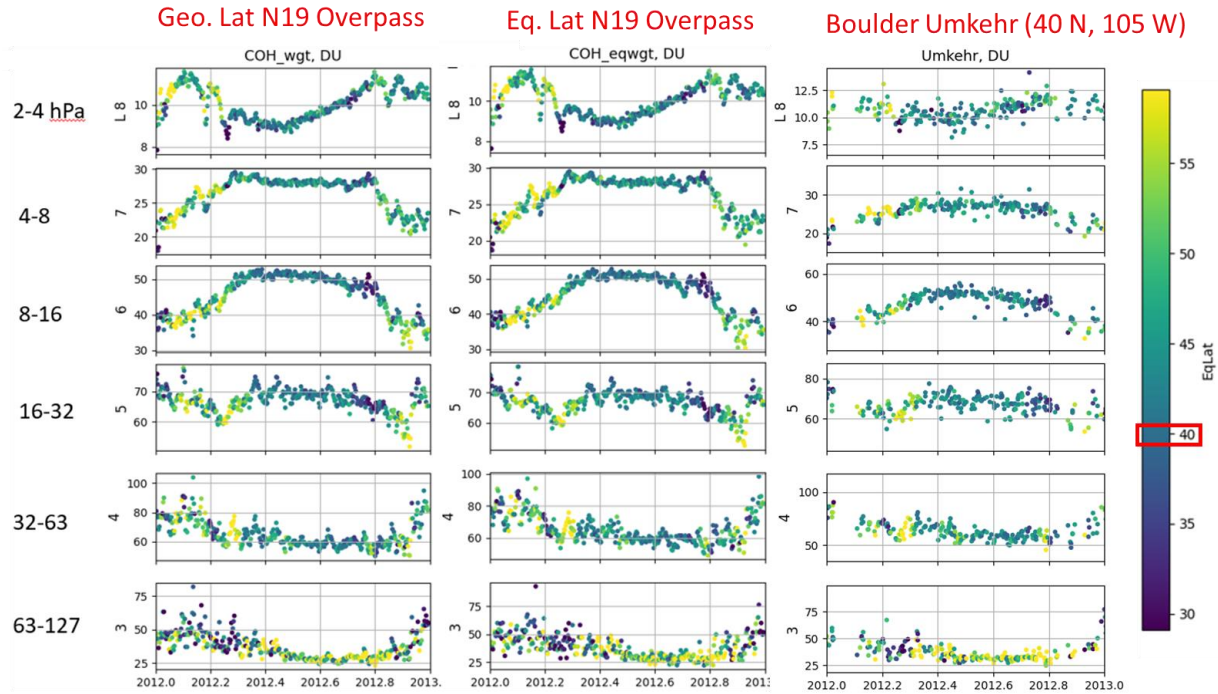
1033

1034 **Figure A7: Shows orbits of SNPP and positions of OMPS NP ozone profiles on January 20, 2012 and January 5, 2012. The**  
 1035 **second row displays a possible EqLat contour overlaid.**

1036 It is informative to create an overpass product using boxes based on EqLat and determine the impact on the data.  
 1037 Since EqLat is layer dependent, the included profiles must be selected independently for each layer. Figure A8 shows  
 1038 COH overpass data for Boulder using geometric coordinates, EqLat based coordinates, and the associated Umkehr  
 1039 data. Color coding shows the EqLat at Boulder for each measurement day with dark blue and yellow indicating days  
 1040 with extreme variation from 40N.

1041

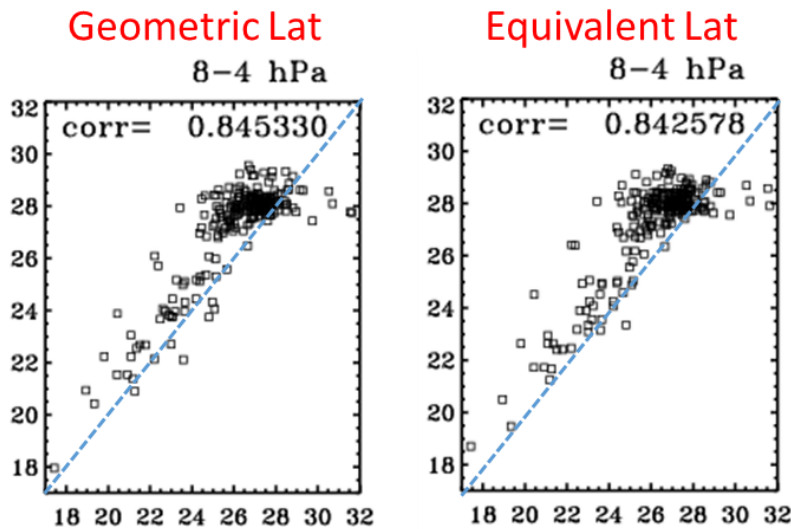
1042



1043

1044 **Figure A8: COH overpass data generated with geometric coordinates, EqLat based coordinates, and the associated Umkehr**  
 1045 **dataset at Boulder for 2012. Data points are color coded for the EqLat at the measurement site. Boulder is at 40 N.**

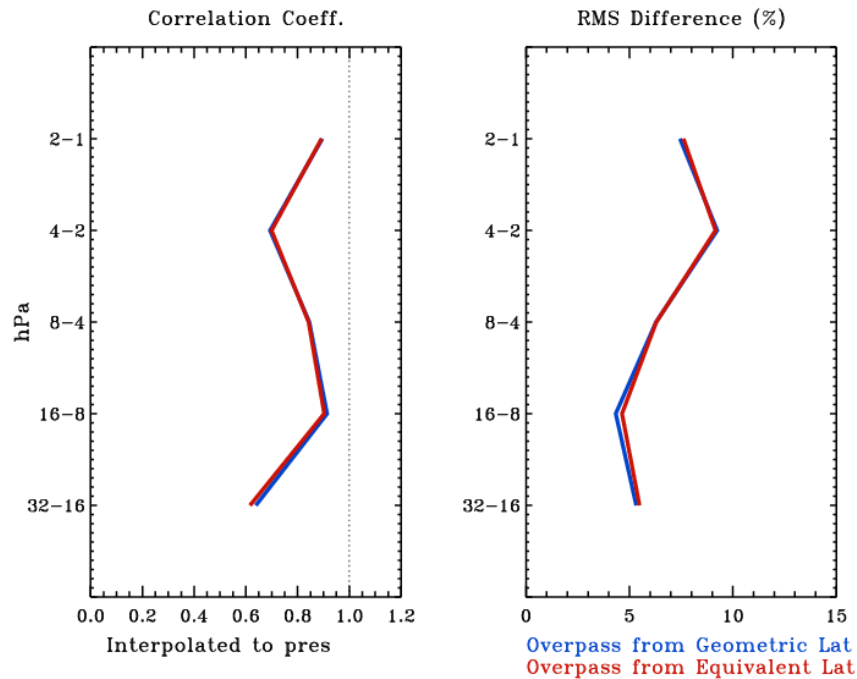
1046 Variation in EqLat is most apparent in Winter months and transitional Fall and Spring, less so in Summer. Yet the  
 1047 value of the COH ozone is not dramatically altered in the time series. Figure A9 shows correlation plots of the COH  
 1048 overpass to Umkehr for the data at layer 7 (4-8 hPa). The pattern of the scatter and the value of the correlation  
 1049 coefficient are not substantially altered for overpass determination using geometric latitude (left) and EqLat (right).  
 1050 Figure A10 shows the vertical distribution of the Correlation coefficient and the RMS Difference for the two COH  
 1051 datasets vs Umkehr. These two metrics are minimally impacted for this sample year in the layers where COH is valid.  
 1052



1053

1054 **Figure A9: Correlation between Umkehr and COH overpass using Geometric Latitude (left) and EqLat (right) to select**  
 1055 **included profiles for layer 7 (4-8 hPa).**

1056



1057 **Figure A10: Profiles of Correlation coefficients and RMS differences between COH overpass data at Boulder for 2012 using**  
 1058 **Geometric Latitude (blue) and EqLat (red) to select data points included in the average.**  
 1059

1060  
 1061 The use of geometric latitude appears to be sufficient in the choice of included data points in the overpass COH product  
 1062 at the layers used in this paper. Likely this is a ramification of the smooth horizontal resolution of the satellite product.

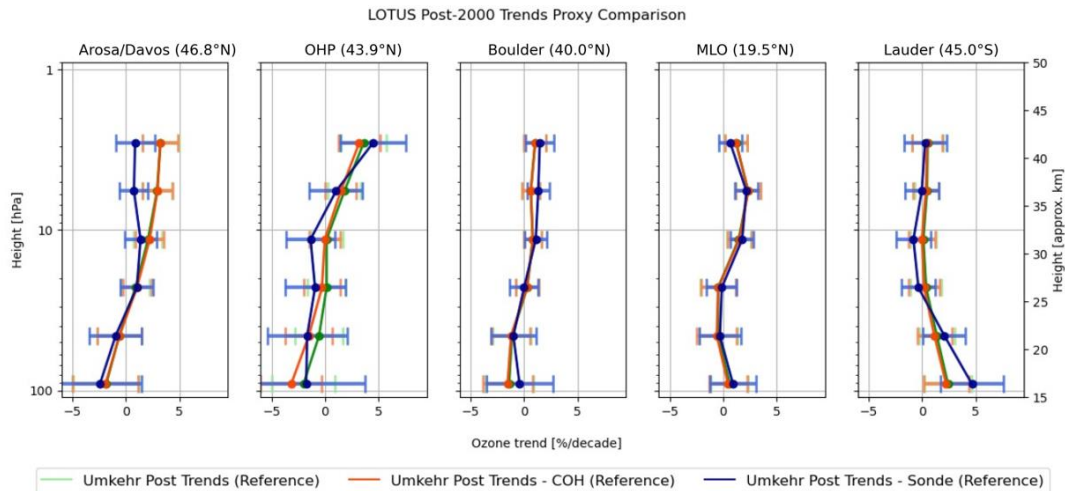
1063 **Appendix D: Temporal Sampling and Impact on Trends**

1064 This paper compares trends for three instrument types each with differing measurement frequency. From each set of  
 1065 measurements a monthly average is constructed. See the data files at  
 1066 [https://gml.noaa.gov/aftp/ozwv/Publications/2023\\_Umkehr\\_Ozone\\_Trends\\_Paper/](https://gml.noaa.gov/aftp/ozwv/Publications/2023_Umkehr_Ozone_Trends_Paper/) for the data and the number of  
 1067 data points in each monthly average with the sampling variations. Umkehr measures once or twice per day depending  
 1068 on cloud interference with the measurement. At Arosa/Davos and Lauder, Umkehr measurements are sparser than  
 1069 the other GB stations, often less than 10 per month. At Boulder beginning in 1983 measurements number 20 or more  
 1070 per month. At OHP the Umkehr record begins in 1983 with a strong 20 or more measurements per month. From  
 1071 1999 to 2016, however, measurements per month are often less than 15 per month. The most Umkehr measurements  
 1072 at MLO are the most abundant, especially after 1985 measuring multiple times in a day, resulting in 50-70 data points  
 1073 contributing to the monthly average. The COH overpass dataset is typically available once per day at each station with  
 1074 occasional misses, contributing usually 27-30 data points per month. Since Umkehr can measure multiple times per  
 1075 day, the COH data matched to Umkehr can contain more profiles in the monthly average than the original full COH  
 1076 data, since the COH overpass data will appear twice in the monthly average, once per each Umkehr measurement.

1077 This occurs often at MLO. Ozonesonde launches are typically one to three times per week depending on the station.  
1078 At Arosa/Davos, sonde measurements are typically about 15 per month. Sonde measurements at the other stations  
1079 usually have approximately 5 measurements per month, with some periods of up to 10 per month. As with COH  
1080 overpass measurements, the sonde dataset matched to Umkehr can have more contributions to the monthly average  
1081 resulting from dates with more than one Umkehr measurement, resulting in multiple sonde matches.  
1082 The trend results in this paper use all available Umkehr data to generate the monthly means. The COH and sonde data  
1083 are matched to Umkehr to use the Umkehr temporal sampling for COH, and to be able to use the Umkehr averaging  
1084 kernels for sonde. It is important to determine how the temporal sampling within the monthly mean data may impact  
1085 trend results. To aid this understanding, we create three subsets of Umkehr data each with different temporal sampling  
1086 and create the corresponding monthly mean: 1) all observations in Umkehr record; 2) Umkehr matched to the COH  
1087 dataset; and 3) Umkehr matched to the sonde dataset. In this way we use the same data, but only vary the temporal  
1088 sampling. Since the COH is measured every day, except in the rare case that the satellite data is missing due to  
1089 instrument issues, sampling 1 and 2 should provide nearly identical results. We expect a strong change in the monthly  
1090 mean and resulting trends for Umkehr record when it is matched with infrequent sampling of ozonesonde profiles  
1091 (especially in Boulder, Hilo and Lauder).

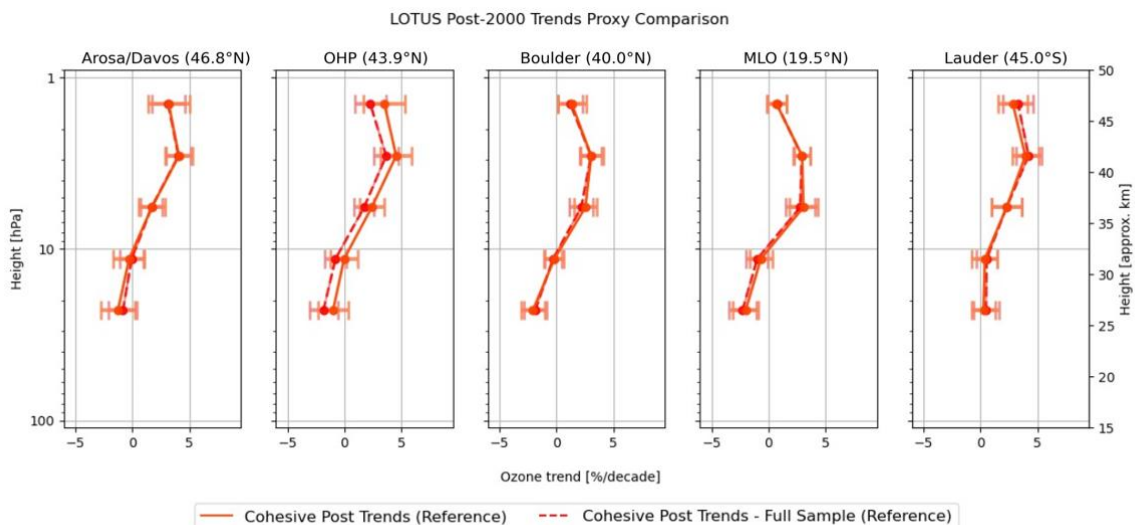
1092 Figure A11 summarizes the results. Each line in Fig. A11 is trend derived from Umkehr data, but with sampling of all  
1093 data, data matched to COH dates, and data matched to sonde dates. In general, the differences are within the envelope  
1094 of trend uncertainty ( $\pm 2$  std errors). As expected, the trends and standard errors for all (green) and COH-matched  
1095 subsampled (orange) Umkehr records are nearly the same. The largest differences in all Umkehr and COH matched  
1096 Umkehr lines are apparent at OHP. We have determined that this arises from occasional months when there is a short  
1097 satellite outage coupled with sparse Umkehr observations at the station. However, trends derived from sonde-matched  
1098 Umkehr data (blue) show deviations from other observations. This is especially clear at Arosa/Davos in the upper  
1099 stratosphere ( $\sim 2-3\%$  above 10 hPa). But since this is above the measurement capability of the ozonesonde, this will  
1100 not impact the ozonesonde trend results at Arosa/Davos. At Lauder the most significant differences are seen in layer  
1101 3 (2.5%), but unfortunately not in the direction to explain sonde differences in the Lauder trend curves as compared to  
1102 Umkehr. Smaller differences are seen at other layers (very small, less than 1 %, differences in layers 6 and 4). At  
1103 OHP small differences of less than 1 % are seen between 50 and 10 hPa, well within error estimates.





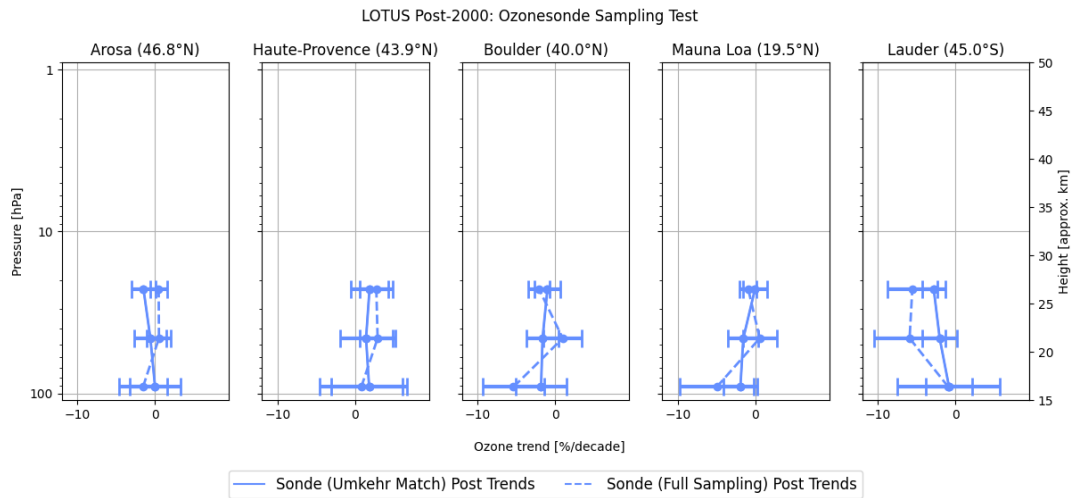
1104  
 1105 **Figure A11: Trend results for the Reference Model using Umkehr data mimicking the temporal sampling of COH and**  
 1106 **sonde. Green is all available Umkehr data; orange is Umkehr data matched to COH measurements dates; blue is Umkehr**  
 1107 **data matched to sonde measurement dates.**

1108 Figure A12 further explores sampling differences by examination of trends of COH data using the full COH dataset,  
 1109 and data sampled to the Umkehr dates in generation of the monthly mean datasets. As with Fig A11, the trend lines  
 1110 are nearly identical at all stations except OHP. At OHP in the early 2000's there are significantly fewer COH points  
 1111 matched to Umkehr because of the drop in Umkehr measurements. This likely impacts the post-2000 trend estimate.  
 1112 The differences remain below 2%, and are within the error estimate of the trends. In summary, the sampling biases  
 1113 between COH overpass and Umkehr data cannot explain the difference in the derived trends (see Fig. 3, most notable  
 1114 in layers 7 and 8 at Boulder and Lauder).  
 1115



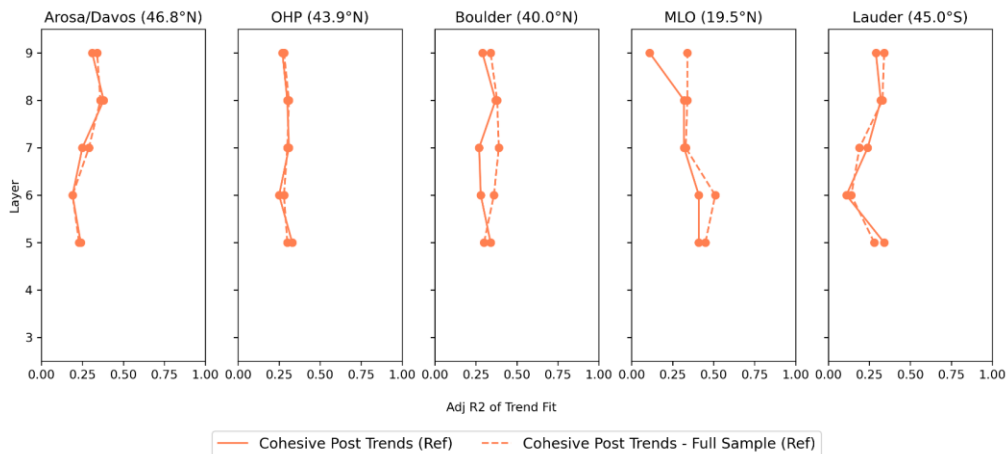
1116  
 1117 **Figure A12: Trend results for the Reference Model exploring variations in sampling of the COH data. Solid orange is COH**  
 1118 **data matching Umkehr sampling; dotted orange is all available COH data.**

1119 Figure A13 explores the impact on trends from sampling differences of the sonde data. Shown are trends with all  
 1120 sonde data, and trends with Umkehr matched data. In this figure only, the sonde data is not AK smoothed since the  
 1121 Umkehr AK are only available on dates when there is an Umkehr measurement. So shown here are trends from sonde  
 1122 data integrated to the Umkehr levels. As with Fig. A11 the only visible impact is seen at OHP and Lauder, though  
 1123 both are within error estimates. At Lauder the trends remain negative for both samplings, but sonde sampled to  
 1124 Umkehr moves closer to the zero line. At OHP the sonde trends are positive, but sonde sampled to Umkehr moves  
 1125 slightly closer to zero. The sampling impact on trends for both OHP and Lauder are likely due to the reduced number  
 1126 of Umkehr data at these sites.



1127  
 1128 **Figure A13: Trend results for Reference model exploring sampling of the sonde data. Solid blue is all sonde data; dashed**  
 1129 **is Umkehr matched sonde data.**

1130 Figure A14 explores the impact of sampling on the adjusted  $R^2$  using the COH overpass data. Shown are the adjusted  
 1131  $R^2$  for all available COH overpass data, and the same using only COH overpass with matches to the Umkehr data. For  
 1132 Arosa/Davos, OHP and Lauder the differences are small. For Boulder and MLO at some layers (Boulder, layers 6,7;  
 1133 MLO layers 6,9), the impact is more apparent with the Full COH exhibiting higher adjusted  $R^2$  at these stations.



1135 **Figure A14: Adjusted R<sup>2</sup> for the Reference Model exploring variations in sampling of the COH data. Solid orange is COH**  
 1136 **data matching Umkehr sampling; dotted orange is all available COH data.**

1137 **Appendix E: Decision process for the Full Model**

1138 The LOTUS styled Reference Model is developed and optimized for zonal average datasets. The Extended Model  
 1139 tests the addition of single predictors to see if fit statistics can be improved for GB and overpass datasets. For  
 1140 Tropospheric Pressure (TP), improvements are consistent among layers and among instrument types. The addition of  
 1141 EqLat also yields consistent results for instrument types and at most stations, though not Mauna Loa. Addition of  
 1142 other predictors gives mixed results depending on level and station. The potential for improving confidence in trend  
 1143 results exists by combining predictors using different choices depending on layer and station. We choose additional  
 1144 predictor combinations with consideration of three criteria: 1) combined predictors should not have a high correlation  
 1145 with each other (usually .2 or less); 2) predictors should reduce the SE of the trend consistently for all instrument  
 1146 types; 3) addition of the predictor should not greatly reduce the adjusted R<sup>2</sup> of the model fit, but preferentially increase  
 1147 it. As seen in Tables 7e and 7f the NAO and the EHF predictors do not make a significant improvement when added  
 1148 to the Reference Model, so we do not include either in the Full Model.

1149 **Mixed Model:**

1150 We have noted a high correlation between the TP and EqLat predictors at all levels especially for Boulder, Mauna  
 1151 Loa and Lauder with correlation adjusted R<sup>2</sup> of .4 to .7, and somewhat less correlated at Arosa/Davos and OHP with  
 1152 adjusted R<sup>2</sup> of .2 and .3. Subsequently, we choose to not use these two predictors together (at the same station/layer  
 1153 combination). The addition of TP at all stations for layers 3 and 4 uniformly decreases the standard errors at all  
 1154 stations for both Umkehr and sonde. The addition of EqLat (with the exception of Umkehr at Boulder, level 5) almost  
 1155 uniformly decreases the standard errors at all stations for layers 5 and 6. There is additional reduction in the SE for  
 1156 layers 7 to 9 for all stations except at Mauna Loa. Thus, we choose TP and EqLat as additional predictors at these  
 1157 layers. QBO C and D, have significant impact in decreasing the SE in layers 4 and 5 for both Umkehr and sonde, and  
 1158 layer 3 for sonde with only a small degradation for Umkehr. QBO-CD shows an improvement in layer 8 at OHP, both  
 1159 COH and Umkehr, and Arosa/Davos and Boulder for COH only. We have tested adding both QBO and EqLat for  
 1160 layer 8 at these 3 stations. For Umkehr measurements, there is no improvement beyond EqLat only with QBO-CD  
 1161 also included. For COH there is additional improvement, but not to the extent of QBO-CD alone. Since the  
 1162 improvement is limited to one layer, and for only COH, we choose to only add the additional QBO-CD for the tropical  
 1163 MLO. Table A1 shows the resulting combination of additional predictors for this Mixed Model.

1164

<b>LOTUS Mixed Model</b>					
<b>Layer</b>	<b>Arosa/Davos</b>	<b>OHP</b>	<b>Boulder</b>	<b>MLO</b>	<b>Lauder</b>
<b>9</b>	EqLat	EqLat	EqLat	Ref	EqLat
<b>8</b>	EqLat	EqLat	EqLat	Ref	EqLat
<b>7</b>	EqLat	EqLat	EqLat	Ref	EqLat

6	EqLat	EqLat	EqLat	EqLat	EqLat
5	EqLat	EqLat	EqLat	EqLat, QBO CD	EqLat
4	TP	TP	TP	TP, QBO CD	TP
3	TP	TP	TP	TP, QBO CD	TP

1165

1166 **Table A1: Details of additional predictor combinations for each level and station in the Mixed Model**

1167 The resulting change in SE from the Reference Model is shown in Table A2. For most stations/layers this is simply a  
 1168 composite of the values from the single EqLat or TP Extended Model results. There remain a few  
 1169 instrument/station/layers where the SE is slightly increased - Arosa/Davos Umkehr layer 8 and Boulder Umkehr layer  
 1170 8, but these are negligible. At Boulder Layer 5 Umkehr the increase in SE is somewhat more at 1.85% difference, but  
 1171 this is still small enough to not be of great concern. For Mauna Loa at layers 3,4 and 5 the model is rerun adding two  
 1172 predictors together and the results are new. Indeed, in these cases the SE is improved beyond the single predictor  
 1173 results of either QBO alone, or TP or EqLat alone with the exception of Sonde layer 5 where the change in SE is just  
 1174 slightly degraded from QBO alone (13.42% vs 13.69% reduction in SE).

LOTUS Model Test: Difference [%] in Standard Error: Mixed Model vs Reference Model																
Pressure	Umkehr	Arosa/Davos			Haute-Provence			Boulder			Mauna Loa			Lauder		
(hPa)	Layer	UMK	COH	SND	UMK	COH	SND	UMK	COH	SND	UMK	COH	SND	UMK	COH	SND
1-2	9		8.4			2.8			1.9			0.0			2.9	
2-4	8	-0.5	0.7		0.1	1.0		-0.4	1.5		0.0	0.0		1.0	3.1	
4-8	7	3.8	3.0		2.1	1.9		5.4	4.1		0.0	0.0		0.5	1.2	
8-16	6	6.1	8.4		2.5	10.8		2.4	7.8		5.3	0.8		3.4	7.7	
16-32	5	7.9	10.8	5.9	1.9	13.3	8.7	-1.9	0.0	0.9	6.6	11.1	13.4	0.8	3.9	
32-63	4	6.6		6.1	5.9		9.9	3.4		3.0	17.3		9.7	8.0		4.1
63-127	3	12.8		10.2	12.8		10.7	6.8		2.5	8.0		4.2	9.8		4.4

1175

1176 **Table A2: Change in the SE of the trend using the Mixed Model.**

1177 Table A3 shows the adjusted R<sup>2</sup> for the proposed Mixed Models. Similarly to the change in SE (Table A2), the  
 1178 adjusted R<sup>2</sup> is a composite of the individual EqLat or TP results from the extended model with the exception of the  
 1179 results for layers 3, 4, and 5 at Mauna Loa where both predictors are included concurrently. At these layers the  
 1180 adjusted R<sup>2</sup> in some cases matches the higher Adj R<sup>2</sup> values of the two predictors, and in others improves with the  
 1181 combination of QBO and TP or EqLat.

LOTUS Model Proxy Tests: (Adjusted R <sup>2</sup> of Model)																
Height	Umkehr	Arosa/Davos			OHP			Boulder			MLO			Lauder		
(hPa)	Layer	UMK	COH	SND	UMK	COH	SND	UMK	COH	SND	UMK	COH	SND	UMK	COH	SND
1-2	9		0.42			0.37			0.36			0.11			0.32	
2-4	8	0.23	0.39		0.14	0.31		0.17	0.39		0.11	0.32		0.18	0.34	
4-8	7	0.35	0.35		0.31	0.41		0.27	0.33		0.26	0.32		0.17	0.27	
8-16	6	0.31	0.35		0.33	0.45		0.33	0.40		0.40	0.51		0.25	0.23	
16-32	5	0.34	0.38	0.26	0.25	0.51	0.23	0.31	0.40	0.19	0.40	0.35	0.37	0.42	0.41	0.24
32-63	4	0.21		0.22	0.29		0.25	0.19		0.13	0.34		0.35	0.42		0.25

63-127	3	0.24		0.23	0.42		0.17	0.22		0.13	0.14		0.21	0.25		0.19
--------	---	------	--	------	------	--	------	------	--	------	------	--	------	------	--	------

1182 **Table A3: Adjusted R<sup>2</sup> for the Mixed Model**

1183 **Augmented Mixed Model**

1184 It is hard to ignore the substantial reduction of SE when adding the AO/AAO predictor especially for layers 3,4 and 5  
 1185 at Mauna Loa, and for layers 3 and 4 at Arosa/Davos. The results for OHP layers 3 and 4 are still compelling, though  
 1186 somewhat less so. So we explore the addition of AO/AAO at these three stations only, for the layers specified. **Table**  
 1187 **A4** summarizes the predictor choices for this Augmented Mixed Model.

1188  
 1189

LOTUS Augmented Mixed Model					
	Arosa/Davos	OHP	Boulder	MLO	Lauder
Layer					
9	EqLat	EqLat	EqLat	Ref	EqLat
8	EqLat	EqLat	EqLat	Ref	EqLat
7	EqLat	EqLat	EqLat	Ref	EqLat
6	EqLat	EqLat	EqLat	EqLat	EqLat
5	EqLat	EqLat	EqLat	EqLat, QBO, AO/AAO	EqLat
4	TP, AO/AAO	TP, AO/AAO	TP	TP, QBO CD, AO/AAO	TP
3	TP, AO/AAO	TP, AO/AAO	TP	TP, QBO CD, AO/AAO	TP

1190 **Table A4: Details of additional predictor choices for each level and station in the Augmented Mixed Model . This differs**  
 1191 **from Table A1 by adding AO/AAO at some levels for Arosa/Davos, OHP and Mauna Loa.**

LOTUS Model Test: Difference [%] in Standard Error: Full Model vs Reference Model																
Pressure	Umkehr	Arosa/Davos			Haute-Provence			Boulder			Mauna Loa			Lauder		
(hPa)	Layer	UMK	COH	SND	UMK	COH	SND	UMK	COH	SND	UMK	COH	SND	UMK	COH	SND
1-2	9		8.4			2.9			1.9			0.0			2.9	
2-4	8	-0.5	0.7		0.1	1.2		-0.4	1.5		0.0	0.0		1.0	3.1	
4-8	7	3.8	3.2		2.1	0.6		5.4	4.1		0.0	0.0		0.5	1.2	
8-16	6	6.1	8.3		2.5	10.9		2.4	7.8		5.3	7.8		3.4	7.7	
16-32	5	7.9	10.6	5.9	1.9	13.4	8.7	-1.9		1.4	13.6	13.0	13.3	0.8	3.9	-1.1
32-63	4	8.7		10.0	6.1		9.4	3.4		2.7	17.3		10.3	8.0		7.4
63-127	3	20.3		18.5	13.5		12.8	6.8		2.2	8.0		5.6	9.8		6.8

1192  
 1193 **Table A5 (the same as Table 9): Change in the SE of the trend using the Augmented Mixed Model.**

1194  
 1195 Table A5 displays the change in the SE from the Reference Model now for the Augmented Mixed Model. Adding  
 1196 AO/AAO at Arosa/Davos (layers 3 and 4) and Mauna Loa (layers 3 to 5) greatly reduces the SE beyond that of the  
 1197 Mixed Model results in Table A2. For OHP (layers 3 and 4) the impact is less dramatic for Umkehr. For sonde  
 1198 measurements at layer 4 the AO/AAO addition has no impact beyond the Mixed Model; for layer 3 the addition of  
 1199 AO/AAO results in less reduction of the SE.

LOTUS Model Proxy Tests: (Adjusted R <sup>2</sup> of the Augmented Mixed Model)																
Height	Umkehr	Arosa/Davos			OHP			Boulder			MLO			Lauder		
(hPa)	Layer	UMK	COH	SND	UMK	COH	SND	UMK	COH	SND	UMK	COH	SND	UMK	COH	SND
1-2	9		0.42			0.37			0.36			0.11			0.32	
2-4	8	0.23	0.39		0.14	0.31		0.17	0.39		0.11	0.32		0.18	0.34	
4-8	7	0.35	0.35		0.31	0.41		0.27	0.33		0.26	0.32		0.17	0.27	
8-16	6	0.31	0.35		0.33	0.45		0.33	0.40		0.40	0.51		0.25	0.23	
16-32	5	0.34	0.38	0.26	0.25	0.51	0.23	0.31	0.40	0.18	0.44	0.53	0.39	0.42	0.41	0.29
32-63	4	0.23		0.25	0.29		0.27	0.19		0.18	0.42		0.38	0.42		0.31
63-127	3	0.31		0.31	0.44		0.21	0.22		0.11	0.19		0.24	0.25		0.21

1200 **Table A6 (The same as Table 12): Adjusted R<sup>2</sup> for the Augmented Mixed Model**

1201 Table A6 displays the Adj R<sup>2</sup> for the Augmented Mixed Model. Adding AO/AAO improves the Adj R<sup>2</sup> results for  
 1202 Arosa/Davos and MLO and has little to no impact at OHP. Based on the criteria outlined at the beginning of this  
 1203 appendix, we assign the Augmented Mixed Model as the ‘Full Model’ in the body of this paper.  
 1204

1205 **Code/Data availability:** All dataset used in this study are publicly available from [https://doi.org/10.15138/1FF4-](https://doi.org/10.15138/1FF4-HC74)  
 1206 [HC74](https://doi.org/10.15138/1FF4-HC74).

1207 **Competing interests:** The authors declare that they have no conflict of interest.

1208 **Author contributions:** IP and JW conceptualized the paper, and IP led the paper preparation. PE, KA, and JW  
 1209 performed the data analysis. KM is responsible for the production of the spatial and temporally matched ground-based  
 1210 and satellite ozone profile data. JW is responsible for producing COH zonally averaged and station overpass ozone  
 1211 profile records. LF is responsible for the retrieval and calibration of the OMPS data. GM, PE, KM and KA are  
 1212 responsible for NOAA Umkehr measurements. EMB is responsible for measurements in Arosa/Davos. RQ is  
 1213 responsible for Umkehr and ozonesonde observations in Lauder, New Zealand. BJ and PC are responsible for  
 1214 ozonesonde observations in Boulder and Hilo. GA is responsible for the ozonesonde observations in OHP. RVM is  
 1215 responsible for HEGIFTOM ozonesonde records and data analyses. RD, SGB, DZ provided context of the LOTUS  
 1216 model use and interpretation of trend analyses. All authors contributed to the writing of the paper.

1217 **Acknowledgements:**

1218 This study was supported in part by NOAA grant NA19NES4320002 (Cooperative Institute for Satellite Earth System  
 1219 Studies - CISESS) at the University of Maryland/ESSIC and NOAA grant NA22OAR4320151, for the Cooperative  
 1220 Institute for Earth System Research and Data Science (CIESRDS). Additional funding is from NOAA Climate  
 1221 Program Office’s Atmospheric Chemistry, Carbon Cycle, and Climate program (AC4), grant numbers  
 1222 NA19OAR4310169 (CU)/ NA19OAR4310171 (UMD). The statements, findings, conclusions, and recommendations  
 1223 are those of the author(s) and do not necessarily reflect the views of NOAA or the U.S. Department of Commerce.

1224 The authors would like to thank the NASA/GSFC Atmospheric Chemistry and Dynamics team for the SBUV/2 v8.6  
1225 profile data, Eric Beach from the NESDIS/STAR for his help with the S-NPP OMPS data, the NOAA GML  
1226 observatory team (Boulder, MLO and Fairbanks observatories), LATMOS (OHP), and NIWA (Lauder) for Umkehr  
1227 and ozonesonde data, Wolfgang Steinbrecht of the DWD for help with interpretation of the Hohenpeißenberg  
1228 ozonesonde data, the MeteoSwiss and PMOD/WRC teams (Arosa/Davos) for Dobson Umkehr data. Some data are  
1229 associated with the Network for the Detection of Atmospheric Composition Change (NDACC) and are available  
1230 through the NDACC website ([www.ndacc.org](http://www.ndacc.org)). Additional thanks are due to Susan Strahan for Equivalent Latitude  
1231 data at each station, to Kai-Lan Chang of CIRES for discussion of statistical interpretation of the thresholds, and to  
1232 Justin Alsing for development of the LOTUS code. North American Regional Reanalysis (NARR) data provided by  
1233 the NOAA PSL, Boulder, Colorado, USA, from their website at <https://psl.noaa.gov>.

## 1234 **References**

1235 Anstey, J.A., T.P. Banyard, N. Butchart, L. Coy, P.A. Newman, S. Osprey, and C.J. Wright, Prospect of increased  
1236 disruption to the QBO in a changing climate, *Geophys. Res. Lett.*, 48 (15), <https://doi.org/10.1029/2021gl093058>,  
1237 2021.

1238  
1239 Ancellet, G., Godin-Beekmann, S., Smit, H. G. J., Stauffer, R. M., Van Malderen, R., Bodichon, R., Pazmino, A.:  
1240 Homogenization of the Observatoire de Haute Provence electrochemical concentration cell (ECC) ozonesonde data  
1241 record: comparison with lidar and satellite observations, *Atmos. Meas. Tech.*, 15, 3105–3120,  
1242 <https://doi.org/10.5194/amt-15-3105-2022>, 2022.

1243  
1244 Bai, K., Liu, C., Shi, R. et al. Comparison of Suomi-NPP OMPS total column ozone with Brewer and Dobson  
1245 spectrophotometers measurements. *Front. Earth Sci.* 9, 369–380 (2015). <https://doi.org/10.1007/s11707-014-0480-5>.

1246  
1247 Ball, W. T., Chiodo, G., Abalos, M., Alsing, J., and Stenke, A., Inconsistencies between chemistry–climate models  
1248 and observed lower stratospheric ozone trends since 1998, *Atmos. Chem. Phys.*, 20, 9737–9752,  
1249 <https://doi.org/10.5194/acp-20-9737-2020>, 2020.

1250  
1251 Bernet, L., Svendby, T., Hansen, G., Orsolini, Y., Dahlback, A., Goutail, F., Pazmiño, A., Petkov, B.,  
1252 and Kylling, A.: Total ozone trends at three northern high-latitude stations, *Atmos. Chem. Phys.*, 23,  
1253 4165–4184, <https://doi.org/10.5194/acp-23-4165-2023>, 2023.

1254 Bhartia, P. K., Herman, J. R., McPeters, R. D., Torres, O.: Effect of Mount Pinatubo aerosols on total ozone  
1255 measurements from backscatter ultraviolet (BUV) experiments, *J. Geophys. Res.*, 98, 18,547- 18,554,  
1256 <https://doi.org/10.1029/93JD01739>, 1993.

1257 Bhartia, P. K., McPeters, R. D., Flynn, L. E., Taylor, S., Kramarova, N. A., Frith, S., Fisher, B., and DeLand, M.:  
1258 Solar Backscatter UV (SBUV) total ozone and profile algorithm, *Atmos. Meas. Tech.*, 6, 2533–2548,  
1259 <https://doi.org/10.5194/amt-6-2533-2013>, 2013.

1260 Björklund, R., Vigouroux, C., Effertz, P., Garcia, O., Geddes, A., Hannigan, J., Miyagawa, K., Kotkamp, M.,  
1261 Langerock, B., Nedoluha, G., Ortega, I., Petropavlovskikh, I., Poyraz, D., Querel, R., Robinson, J., Shiona, H., Smale,  
1262 D., Smale, P., Van Malderen, R., and De Mazière, M.: Intercomparison of long-term ground-based measurements of  
1263 tropospheric and stratospheric ozone at Lauder, New Zealand (45S), *EGUsphere* [preprint],  
1264 <https://doi.org/10.5194/egusphere-2023-2668>, 2023.

1265 Boynard, A., Hurtmans, D., Garane, K., Goutail, F., Hadji-Lazaro, J., Koukouli, M. E., Wespes, C., Vigouroux, C.,  
1266 Keppens, A., Pommereau, J.-P., Pazmino, A., Balis, D., Loyola, D., Valks, P., Sussmann, R., Smale, D., Coheur, P.-  
1267 F., and Clerbaux, C.: Validation of the IASI FORLI/EUMETSAT ozone products using satellite (GOME-2), ground-  
1268 based (Brewer–Dobson, SAOZ, FTIR) and ozonesonde measurements, *Atmos. Meas. Tech.*, 11, 5125–5152,  
1269 <https://doi.org/10.5194/amt-11-5125-2018>, 2018.

1270 Chang, K.-L., Cooper, O. R., Gaudel, A., Petropavlovskikh, I., and Thouret, V., Statistical regularization for trend  
1271 detection: an integrated approach for detecting long-term trends from sparse tropospheric ozone profiles, *Atmos.*  
1272 *Chem. Phys.*, 20, 9915–9938, <https://doi.org/10.5194/acp-20-9915-2020>, 2020.

1273 Chang, K. L., Schultz, M. G., Lan, X., McClure-Begley, A., Petropavlovskikh, I., Xu, X., & Ziemke, J. R., Trend  
1274 detection of atmospheric time series: Incorporating appropriate uncertainty estimates and handling extreme events,  
1275 *Elem Sci Anth*, 9(1), 00035, <https://doi.org/10.1525/elementa.2021.00035>, 2021.

1276 Chang, K.-L., Schultz, M.G., Koren, G., Selke, N., Guidance note on best statistical practices for TOAR analyses, in  
1277 TOAR tropospheric ozone assessment report, 2023, available at [https://igacproject.org/sites/default/files/2023-](https://igacproject.org/sites/default/files/2023-04/STAT_recommendations_TOAR_analyses_0.pdf)  
1278 [04/STAT\\_recommendations\\_TOAR\\_analyses\\_0.pdf](https://igacproject.org/sites/default/files/2023-04/STAT_recommendations_TOAR_analyses_0.pdf), last access 12/07/2023.

1279 Chang, K.-L., Cooper, O.R., Gaudel, A., Petropavlovskikh, I., Effertz, P., Morris, G., McDonald, B.C., Challenges of  
1280 detecting free tropospheric ozone trends in a sparsely sampled environment, in Special issue: Tropospheric Ozone  
1281 Assessment Report Phase II (TOAR-II) Community Special Issue (ACP/AMT/BG/GMD inter-journal SI), 2023  
1282 preprint.

1283 Cochran, D., Orcutt, G. H.: Application of least squares regression to relationships containing auto-correlated error  
1284 terms, *Journal of the American Statistical Association*, 44: 245, 32-  
1285 61, <https://doi.org/10.1080/01621459.1949.10483290>, 1949 .

1286 DeLuisi, J. J., Longenecker, D. U., Mateer, C. L., Wuebbles, D. J.: An analysis of northern middle-latitude Umkehr  
1287 measurements corrected for stratospheric aerosols for 1979–1986, *J. Geophys. Res.*, 94, 9837–9846,  
1288 <https://doi.org/10.1029/JD094iD07p09837>, 1989.



1289 Diallo, M., Riese, M., Birner, T., Konopka, P., Müller, R., Hegglin, M. I., Santee, M. L., Baldwin, M., Legras, B., and  
1290 Ploeger, F.: Response of stratospheric water vapor and ozone to the unusual timing of El Niño and the QBO disruption  
1291 in 2015–2016, *Atmos. Chem. Phys.*, 18, 13055–13073, <https://doi.org/10.5194/acp-18-13055-2018>, 2018.  
1292

1293 Diallo, M. A., Ploeger, F., Hegglin, M. I., Ern, M., Groß, J.-U., Khaykin, S., and Riese, M.: Stratospheric water  
1294 vapour and ozone response to the quasi-biennial oscillation disruptions in 2016 and 2020, *Atmos. Chem. Phys.*, 22,  
1295 14303–14321, <https://doi.org/10.5194/acp-22-14303-2022>, 2022.  
1296

1297 EEAP (Environmental Effects Assessment Panel): 2022 Quadrennial Assessment - Environmental effects of  
1298 stratospheric ozone depletion, UV radiation, and interactions with climate change, 2023,  
1299 <https://ozone.unep.org/system/files/documents/EEAP-2022-Assessment-Report-May2023.pdf>, last access March 5,  
1300 2024.  
1301

1302 Evans, R.D., Irina Petropavlovskikh, Audra McClure-Begley, Glen McConville, Dorothy Quincy, and Koji  
1303 Miyagawa, Technical note: The US Dobson station network data record prior to 2015, re-evaluation of NDACC and  
1304 WOUDC archived records with WinDobson processing software, *Atmospheric Chemistry and Physics*, 17, 12051–  
1305 12070, <https://doi.org/10.5194/acp-17-12051-2017>, 2017.  
1306

1307 Fioletov, V. E., Labow, G., Evans, R., Hare, E. W., Köhler, U., McElroy, C. T., Miyagawa, K., Redondas, A.,  
1308 Savastiouk, V., Shalamyansky, A. M., Staehelin, J., Vanicek, K., and Weber, M.: Performance of the ground-based  
1309 total ozone network assessed using satellite data, *J. Geophys. Res.*, 113, D14313,  
1310 <https://doi.org/10.1029/2008JD009809>, 2008.  
1311

1312 Frith, S. M., Kramarova, N. A., Stolarski, R. S., McPeters, R. D., Bhartia, P. K., G. J. Labow: Recent changes in total  
1313 column ozone based on the SBUV Version 8.6 Merged Ozone Data Set, *J. Geophys. Res. Atmos.*, 119, 9735–9751,  
1314 <https://doi.org/10.1002/2014JD021889>, 2014.

1315 Frith, S. M., Kramarova, N. A., Bhartia, P. K., McPeters, R. D., Labow, G. J., J. R. Ziemke, J. R., Haffner, D.: Recent  
1316 Advances in the SBUV Merged Ozone Dataset (MOD) for LOTUS Phase 2 Analysis of Stratospheric Ozone Trends  
1317 and Uncertainties, LOTUS Phase 2 Workshop (Virtual), May 28, 2020.

1318 Godin-Beekmann, S., Azouz, N., Sofieva, V., Hubert, D., Petropavlovskikh, I., Effertz, P., Ancellet, G., Degenstein,  
1319 D., Zawada, D., Froidevaux, L., Frith, S., Wild, J., Davis, S., Steinbrecht, W., Leblanc, T., Querel, R., Tourpali, K.,  
1320 Damadeo, R., Maillard Barras, E., Stübi, R., Vigouroux, C., Arosio, C., Nedoluha, G., Boyd, I., van Malderen, R.:  
1321 Updated trends of the stratospheric ozone vertical distribution in the 60° S–60° N latitude range based on the LOTUS  
1322 regression model, *Atmos. Chem. Phys.*, 22, 11657–11673, <https://doi.org/10.5194/acp-22-11657-2022>, 2022.  
1323

1324 Harris, N.R.P., B. Hassler, F. Tummon, G. E. Bodeker, D. Hubert, I. Petropavlovskikh, W. Steinbrecht, J. Anderson,  
1325 P. K. Bhartia, C. D. Boone, A. Bourassa, S. M. Davis, D. Degenstein, A. Delcloo, S. M. Frith, L. Froidevaux, S.  
1326 Godin-Beekmann, N. Jones, M. J. Kurylo, E. Kyrölä, M. Laine, S. T. Leblanc, J.-C. Lambert, B. Liley, E. Mahieu, A.

1327 Maycock, M. de Mazière, A. Parrish, R. Querel, K. H. Rosenlof, C. Roth, C. Sioris, J. Staehelin, R. S. Stolarski, R.  
1328 Stübi, J. Tamminen, C. Vigouroux, K. A. Walker, H. J. Wang, J. Wild, and J. M. Zawodny, Past changes in the vertical  
1329 distribution of ozone – Part 3: Analysis and interpretation of trends, *Atmos. Chem. Phys.*, 15, 9965-9982,  
1330 <https://doi.org/10.5194/acp-15-9965-2015>, 2015.

1331

1332 Hassler, B., I. Petropavlovskikh, J. Staehelin, T. August, P. K. Bhartia, C. Clerbaux, D. Degenstein, M. De Mazière,  
1333 B. M. Dinelli, A. Dudhia, G. Dufour, S. M. Frith, L. Froidevaux, S. Godin-Beekmann, J. Granville, N. R. P. Harris,  
1334 K. Hoppel, D. Hubert, Y. Kasai, M. J. Kurylo, E. Kyrölä, J.-C. Lambert, P. F. Levelt, C. T. McElroy, R. D. McPeters,  
1335 R. Munro, H. Nakajima, A. Parrish, P. Raspollini, E. E. Remsberg, K. H. Rosenlof, A. Rozanov, T. Sano, Y. Sasano,  
1336 M. Shiotani, H. G. J. Smit, G. Stiller, J. Tamminen, D. W. Tarasick, J. Urban, R. J. van der A, J. P. Veefkind, C.  
1337 Vigouroux, T. von Clarmann, C. von Savigny, K. A. Walker, M. Weber, J. Wild, and J. M. Zawodny, Past changes in  
1338 the vertical distribution of ozone – Part 1: Measurement techniques, uncertainties and availability, *Atmos. Meas.*  
1339 *Tech.*, 7, 1395-1427, <https://doi.org/10.5194/amt-7-1395-2014>, 2014.

1340

1341 Hassler, B., Kremser, S., Bodeker, G. E., Lewis, J., Nesbit, K., Davis, S. M., Chipperfield, M. P., Dhomse, S. S., and  
1342 Dameris, M.: An updated version of a gap-free monthly mean zonal mean ozone database, *Earth Syst. Sci. Data*, 10,  
1343 1473–1490, <https://doi.org/10.5194/essd-10-1473-2018>, 2018.

1344

1345 Hassler, B., P. Young, P. (Lead Authors), Ball, W. T., Damadeo, R., Keeble, J., Maillard Barras, E., Sofieva, V.,  
1346 Zeng, G.: Update on Global Ozone: Past, Present, and Future, Chapter 3 in *Scientific Assessment of Ozone Depletion:*  
1347 *2022*, GAW Report No. 278, 509 pp., WMO, Geneva, 2022.

1348

1349 Hubert, D., Lambert, J.-C., Verhoelst, T., Granville, J., Keppens, A., Baray, J.-L., Bourassa, A. E., Cortesi, U.,  
1350 Degenstein, D. A., Froidevaux, L., Godin-Beekmann, S., Hoppel, K. W., Johnson, B. J., Kyrölä, E., Leblanc, T.,  
1351 Lichtenberg, G., Marchand, M., McElroy, C. T., Murtagh, D., Nakane, H., Portafaix, T., Querel, R., Russell III, J. M.,  
1352 Salvador, J., Smit, H. G. J., Stebel, K., Steinbrecht, W., Strawbridge, K. B., Stübi, R., Swart, D. P. J., Taha, G.,  
1353 Tarasick, D. W., Thompson, A. M., Urban, J., van Gijssel, J. A. E., Van Malderen, R., von der Gathen, P., Walker, K.  
1354 A., Wolfram, E., and Zawodny, J. M.: Ground-based assessment of the bias and long-term stability of 14 limb and  
1355 occultation ozone profile data records, *Atmos. Meas. Tech.*, 9, 2497–2534, <https://doi.org/10.5194/amt-9-2497-2016>,  
1356 2016.

1357

1358 E. Kalnay, Kanamitsu, M., Kistler, R., Collins, W., Deaven, D., Gandin, L., Iredell, M., Saha, S., White, G., Woollen,  
1359 J., Zhu, Y., Chelliah, M., Ebisuzaki, W., Higgins, W., Janowiak, J., Mo, K.C., Ropelewski, C., Wang, J., Leetmaa,  
1360 A., Reynolds, R., Jenne, R., and Joseph, D., The NCEP/NCAR 40-year reanalysis project, *Bull. Amer. Meteor. Soc.*,  
1361 77, 437-470, [https://doi.org/10.1175/1520-0477\(1996\)077<0437:TNYRP>2.0.CO;2](https://doi.org/10.1175/1520-0477(1996)077<0437:TNYRP>2.0.CO;2), 1996.

1362

1363 Knudsen, B. M., and J. U. Grooss, Northern midlatitude stratospheric ozone dilution in spring modeled with simulated  
1364 mixing. *J. Geophys. Res.*, 105, 6885–6890, <https://doi.org/10.1029/1999JD901076>, 2000.  
1365

1366 Koukoulis, M. E., Zara, M., Lerot, C., Fragkos, K., Balis, D., van Roozendaal, M., Allart, M. A. F., and van der A, R.  
1367 J.: The impact of the ozone effective temperature on satellite validation using the Dobson spectrophotometer network,  
1368 *Atmos. Meas. Tech.*, 9, 2055–2065, <https://doi.org/10.5194/amt-9-2055-2016>, 2016.  
1369

1370 Kramarova, N. A., Frith, S. M., Bhartia, P. K., McPeters, R. D., Taylor, S. L., Fisher, B. L., Labow, G. J., DeLand,  
1371 M. T.: Validation of ozone monthly zonal mean profiles obtained from the version 8.6 Solar Backscatter Ultraviolet  
1372 algorithm, *Atmos. Chem. Phys.*, 13, 6887-6905, <https://doi.org/10.5194/acp-13-6887-2013>, 2013a.

1373 Kramarova, N. A., Bhartia, P. K., Frith, S. M., McPeters, R. D., and Stolarski, R. S.: Interpreting SBUV smoothing  
1374 errors: an example using the quasi-biennial oscillation, *Atmos. Meas. Tech.*, 6, 2089–2099,  
1375 <https://doi.org/10.5194/amt-6-2089-2013>, 2013b.

1376 Lary, D.J., Chipperfield, M.P., Pyle, J.A., Norton, W.A. Riishøjgaard, L.P. (1995), Three-dimensional tracer  
1377 initialization and general diagnostics using equivalent PV latitude–potential-temperature coordinates, *Q.J.R.*  
1378 *Meteorol. Soc.*, 121: 187-210, <https://doi.org/10.1002/qj.49712152109>, 1995.  
1379

1380 Lawrence, Z. D., Perlwitz, J., Butler, A. H., Manney, G. L., Newman, P. A., Lee, S. H., & Nash, E. R., The  
1381 remarkably strong Arctic stratospheric polar vortex of winter 2020: Links to record-breaking Arctic Oscillation and  
1382 ozone loss. *Journal of Geophysical Research: Atmospheres*, 125, e2020JD033271.  
1383 <https://doi.org/10.1029/2020JD033271>, 2020.  
1384

1385 Lee, H., and Smith, A. K., Simulation of the combined effects of solar cycle, quasi-biennial oscillation, and volcanic  
1386 forcing on stratospheric ozone changes in recent decades, *J. Geophys. Res.*, 108, D2, 4049,  
1387 <https://doi.org/10.1029/2001JD001503>, 2003.  
1388

1389 Madronich, S., Lee-Taylor, J. M., Wagner, M., Kyle, J., Hu, Z., & Landolfi, R. (2021). Estimation of skin and ocular  
1390 damage avoided in the United States through implementation of the Montreal Protocol on Substances that Deplete the  
1391 Ozone Layer. *ACS Earth and Space Chemistry*, 5(8), 1876-1888. <https://doi.org/10.1021/acsearthspacechem.1c00183>.  
1392

1393 Maillard Barras, E., Haeefe, A., Stübi, R., Jouberton, A., Schill, H., Petropavlovskikh, I., Miyagawa, K., Stanek, M.,  
1394 and Froidevaux, L.: Dynamical linear modeling estimates of long-term ozone trends from homogenized Dobson  
1395 Umkehr profiles at Arosa/Davos, Switzerland, *Atmos. Chem. Phys.*, 22, 14283–14302, [https://doi.org/10.5194/acp-](https://doi.org/10.5194/acp-22-14283-2022)  
1396 [22-14283-2022](https://doi.org/10.5194/acp-22-14283-2022), 2022.  
1397

1398 Manney, G. L., and M. I. Hegglin, 2018: Seasonal and Regional Variations of Long-Term Changes in Upper-  
1399 Tropospheric Jets from Reanalyses. *J. Climate*, 31, 423–448, <https://doi.org/10.1175/JCLI-D-17-0303.1>.  
1400

1401 Manney, G. L., and Coauthors, Unprecedented Arctic ozone loss in 2011. *Nature*, 478, 469–475,  
1402 <https://doi.org/10.1038/nature10556>, 2011.  
1403

1404 McPeters, R. D., Bhartia, P. K., Haffner, D., Labow, G. J., Flynn, L.: The version 8.6 SBUV ozone data record: An  
1405 overview, *J. Geophys. Res. Atmos.*, 118, 8032–8039, <https://doi.org/10.1002/jgrd.50597>, 2013.

1406 Meng, L., Liu, J., Tarasick, D.W., Randel, W.J., Steiner, A.K., Wilhelmsen, H., Wang, L., Haimberger, L., Continuous  
1407 rise of the tropopause in the Northern Hemisphere over 1980–2020, *Sci. Adv.* 7, eabi8065,  
1408 <https://doi.org/10.1126/sciadv.abi8065>, 2021.

1409 Millán, L. F., Hoor, P., Hegglin, M. I., Manney, G. L., Boenisch, H., Jeffery, P., Kunkel, D., Petropavlovskikh, I., Ye,  
1410 H., Leblanc, T., and Walker, K.: Exploring ozone variability in the upper troposphere and lower stratosphere using  
1411 dynamical coordinates, *EGUsphere* [preprint], <https://doi.org/10.5194/egusphere-2024-144>, 2024.

1412 Petropavlovskikh, I., Bhartia, P. K., and DeLuisi, J.: New Umkehr ozone profile retrieval algorithm optimized for  
1413 climatological studies, *Geophys. Res. Lett.*, 32, L16808, <https://doi.org/10.1029/2005GL023323>, 2005.

1414 Petropavlovskikh, I., Miyagawa, K., McClure-Beegle, A., Johnson, B., Wild, J., Strahan, S., Wargan, K., Querel, R.,  
1415 Flynn, L., Beach, E., Ancellet, G., and Godin-Beekmann, S.: Optimized Umkehr profile algorithm for ozone trend  
1416 analyses, *Atmos. Meas. Tech.*, 15, 1849–1870, <https://doi.org/10.5194/amt-15-1849-2022>, 2022.

1417 Rodgers, C. D.: *Inverse Methods for Atmospheric Sounding : Theory and Practice.*, Series on Atmospheric, Oceanic  
1418 and Planetary Physics, World Scientific Publishing Company, Hackensack, N. J., <https://doi.org/10.1142/3171>, 2000.

1419 Savin, N. E., & White, K. J. (1978). Testing for Autocorrelation with Missing observations. *Econometrica* (Pre-1986),  
1420 46(1), 59.

1421 Smit, H. G. J. and the ASOPOS panel (Assessment of Standard Operating Procedures for Ozonesondes): Quality  
1422 assurance and quality control for ozonesonde measurements in GAW, World Meteorological Organization, GAW  
1423 Report #201, Geneva, Switzerland, available at: [https://library.wmo.int/doc\\_num.php?explnum\\_id=7167](https://library.wmo.int/doc_num.php?explnum_id=7167), 2014.  
1424

1425 Smit, H. G. J., Thompson, A. M. and the ASOPOS 2.0 panel (Assessment of Standard Operating Procedures for  
1426 Ozonesondes, v2.0): Ozonesonde measurement principles and best operational practices, World Meteorological  
1427 Organization, GAW Report #268, Geneva, Switzerland, available at:  
1428 [https://library.wmo.int/doc\\_num.php?explnum\\_id=10884](https://library.wmo.int/doc_num.php?explnum_id=10884), 2021.  
1429

1430 SPARC/IO3C/GAW, SPARC/IO3C/GAW Report on Long-term Ozone Trends and Uncertainties in the Stratosphere.  
1431 I. Petropavlovskikh, S. Godin-Beekmann, D. Hubert, R. Damadeo, B. Hassler, V. Sofieva (Eds.), SPARC Report No.  
1432 9, GAW Report No. 241, WCRP-17/2018, <https://doi.org/10.17874/f899e57a20b>, available at [www.sparc-](http://www.sparc-climate.org/publications/sparc-reports/sparc-report-no9)  
1433 [climate.org/publications/sparc-reports/sparc-report-no9](http://www.sparc-climate.org/publications/sparc-reports/sparc-report-no9), 2019.  
1434

1435 Staehelin, J., Pierre Viatte, Rene Stübi, Fiona Tummon, and Thomas Peter, 2018, Stratospheric ozone measurements  
1436 at Arosa (Switzerland): history and scientific relevance, *Atmospheric Chemistry and Physics*, 18, 6567–6584,  
1437 <https://doi.org/10.5194/acp-18-6567-2018>.  
1438

1439 Stauffer, R.M., Thompson, A. M., Kollonige, D. E., Tarasick, D. W., Van Malderen, R., Smit, H. G. J., Vömel, H.,  
1440 Morris, G.A., Johnson, B.J., Cullis, P.D., Stübi, R., Davies. J., Yan, M.M., An Examination of the Recent Stability of  
1441 Ozonesonde Global Network Data, *EARTH and Space Science*, 9, e2022EA002459.  
1442 <https://doi.org/10.1029/2022EA002459>, 2022.  
1443

1444 Stauffer, R. M., Thompson, A. M., Kollonige, D. E., Komala, N., Al-Ghazali, H. K., Risdianto, D. Y., Dindang, A.,  
1445 Fairudz bin Jamaluddin, A., Sammathuria, M. K., Zakaria, N. B., Johnson, B. J., and Cullis, P. D.: Dynamical drivers  
1446 of free-tropospheric ozone increases over equatorial Southeast Asia, *EGU sphere* [preprint],  
1447 <https://doi.org/10.5194/egusphere-2023-2618>, 2023.  
1448

1449 Stauffer, R. M., Thompson, A. M., Oman, L. D., & Strahan, S. E., The effects of a 1998 observing system change on  
1450 MERRA-2-based ozone profile simulations. *Journal of Geophysical Research: Atmospheres*, 124, 7429–7441,  
1451 <https://doi.org/10.1029/2019JD030257>, 2019.  
1452

1453 Steinbrecht, W., U. Köhler, H. Claude, M. Weber, J. P. Burrows, and R. J. van der A, Very high ozone columns at  
1454 northern mid-latitudes in 2010, *Geophys. Res. Lett.*, 38, L06803, <https://doi.org/10.1029/2010GL046634>, 2011.  
1455

1456 Sterling, C. W, Johnson, B. J., Oltmans, S. J., Smit, H. G. J., Jordan, A.F., Cullis, P. D., Hall, E. G., Thompson, A.  
1457 M., Jacquelyn C. Witte, J. C.: Homogenizing and estimating the uncertainty in NOAA's long-term vertical ozone  
1458 profile records measured with the electrochemical concentration cell  
1459 ozonesonde, *Atmos. Meas. Tech.*, 11, 3661–3687, <https://doi.org/10.5194/amt-11-3661-2018>, 2018.  
1460

1461 Szelag, M. E., Sofieva, V. F., Degenstein, D., Roth, C., Davis, S., and Froidevaux, L.: Seasonal stratospheric ozone  
1462 trends over 2000–2018 derived from several merged data sets, *Atmospheric Chemistry and Physics*, 20, 7035–7047,  
1463 <https://doi.org/10.5194/acp-20-7035-2020>, 2020.  
1464

1465 Tarasick, D. W., Davies, J., Smit, H. G. J., Oltmans, S. J.: A re-evaluated Canadian ozonesonde record: measurements  
1466 of the vertical distribution of ozone over Canada from 1966 to 2013, *Atmos. Meas. Tech.*, 9, 195–214,  
1467 <https://doi.org/10.5194/amt-9-195-2016>, 2016.  
1468

1469 Thompson, A. M., Witte, J. C., Sterling, C., Jordan, A., Johnson, B. J., Oltmans, S. J., Fujiwara, M., Vömel, H.,  
1470 Allaart, M., Piders, A., Coetzee, G. J. R., Posny, F., Corrales, E., Diaz, J. A., Félix, C., Komala, N., Lai, N., Nguyen,  
1471 H. T. A., Maata, M., Mani, F., Zainal, Z., Ogino, S., Paredes, F., Penha, T. L. B., da Silva, F. R., Sallons-Mitro, S.,

1472 Selkirk, H. B., Schmidlin, F. J., Stübi, R., Thiongo, K.: First reprocessing of Southern Hemisphere ADditional  
1473 OZonesondes (SHADOZ) Ozone Profiles (1998-2016). 2. Comparisons with satellites and ground-based instruments,  
1474 J. Geophys. Res., 122, <https://doi.org/10.1002/2017JD027406>, 2017.  
1475

1476 Thompson, A. M., H. G. J. Smit, J. C. Witte, R. M. Stauffer, B. J. Johnson, G. Morris, P. von der Gathen, R. Van  
1477 Malderen, J. Davies, A. PETERS, M. Allaart, F. Posny, R. Kivi, P. Cullis, N. Thi Hoang Anh, E. Corrales, T. Machinini,  
1478 F. R. da Silva, G. Paiman, K. Thiong'o, Z. Zainal, G. B. Brothers, K. R. Wolff, T. Nakano, R. Stübi, G. Romanens,  
1479 G.J. R. Coetzee, J. A. Diaz, S. Mitro, M. Mohamad and S.-Y. Ogino, Ozonesonde Quality Assurance: The JOSIE–  
1480 SHADOZ (2017) Experience, Bulletin of the American Meteorological Society, 100, 1, 155-171, 10.1175/BAMS-D-  
1481 17-0311.1, 2019.

1482 Thompson, A. M., Stauffer, R. M., Wargan, K., Witte, J. C., Kollonige, D. E., & Ziemke, J. R.: Regional and seasonal  
1483 trends in tropical ozone from SHADOZ profiles: Reference for models and satellite products, J. Geophys. Res.-  
1484 Atmos., 126, e2021JD034691. <https://doi.org/10.1029/2021JD034691>, 2021.

1485 Torres, O., Herman, J. R., Bhartia, P. K., and Ahmad, Z.: Properties of Mount-Pinatubo Aerosols as Derived from  
1486 Nimbus-7 Total Ozone Mapping Spectrometer Measurements, J. Geophys. Res.-Atmos., 100, 14043–14055,  
1487 <https://doi.org/10.1029/95JD01224>, 1995.

1488 Tweedy, O. V., Kramarova, N. A., Strahan, S. E., Newman, P. A., Coy, L., Randel, W. J., Park, M., Waugh, D. W.,  
1489 and Frith, S. M.: Response of trace gases to the disrupted 2015–2016 quasi-biennial oscillation, Atmos. Chem. Phys.,  
1490 17, 6813–6823, <https://doi.org/10.5194/acp-17-6813-2017>, 2017.

1491 Van Malderen, R., Marc A. F. Allaart, M. A. F., Hugo De Backer, H., Herman G. J. Smit, H. G. J., Dirk De Muer, D.  
1492 D.: On instrumental errors and related correction strategies of ozonesondes: possible effect on calculated ozone trends  
1493 for the nearby sites Uccle and De Bilt, Atmos. Meas. Tech., 9, 3793–3816, <https://doi.org/10.5194/amt-9-3793-2016>,  
1494 2016.  
1495

1496 Wallace, J.M., The general circulation of the tropical lower stratosphere. Rev. Geophys. Space Phys., 11, 191–222,  
1497 <https://doi.org/10.1029/RG011I002P00191>, 1973.  
1498

1499 Wallace, J.M., L. Panetta, and J. Estberg, Representation of the equatorial stratospheric quasi-biennial oscillation in  
1500 EOF phase space. J. Atmos. Sci., 50, 1751–1762, [https://doi.org/10.1175/1520-  
1501 0469\(1993\)050<1751:ROTESQ>2.0.CO;2](https://doi.org/10.1175/1520-0469(1993)050<1751:ROTESQ>2.0.CO;2), 1993.  
1502

1503 Wargan, K., C. Orbe, S. Pawson, et al. J. R. Ziemke, L. D. Oman, M. A. Olsen, L. Coy, and K. E. Knowland. 2018.  
1504 Recent decline in extratropical lower stratospheric ozone attributed to circulation changes Geophysical Research  
1505 Letters, <https://doi.org/10.1029/2018gl077406>.  
1506

1507 Wasserstein, R. L., Schirm A.L., Lazar, N.A., Moving to a World Beyond “ $p < 0.05$ ”, *The American Statistician*,  
1508 73:sup1, 1-19, <https://doi.org/10.1080/00031305.2019.1583913>, 2019.  
1509

1510 Weber, M., Arosio, C., Coldewey-Egbers, M., Fioletov, V. E., Frith, S. M., Wild, J. D., Tourpali, K., Burrows, J. P.,  
1511 and Loyola, D.: Global total ozone recovery trends attributed to ozone-depleting substance (ODS) changes derived  
1512 from five merged ozone datasets, *Atmos. Chem. Phys.*, 22, 6843–6859, <https://doi.org/10.5194/acp-22-6843-2022>,  
1513 2022a.  
1514

1515 Weber, M., W. Steinbrecht, C. Arosio, R. van der A, S. M. Frith, J. Anderson, L. Ciasto, M. Coldewey-Egbers, S.  
1516 Davis, D. Degenstein, V. E. Fioletov, L. Froidevaux, D. Hubert, D. Loyola, C. Roth, A. Rozanov, V. Sofieva, K.  
1517 Tourpali, R. Wang, and J. D. Wild: Stratospheric Ozone [in “State of the Climate in 2020“], *Bull. Amer. Meteor.*, 103  
1518 (8), S90–S92, <https://doi.org/10.1175/BAMS-D-22-0092.1>, 2022b.  
1519

1520 Wild, J.D., S.-K. Yang, and C.S. Long, Ozone Profile Trends: An SBUV/2 Perspective (QOS2016-133), in  
1521 Proceedings of the Quadrennial Ozone Symposium, Edinburgh, Scotland,  
1522 <https://meetingorganizer.copernicus.org/QOS2016/QOS2016-133.pdf>, last access February 6, 2024, 2016.  
1523

1524 Witte, J. C., Thompson, A. M., Herman G. J. Smit, H. G. J., Fujiwara, M., Posny, F., Coetzee, G. J. R., Northam, E.  
1525 T., Johnson, B. J., Sterling, C. W., Mohamad, M., Ogino, S-Y., Jordan, A., da Silva, F. R.: First reprocessing of  
1526 Southern Hemisphere ADditional OZonesondes (SHADOZ) profile records (1998-2015) 1: Methodology and  
1527 evaluation, *J. Geophys. Res.*, 122, <https://doi.org/10.1002/2016JD026403>, 2017.  
1528

1529 Witte, J. C., Thompson, A., M., Smit, H. G. J., Vömel, H., Posny, F., Stübi, R.: First reprocessing of Southern  
1530 Hemisphere Additional Ozonesondes (SHADOZ) Profile Records. 3. Uncertainty in ozone profile and total column,  
1531 *J. Geophys. Res.*, 123(6), 3243-3268, <https://doi.org/10.1002/2017JD027791>, 2018.  
1532

1533 Witte, J. C., Thompson, A. M., Schmidlin, F. J., Northam, E. T., Wolff, K. R., Brothers, G. B.: The NASA Wallops  
1534 Flight Facility digital ozonesonde record: Reprocessing, uncertainties, and dual launches. *J. Geophys. Res.*, 124, 3565–  
1535 3582, <https://doi.org/10.1029/2018JD030098>, 2019.  
1536

1537 WMO (World Meteorological Organization), Scientific Assessment of Ozone Depletion: 2014, Global Ozone  
1538 Research and Monitoring Project-Report No. 55, 416 pp., WMO: Geneva, Switzerland,  
1539 available at: <https://www.esrl.noaa.gov/csd/assessments/ozone/2014/>, 2014.  
1540

1541 WMO (World Meteorological Organization), Scientific Assessment of Ozone Depletion: 2018, Global Ozone  
1542 Research and Monitoring Project-Report No. 58, 588 pp., WMO: Geneva, Switzerland,  
1543 <https://library.wmo.int/idurl/4/56362>, 2018.

1544  
1545 WMO (World Meteorological Organization), Scientific Assessment of Ozone Depletion: 2022, GAW Report No. 278,  
1546 509 pp.; WMO: Geneva, Switzerland, <https://ozone.unep.org/science/assessment/sap>, 2022.  
1547  
1548 Wohltmann, I., Rex, M., Brunner, D., and Mäder, J., Integrated equivalent latitude as a proxy for dynamical changes  
1549 in ozone column, *Geophys. Res. Lett.*, 32, L09811, <https://doi.org/10.1029/2005GL022497>, 2005.  
1550  
1551 Wolter, K., and M. S. Timlin, El Niño/Southern Oscillation behaviour since 1871 as diagnosed in an extended  
1552 multivariate ENSO index (MEI.ext). *Intl. J. Climatology*, 31, 14pp., 1074-1087, <https://doi.org/10.1002/joc.2336>,  
1553 2011.  
1554  
1555 Yoon, S., Kotsakis, A., Alvarez, S. L., Spsychala, M. G., Klovenski, E., Walter, P., Morris, G., Corrales, E., Alan, A.,  
1556 Diaz, J. A., and Flynn, J. H., Development and testing of a novel sulfur dioxide sonde, *Atmos. Meas. Tech.*, 15, 4373–  
1557 4384, <https://doi.org/10.5194/amt-15-4373-2022>, 2022.  
1558  
1559 Zhang, J., and Coauthors, Influence of the Arctic Oscillation on the Vertical Distribution of Wintertime Ozone in the  
1560 Stratosphere and Upper Troposphere over the Northern Hemisphere. *J. Climate*, 30, 2905–2919,  
1561 <https://doi.org/10.1175/JCLI-D-16-0651.1>, 2017.  
1562  
1563 Zerefos, C., Kapsomenakis, J., Eleftheratos, K., Tourpali, K., Petropavlovskikh, I., Hubert, D., Godin-Beekmann, S.,  
1564 Steinbrecht, W., Frith, S., Sofieva, V., and Hassler, B.: Representativeness of single lidar stations for zonally averaged  
1565 ozone profiles, their trends and attribution to proxies, *Atmos. Chem. Phys.*, 18, 6427–6440,  
1566 <https://doi.org/10.5194/acp-18-6427-2018>, 2018.